



January 2018

An Investigation Of Particulate Matter Air Pollution Using Caliop Observations

Travis Toth

[How does access to this work benefit you? Let us know!](#)

Follow this and additional works at: <https://commons.und.edu/theses>

Recommended Citation

Toth, Travis, "An Investigation Of Particulate Matter Air Pollution Using Caliop Observations" (2018).
Theses and Dissertations. 2366.
<https://commons.und.edu/theses/2366>

This Dissertation is brought to you for free and open access by the Theses, Dissertations, and Senior Projects at UND Scholarly Commons. It has been accepted for inclusion in Theses and Dissertations by an authorized administrator of UND Scholarly Commons. For more information, please contact und.common@library.und.edu.

AN INVESTIGATION OF PARTICULATE MATTER AIR POLLUTION
USING CALIOP OBSERVATIONS

by

Travis Dean Toth
Bachelor of Science, Millersville University, 2010
Master of Science, University of North Dakota, 2012

A Dissertation

Submitted to the Graduate Faculty

of the

University of North Dakota

in partial fulfillment of the requirements

for the degree of

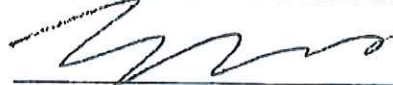
Doctor of Philosophy

Grand Forks, North Dakota

May
2018

Copyright 2018 Travis D. Toth

This dissertation, submitted by Travis D. Toth in partial fulfillment of the requirements for the Degree of Doctor of Philosophy from the University of North Dakota, has been read by the Faculty Advisory Committee under whom the work has been done and is hereby approved.



Jianglong Zhang, Chairperson



Cedric Grainger

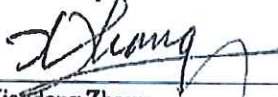


Xiquan Dong

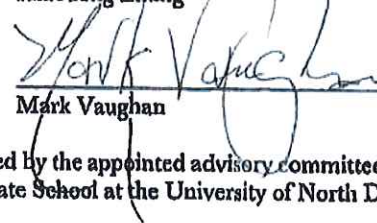
27 Apr. 2018



James Campbell



Xiaodong Zhang



Mark Vaughan

This dissertation is being submitted by the appointed advisory committee as having met all of the requirements of the Graduate School at the University of North Dakota and is hereby approved.



Grant McGimpsey
Dean of the Graduate School

May 1, 2018

Date

PERMISSION

Title An Investigation of Particulate Matter Air Pollution Using CALIOP
Observations

Department Atmospheric Sciences

Degree Doctor of Philosophy

In presenting this dissertation in partial fulfillment of the requirements for a graduate degree from the University of North Dakota, I agree that the library of this University shall make it freely available for inspection. I further agree that permission for extensive copying for scholarly purposes may be granted by the professor who supervised my dissertation work or, in their absence, by the chairperson of the department or the dean of the Graduate School. It is understood that any copying or publication or other use of this dissertation or part thereof for financial gain shall not be allowed without my written permission. It is also understood that due recognition shall be given to me and to the University of North Dakota in any scholarly use which may be made of any material in my dissertation.

Travis Toth
May 2, 2018

TABLE OF CONTENTS

LIST OF FIGURES.....	vi
LIST OF TABLES.....	xiii
ACKNOWLEDGEMENTS	xv
ABSTRACT.....	xvii
CHAPTER	
I. INTRODUCTION.....	1
II. DATASETS.....	7
III. IMPACT OF DATA QUALITY AND SURFACE-TO-COLUMN REPRESENTATIVENESS ON THE PM _{2.5} /SATELLITE AOT RELATIONSHIP FOR THE CONTIGUOUS UNITED STATES.....	13
IV. MINIMUM AEROSOL LAYER DETECTION SENSITIVITIES AND THEIR SUBSEQUENT IMPACTS ON AEROSOL OPTICAL THICKNESS RETRIEVALS IN CALIPSO LEVEL 2 DATA PRODUCTS.....	45
V. A BULK-MASS-MODELING-BASED METHOD FOR RETRIEVING PARTICULATE MATTER POLLUTION USING CALIOP OBSERVATIONS	79
VI. TEMPORAL VARIABILITY OF AEROSOL OPTICAL THICKNESS VERTICAL DISTRIBUTION OBSERVED FROM CALIOP.....	107
VII. SUMMARY AND CONCLUSIONS.....	152
BIBLIOGRAPHY.....	156

LIST OF FIGURES

Figure	Page
1. For the period 2008-2009, U.S. Environmental Protection Agency (EPA) sites with available PM _{2.5} measurements at (a) hourly and (b) daily intervals, respectively. The sites are colored-coded based on number of days with observations, as red (fewer than 100), black (between 100 and 300), or blue (greater than 300).....	21
2. Two-year (2008-2009) scatterplots of operational Terra MODIS (in light blue) and MISR (in red) AOT, averaged within 40 km of each respective PM _{2.5} -monitoring site, versus hourly PM _{2.5} concentrations for the (a) Eastern and (b) Pacific U.S. time zones. Also plotted are averages of PM _{2.5} for each 0.1 AOT bin, represented with triangles (in dark blue) for Terra MODIS and squares (in orange) for MISR. Error bars (+/- 1 standard deviation) for the bin averages are also shown.....	24
3. Two-year (2008-2009) scatterplots of daily 1° x 1° DA Terra MODIS (in light blue) and daily 1° x 1° MISR (in red) AOT versus daily PM _{2.5} concentrations for the (a) Eastern and (b) Pacific U.S. time zones. Averages of PM _{2.5} are plotted for each 0.1 AOT bin, represented with triangles (in dark blue) for Terra MODIS and squares (in orange) for MISR. Error bars (+/- 1 standard deviation) for the bin averages are also shown.....	27
4. For the period 2008-2009, the U.S. Environmental Protection Agency (EPA) daily PM _{2.5} sites used in this study. Sites are color-coded based on the correlation between daily PM _{2.5} observations and daily 1° x 1° (a) operational and (b) DA Terra MODIS AOT.....	29
5. For the period 2008-2009, the U.S. Environmental Protection Agency (EPA) daily PM _{2.5} sites used in this study. Sites are color-coded based on the correlation between daily PM _{2.5} observations and daily 1° x 1° (a) operational and (b) DA MISR AOT.....	30
6. Two-year (2008-2009) 1° x 1° average CALIOP 0.532 μm extinction, relative to the number of cloud-free 5 km CALIOP profiles in each 1° x 1° bin, for atmospheric layers a.g.l. of (a) 0-500 m, (b) 500-1500 m, (c) 1500-2500 m, and (d) 2500-3500 m.....	33

7. Two-year (2008-2009) 1° x 1° average contribution percentage of 0 to 500 m a.g.l. integrated CALIOP extinction to total column AOT (at 0.532 μm) relative to the number of cloud-free CALIOP profiles in each 1° x 1° bin, for the contiguous United States.....	34
8. From 2006 to 2011, fraction of CALIOP-integrated 0.532 μm extinction below 500 m a.g.l. for the contiguous United States.....	35
9. Two-year (2008-2009) 1° x 1° average (a) contribution percentage of above 2 km a.g.l. CALIOP AOT to total column AOT (at 0.532 μm) and (b) frequency of occurrence of AOT above 2 km a.g.l., both relative to the number of cloud-free CALIOP profiles in each 1° x 1° bin, for the contiguous United States.....	36
10. For the Eastern (in blue) and Pacific (in red) U.S. Time zones, two-year (2008-2009) scatterplots of hourly PM _{2.5} concentrations versus (a) cloud-free 5 km CALIOP dry mass 0.532 μm extinction at the 200-300 m a.g.l. layer, and (b) operational Aqua MODIS AOT, both averaged within 40 km and the hour of each respective PM _{2.5} measurement.....	39
11. For the Eastern (blue) and Pacific (red) U.S. Time zones, two-year (2008-2009) scatterplots of daily PM _{2.5} concentrations versus (a) cloud-free 5 km CALIOP dry mass 0.532 μm extinction at the 200-300 m a.g.l. layer (averaged within 100 km), and (b) operational Aqua MODIS AOT (averaged within 1°) and the day of each respective PM _{2.5} measurement.....	41
12. For data collected during daytime on July 2 nd , 2010 over the Arctic, browse image curtain plots of CALIPSO (a) 532 nm total attenuated backscatter (km ⁻¹ sr ⁻¹) and (b) corresponding vertical feature mask (VFM). The white box represents an example segment of the granule for which range bins in the associated Level 2 (L2) aerosol extinction coefficient profile are all retrieval fill values (RFVs), as the VFM classified these bins as either surface (green) or clear air (blue) features. The white arrow indicates a column in which some aerosol has been detected (orange), and the resultant L2 aerosol extinction profile for this column is shown in (c).....	53
13. For February 2008, mean profiles of (a, c) Level 1.5 total attenuated backscatter (TAB) and (b, d) attenuated scattering ratio (TAB/molecular attenuated backscatter) over global oceans, corresponding to Level 2 all-RFV (in blue) and non-all-RFV (AOT > 0; in red) profiles. The left column is from an analysis of all cloud-free CALIOP points over global oceans and the right column represents only those collocated with MODIS AOTs between 0.03 and 0.07.....	55

14. For 2010-2011, (a) the frequency of occurrence (%) of cloud-free CALIOP profiles at 2° x 5° latitude/longitude grid spacing. Also shown are the corresponding cloud-free mean CALIOP column AOTs (b) without and (c) with all-RFV profiles, and (d) the ratio of (b) to (c).....	59
15. For 2010-2011, histograms of all over-ocean cloud-free CALIOP profiles (in green) and all-RFV profiles (in purple) as a function of collocated Aqua MODIS AOT (0.01 bins), for (a) 30° to 60° N, (b) -30° to 30° N, and (c) -60° to -30° N.....	61
16. For 2010-2011, (a) frequency of occurrence (%) of valid (“Good” or “Very Good”) over-ocean Level 2 (L2) MODIS AOT retrievals, relative to all over-ocean L2 MODIS AOT retrievals, for every 2° x 5° latitude/longitude grid box. Also shown is (b) the corresponding spatial distribution of mean L2 MODIS AOT for the same time period. This analysis includes only those MODIS points collocated with CALIOP.....	62
17. 2010-2011 frequency of occurrence (%) of over-ocean cloud-free CALIOP all-RFV profiles, relative to all cloud-free CALIOP profiles, as a function of collocated Aqua MODIS AOT (0.01 bins), for 30° to 60° N (in red), -30° to 30° N (in blue), and -60° to -30° N (in black).....	65
18. Map of the ninety-three coastal/island AERONET sites with Level 2.0 data, for the 2007-2008 and 2010-2011 periods, used for collocation with over-ocean CALIOP aerosol observations.....	66
19. For the 2007-2008 and 2010-2011 periods, (a) histograms of all cloud-free CALIOP profiles (in green) and all-RFV profiles (in purple), and (b) corresponding frequency of occurrence (%) of cloud-free CALIOP all-RFV profiles, relative to all cloud-free CALIOP profiles, both as a function of collocated coastal/island AERONET AOT (0.01 bins).....	68
20. For February 2008 over cloud-free global oceans, the all-RFV aerosol extinction coefficient profiles derived from the inversion algorithm. The black curve represents all cloud-free CALIOP profiles over global oceans, while the green curve is from an analysis restricted to only those CALIOP points collocated with MODIS AOTs between 0.03 and 0.07.....	71
21. For 2008-2009, scatterplot of mean PM _{2.5} concentration from ground-based U.S. EPA stations and mean column AOT (550 nm) from collocated Collection 6 (C6) Aqua MODIS observations.....	80

22. For 2008-2009 over the CONUS, (a) mean PM _{2.5} concentration ($\mu\text{g m}^{-3}$) for those U.S. EPA stations with reported daily measurements, and (c) $1^\circ \times 1^\circ$ average CALIOP-derived PM _{2.5} concentrations for the 100–1000 m AGL atmospheric layer, using Equation 3, for combined daytime and nighttime conditions. Also shown are the pairwise PM _{2.5} concentrations from (b) EPA daily measurements and (d) those derived from CALIOP (day and night combined), both averaged for each EPA station for the 2008-2009 period. For all four plots, values greater than $20 \mu\text{g m}^{-3}$ are colored red.....	87
23. For 2008-2009 over the CONUS, $1^\circ \times 1^\circ$ average CALIOP extinction, relative to the number of cloud-free 5 km CALIOP profiles in each $1^\circ \times 1^\circ$ bin, for the 100 – 1000 m AGL atmospheric layer, for (a) daytime and (b) nighttime measurements. Also shown are the corresponding CALIOP-derived PM _{2.5} concentrations, using Equation 3 for (c) daytime and (d) nighttime conditions. Values greater than 0.2 km^{-1} and $20 \mu\text{g m}^{-3}$ for (a, b) and (c, d), respectively, are colored red. Scatterplots of mean PM _{2.5} concentration from ground-based U.S. EPA stations and those derived from collocated near-surface CALIOP observations are shown in the bottom row, using (e) daytime and (f) nighttime CALIOP data.....	90
24. Scatterplot of mean PM _{2.5} concentration from ground-based U.S. EPA stations and those derived from collocated near-surface CALIOP observations using combined daytime and nighttime CALIOP data.....	92
25. Root-mean-square errors of CALIOP-derived PM _{2.5} against EPA PM _{2.5} as a function of CALIOP-derived PM _{2.5} using both daytime (in red) and nighttime (in blue) CALIOP observations.....	94
26. Two-year (2008-2009) histograms of mean PM _{2.5} concentrations from the U.S. EPA (in black) and those derived from aerosol extinction using nighttime (in blue) and daytime (in red) CALIOP data. The U.S. EPA data shown are not collocated, while those derived using CALIOP are spatially (but not temporally) collocated, with EPA station observations.....	96
27. Two-year (2008-2009) histograms of mean PM _{2.5} concentrations from the U.S. EPA and those derived from spatially and temporally collocated aerosol extinction using (a) daytime and (b) nighttime CALIOP data.....	97
28. For 2008-2009, scatterplots of mean PM _{2.5} concentration from ground-based U.S. EPA stations and mean column AOT from collocated CALIOP observations, using (a) daytime and (b) nighttime CALIOP data.....	98

29. Two-year (2008-2009) scatterplots of mean $PM_{2.5}$ concentration from ground-based U.S. EPA stations and those derived from collocated near-surface CALIOP observations as a function of CALIOP-based backscatter color ratio (1064 nm/532 nm; χ). The results are separated by the median of the χ distribution, i.e., the left (right) column for χ less than or equal to (greater than) the median of each subset. Daytime analyses (a, b) are shown on the top row and nighttime analyses (c, d) are shown in the bottom row. The green circle in (a) represents an outlier and was not included in the computation of the slope.....	100
30. Two-year (2008-2009) scatterplots of mean $PM_{2.5}$ concentration from ground-based U.S. EPA stations and those derived from collocated near-surface CALIOP observations as a function of CALIOP aerosol type. The polluted continental/smoke (polluted dust) analyses are shown in the left (right) column. Daytime analyses (a, b) are shown on the top row and nighttime analyses (c, d) are shown in the bottom row.....	102
31. Two-year (2008-2009) scatterplot of mean $PM_{2.5}$ concentration from ground-based U.S. EPA stations and those derived from collocated daytime near-surface CALIOP observations for the dust CALIOP aerosol type.....	103
32. Vertical profiles of total number of valid CALIOP AOT observations for June 2006 through December 2014 for the daytime (in red) and nighttime (in blue) analyses.....	116
33. For September 2006 over global oceans, average profiles of 0.532 μm extinction coefficient from the all-sky CALIPSO Version 3.0 Level 3.0 Aerosol Profile Product (in red; CAL_LID_L3_APro_AllSky-Standard-V3-00) and the Level 3.0 dataset derived for this study (in black) for (a) daytime and (b) nighttime.....	118
34. From June 2006 to December 2014, daytime and nighttime mean total-column CALIOP AOT for (a, c) December through May and (b, d) June through November, at $2^\circ \times 5^\circ$ (latitude/longitude) resolution. (e, f) Corresponding $2^\circ \times 5^\circ$ (latitude/longitude) daytime minus nighttime AOTs for each seasonal period are also shown.....	121
35. From June 2006 to December 2014, layer mean CALIOP AOT for (a, e) 0.0 – 0.5 km, (b, f) 0.5 – 1.0 km, (c, g) 1.0 – 2.0 km, and (d, h) > 2.0 km above ground level (AGL), at $2^\circ \times 5^\circ$ (latitude/longitude) resolution. Daytime analyses are shown in Figs. 35a-35d, with nighttime analyses in Figs. 35e-35h.....	122

36. Time series of monthly mean AERONET AOT (interpolated to 0.532 μm) and the corresponding deseasonalized AOT anomalies at (a, c) Amsterdam Island (37.8° S, 77.5° E; January 2007 – December 2013) and (b, d) Midway Island (28.2° N, 177.4° W; June 2006 – December 2014). The time series of monthly mean 2° x 5° (latitude/longitude) daytime CALIOP AOT (0.532 μm) and the corresponding deseasonalized AOT anomalies for the closest grid box to each site is also shown. The trend (ω) and corresponding uncertainty (σ) for each time series are also included.....	125
37. From June 2006 to December 2014, the standard deviation (STDDEV) of monthly mean CALIOP total-column AOT for the closest 2° x 5° (latitude/longitude) grid box to (a, c) Amsterdam Island (37.8° S, 77.5° E) and (b, d) Midway Island (28.2° N, 177.4° W). Daytime analyses are shown in the left column, with nighttime analyses in the right column. The trends (STDDEV/year) of each dataset are also shown.....	126
38. June 2006 to December 2014 monthly global mean CALIOP AOT, and corresponding deseasonalized AOT anomalies, for the total-column and each layer for (a, c) daytime and (b, d) nighttime.....	127
39. For the June 2006 to December 2014 period, monthly mean CALIOP AOT for the total-column and each of the four layers for global (a, b) land and (c, d) oceans. Daytime analyses are shown in Figs. 39a and 39c, with nighttime analyses in Figs. 39b and 39d.....	130
40. For June 2006 to December 2014, daytime and nighttime trends per year of the de-seasonalized monthly mean CALIOP AOT for the total-column and each of the four layers for global (a) land and (b) oceans.....	131
41. From June 2006 to December 2014, trends (AOT per year) of the de-seasonalized monthly mean total-column CALIOP AOT for every 2° x 5° (latitude/longitude) for (a) daytime and (b) nighttime.....	136
42. From June 2006 to December 2014, trends (AOT per year) of the de-seasonalized monthly mean layer CALIOP AOT for (a, e) 0.0 - 0.5 km, (b, f) 0.5 – 1.0 km, (c, g) 1.0 – 2.0 km, and (d, h) > 2.0 km for every 2° x 5° (latitude/longitude). Daytime analyses are shown in Figs. 42a-42d, with nighttime analyses in Figures 42e-42h.....	139
43. For June 2006 to December 2014, trends (AOT per year) of the de-seasonalized monthly mean CALIOP AOT for the total-column and each of the four layers for the globe and each region for (a) daytime and (b) nighttime. The ten regions presented are Western U.S. (WUS), Eastern U.S. (EUS), South America (SAM), Northern Africa (NAF), Southern Africa (SAF), Europe (EUR), the Middle East (ME), India (INDIA), Eastern China (ECHINA), and Indonesia (INDO).....	140

44. For June 2006 to December 2014, global total-column/layer trends (AOT per year) of the de-seasonalized monthly mean CALIOP AOT from the analysis shown in Fig. 43 and two sensitivity studies for (a) daytime and (b) nighttime. See the text for details of each sensitivity study.....142

45. For June 2006 to December 2014, (a, b) mean total-column daytime AOT and (c, d) trends (AOT per year) of the de-seasonalized monthly mean total-column daytime AOT at 2° x 5° (latitude/longitude) resolution, from the collocated Collection 6 (C6) Aqua MODIS (Figs. 45a and 45c) and CALIOP (Figs. 45b and 45d) analyses.....144

46. For June 2006 to December 2014, global and regional trends (AOT per year) of the de-seasonalized monthly mean daytime AOT for the total-column and each layer from the collocated Collection 6 (C6) Aqua MODIS/CALIOP analysis. The ten regions presented are Western U.S. (WUS), Eastern U.S. (EUS), South America (SAM), Northern Africa (NAF), Southern Africa (SAF), Europe (EUR), the Middle East (ME), India (INDIA), Eastern China (ECHINA), and Indonesia (INDO).....146

LIST OF TABLES

Table	Page
1. Correlation coefficients and data counts of the 40 km average operational Aqua/Terra MODIS and MISR AOT/hourly PM _{2.5} collocation analyses for the Eastern, Central, Mountain, and Pacific time zones and contiguous United States total for the entire two-year (2008-2009) study period, December through May 2008-2009 (DJFMAM), and June through November 2008-2009 (JJASON).....	22
2. Correlation coefficients and data counts of the daily 1° x 1° average operational/DA Aqua/Terra MODIS and MISR AOT/daily PM _{2.5} collocation analyses for the Eastern, Central, Mountain, and Pacific time zones and contiguous United States total for the entire two-year (2008-2009) study period, December through May 2008-2009 (DJFMAM), and June through November 2008-2009 (JJASON).....	26
3. Correlation coefficients and data counts for the hourly PM _{2.5} /40 km average operational AOT and daily PM _{2.5} /1° x 1° average DA AOT common point analyses for the Eastern, Central, Mountain, and Pacific time zones and contiguous United States total for the two-year (2008-2009) study period.....	31
4. Correlation coefficients and data counts for the hourly PM _{2.5} /average AERONET AOT (0.670 μm) collocation analysis (AERONET AOT averaged within the hour and 0.3° latitude/longitude of an hourly PM _{2.5} measurement) for the Eastern, Central, Mountain, and Pacific time zones and contiguous United States total for the two-year (2008-2009) study period.....	31
5. Two-year (2008-2009) correlation coefficients of hourly PM _{2.5} observations and 40 km average CALIOP extinction (both uncorrected and dry mass) at various 100 m a.g.l. atmospheric layers.....	38
6. Statistical summary of the results for this study, for the 2007-2008 and 2010-2011 periods, both globally and for global oceans only. The values in bold and parentheses represent the percentages of each category relative to the entire CALIOP aerosol profile archive for each respective period.....	58

7. Mean, median, and standard deviation of AOTs derived from Aqua MODIS (2010-2011) and AERONET (2007-2008; 2010-2011), both independently collocated with CALIOP all-RFV profiles.....	63
8. For February 2008 over cloud-free global oceans, the mean and standard deviation of collocated CALIOP and MODIS AOTs for various scenarios related to the treatment of non-all-RFV and all-RFV CALIOP aerosol profiles. For those scenarios that involve correction, [1] refers to analyses including all cloud-free CALIOP profiles over global oceans, while [2] refers to analyses restricted to CALIOP points collocated with MODIS AOTs of 0.03 to 0.07. The corresponding aerosol extinction profiles used for RFV correction are shown in Fig. 20. Key results are highlighted in yellow.....	72
9. All-RFV CALIOP occurrence frequencies for two months (January and February 2008) from various analyses using daytime and nighttime data, as well as their corresponding absolute differences.....	73
10. The QA metrics implemented to construct the CALIOP aerosol extinction profiles. The Integrated_Attenuated_Backscatter_532 (L2_05kmALay product) threshold is checked for each aerosol layer within a 5 km CALIOP column, while all other parameters (L2_05kmAProf product) are a function of range within the aerosol profile. Also shown are the values used for construction of aerosol extinction profiles for the official Level 3.0 aerosol profile product (CAL_LID_L3_APro). See Winker et al. (2013) for details on the implementation of these metrics.....	113
11. For both daytime and nighttime analyses, and for each region, the signs of the total-column trend (AOT per year) from the linear least-squares fitting (LSF) method. Red indicates a positive trend and blue represents a negative trend. Those trends that are significant at the 90% confidence interval or greater, as determined by the Mann-Kendall (MK) test, are indicated. Also shown for each region are the altitudes of largest AOT and those of the primary contributor to the total-column trend.....	123
12. For the globe and selected regions, daytime and nighttime trends (AOT per 8.58 years) for the total-column and each layer. Trends computed from both the linear least-squares fitting (LSF) and Sen's slope (SS; Sen, 1968) methods are shown. Bold values indicate trends that are significant at the 90% confidence interval or greater, as determined by the Mann-Kendall test.....	129
13. Trends (AOT per year) for selected regions from Terra MODIS/MISR (Zhang and Reid, 2010), SeaWiFS (Hsu et al., 2012), and AERONET (Li et al., 2014b) observations. Also shown are daytime total-column trend from CALIOP aerosol profile observations. The number in parentheses for the Terra MODIS/MISR and SeaWiFS columns represents the CALIOP total-column trends using the latitude/longitude boundaries defined by each passive-based study.....	134

ACKNOWLEDGEMENTS

I wish to express my sincere gratitude to my adviser, Dr. Jianglong Zhang, for his continual guidance and support throughout the course of my doctoral program. He has taught me many lessons on how to conduct a thorough scientific investigation and report results in peer-reviewed journal articles, and has helped me to become an independent researcher. I also thank the members of my doctoral committee with expertise in lidar remote sensing, Dr. James Campbell and Mark Vaughan. They have provided invaluable guidance and help with the research topics of this dissertation. I also thank the other members of my doctoral committee, Drs. Cedric Grainger, Xiquan Dong, and Xiaodong Zhang for their comments and guidance in improving this work.

Thank you to all of my family and friends for their encouragement, love, and support. Also, thank you to all of the graduate students in the Atmospheric Sciences Department, especially those in my research group, for the fun times during my graduate school experience. Special thanks to the researchers I have had the privilege of collaborating with throughout my PhD studies, including Drs. Jeffrey Reid, Edward Hyer, Doug Westphal, and Yingxi Shi, as well as Jason Tackett and Jared Marquis. Mark Vaughan and John Hair, along with the remainder of the CALIPSO and HSRL teams at NASA Langley Research Center, are also thanked for the guidance and support they provided me during the summers I spent as a NASA Pathways intern throughout my doctoral program.

This research was funded by the NASA Earth and Space Science Fellowship

program, as well as the Office of Naval Research Code 322 and contract N00014-16-1-2040 (grant 11843919), NASA grants NNX14AJ13G and NNX17AG52G, and the NASA Interdisciplinary Science Program. CALIPSO and MISR data were obtained from the NASA Langley Research Center Atmospheric Science Data Center. MODIS data were obtained from NASA Goddard Space Flight Center. The DA-quality MODIS data were obtained from the Global Ocean Data Assimilation Experiment (GODAE) server. The PM_{2.5} data were obtained from the EPA AQS site. The AERONET program and their contributing principal investigators and their staff are acknowledged and appreciated for establishing and maintaining the AERONET sites used in this investigation.

ABSTRACT

Particulate matter with aerodynamic diameters smaller than $2.5\ \mu\text{m}$ ($\text{PM}_{2.5}$) contributes greatly to air pollution and poses significant threats to human health. Space-borne passive aerosol measurements, with their large spatial coverage, have been applied for estimating surface-based $\text{PM}_{2.5}$ concentrations. Specifically, column-integrated aerosol optical thickness (AOT) observations, like those from the National Aeronautics and Space Administration (NASA) Moderate Resolution Imaging Spectroradiometer (MODIS) and Multi-angle Imaging Spectroradiometer (MISR) instruments, have been leveraged for this task. In this doctoral research study, the issues and limitations with estimating $\text{PM}_{2.5}$ from passively-retrieved MODIS and MISR AOT over the contiguous United States (CONUS) were first explored. Second, the potential of using active space-borne NASA Cloud-Aerosol Lidar with Orthogonal Polarization (CALIOP) near-surface aerosol extinction retrievals for $\text{PM}_{2.5}$ estimation is studied. This includes exploration of various factors that affect CALIOP aerosol data processing, including the retrieval fill value (RFV) issue that results from CALIOP minimum aerosol detection limits. Next, an innovative approach for deriving $\text{PM}_{2.5}$ concentrations directly from CALIOP near-surface aerosol extinction data has been explored using a bulk-mass-modeling-based method, and were validated against in situ $\text{PM}_{2.5}$ from U.S. Environmental Protection Agency (EPA) ground stations. Lastly, temporal variations of CALIOP-based aerosol vertical distribution, including trends of near-surface aerosol loading, were examined globally and regionally to infer possible changes in surface air quality.

CHAPTER I

INTRODUCTION

Aerosols are tiny solid and/or liquid particles suspended in a gas. In Earth's atmosphere, aerosols are very heterogeneous temporally and spatially due to their short residence times and strong dependence of local sources. Atmospheric aerosols exhibit both natural and anthropogenic origins, with types including sea spray, desert dust, biomass burning (smoke), sulfates, and volcanic emissions (e.g., Boucher, 2015). As an important component of the climate system, aerosols impact the radiation budget of Earth by scattering and absorbing solar radiation (i.e., the aerosol direct effect), as well as influence the formation of clouds in the atmosphere (i.e., the aerosol indirect effect; e.g., Kaufman et al., 2002). Additionally, aerosols contribute to atmospheric pollution, and thus degrade air quality (AQ) and pose a threat to human health (e.g., Schwartz and Neas, 2000; Pope et al., 2002).

Of specific concern for health are aerosols, or particulate matter (PM), with aerodynamic diameters smaller than $2.5\ \mu\text{m}$ ($\text{PM}_{2.5}$). These particulates are small enough to be carried into the lungs, and can lead to millions of premature deaths each year (e.g., Silva et al., 2013; Fuzzi et al., 2015). Thus, governments across the globe have instituted PM measurements as standard metrics for characterizing AQ in their respective countries. In the United States (U.S.), the Environmental Protection Agency (EPA) has monitored PM concentrations using in situ instruments at ground stations since the passage of the Clean Air Act in 1970 (Greenstone, 2002). Research conducted after this time confirmed

the harmful effects of $PM_{2.5}$, leading to the U.S. EPA increasing its effort to monitor, and set strict limits on, $PM_{2.5}$ concentrations in 1997 (Federal Register, 1997).

Due to the high cost of maintaining EPA ground stations and their lack of spatial coverage over portions of the U.S., alternative methods of monitoring $PM_{2.5}$ have been investigated. For example, a number of studies have attempted estimates of surface-based $PM_{2.5}$ through linear regression analyses using satellite-derived aerosol optical thickness (AOT; an indicator of aerosol concentration in the atmosphere) from passive imaging radiometric sensors (e.g., Wang and Christopher, 2003; Engel-Cox et al., 2004; Kumar et al., 2007; Liu et al., 2007; Hutchison et al., 2008; Hoff and Christopher, 2009). Examples of such sensors are the National Aeronautics and Space Administration (NASA) Moderate Resolution Imaging Spectroradiometer (MODIS) and Multi-angle Imaging Spectroradiometer (MISR). Large ranges in $PM_{2.5}$ /AOT correlations have been found, with impacts from environmental parameters (e.g., relative humidity; Shinozuka et al. 2007) and the spatial (i.e., for a particular EPA site versus a regional or national analysis) and temporal (i.e., hourly/daily versus seasonally/annually) scopes of the comparisons. Still, the primary advantage of estimating surface $PM_{2.5}$ using satellite AOT is that satellites provide larger spatial coverage than what can be inferred from ground stations.

There are important issues, however, that need to be considered prior to applying satellite-based AOT data as a proxy for $PM_{2.5}$. For one, since AOT derived from passive sensors is a column-integrated value and $PM_{2.5}$ concentration is a surface measurement, the AOT/ $PM_{2.5}$ relationship could be affected by the representativeness of surface aerosol particle presence to that of the entire column (i.e., AOT). To help mitigate this issue, airborne and ground-based lidars, which provide information on aerosol vertical

distribution, have been used to investigate the relationship between column-integrated AOT and surface-based $\text{PM}_{2.5}$ through meteorological parameters such as mixed layer height (e.g., Engel-Cox et al., 2006; Gupta et al., 2006; Shinozuka et al. 2007; Boyouk et al., 2010; Chu et al., 2013). Additionally, chemical transport models (CTMs) have been used to simulate aerosol vertical structure, also to help mitigate the surface-to-column aerosol representativeness issue (e.g., Liu et al., 2004; Van Donkelaar et al., 2006; 2010; Hyer and Chew, 2010). The primary focus and intent of these lidar- and CTM- based studies is still, however, to simply improve the $\text{PM}_{2.5}/\text{AOT}$ relationship. Also note that AOT is a unitless parameter and $\text{PM}_{2.5}$ is in the units of $\mu\text{g}/\text{m}^3$. Thus, the $\text{PM}_{2.5}/\text{AOT}$ relationship is essentially a non-physical-based relationship.

Another issue that warrants attention is the quality of the satellite-based passive aerosol data that are employed for AQ and $\text{PM}_{2.5}$ applications. For example, uncertainties exist in satellite-retrieved passively-sensed AOT (e.g., from MODIS and MISR) values due to cloud contamination, inaccurate optical models used in the retrieval process, and heterogeneous surface boundary conditions (e.g., Zhang and Reid, 2006; Shi et al., 2011a; Toth et al., 2013). The impact of suppressing these uncertainties (i.e., increasing AOT data quality through cloud screening, snow filter, and corrections for albedo and regional slope bias) on the $\text{AOT}/\text{PM}_{2.5}$ relationship has yet to be investigated.

While progress has been made in studying surface $\text{PM}_{2.5}$ through passive AOT retrievals, the advancement of this topic is fundamentally limited because passive sensors provide only total-column aerosol observations. In contrast, the space-based active NASA Cloud-Aerosol Lidar with Orthogonal Polarization (CALIOP) instrument provides unique range-resolved measurements of aerosol optical properties near the ground (where we care about $\text{PM}_{2.5}$ pollution), and is not limited to the AOT perspective of passive sensors.

Therefore, in this doctoral research, for the first time, the feasibility of using CALIOP near-surface aerosol extinction to directly derive $\text{PM}_{2.5}$ concentrations is examined from a semi-physical-based method, based upon the long-established relationship between light scattering and aerosol mass concentration (e.g., Charlson et al., 1968). The advantage of this method is that $\text{PM}_{2.5}$ concentration can be estimated semi-physically from CALIOP aerosol extinction values with the use of bulk mass extinction efficiencies, rather than a proxy relationship as shown in the $\text{PM}_{2.5}/\text{AOT}$ studies.

However, several issues with CALIOP aerosol data first need to be accounted for before their use in AQ studies. For example, uncertainties exist in aerosol extinction retrievals, mainly due to the extinction-to-backscatter ratio (lidar ratio) and calibration-related issues (Young et al., 2013). Thus, a range of quality assurance (QA) parameters and procedures for the CALIOP Level 2 (L2) aerosol extinction product must be applied, and these choices may impact the derived aerosol extinction coefficient profile. Also, in CALIOP L2 data analysis, range bins with signals below the noise floor are often set to retrieval fill values (RFVs). Different approaches have been adopted in the community for processing range bins with RFVs, which can impact estimates of mean near-surface extinction, thus requiring careful consideration. Additionally, CALIOP exhibits sparse spatial (~ 70 m swath) and temporal (repeat cycle of ~ 16 days) sampling (Winker et al., 2009), and thus sampling-related biases in using CALIOP aerosol observations for $\text{PM}_{2.5}$ studies requires investigation.

Lastly, one application of aerosol-extinction-derived $\text{PM}_{2.5}$ concentrations is assessment of trends in $\text{PM}_{2.5}$ near the surface. As stated in the 2017-2027 Decadal Survey, long-term AQ trends are an important priority for the next decade (National Academies of Sciences, Engineering, and Medicine, 2018). While past studies have looked at trends of

column-integrated aerosol concentrations (i.e., AOT) from passive sensors (e.g., Mishchenko et al., 2007; Zhang and Reid, 2010; Li et al., 2014a), trends in aerosol vertical distribution have not been thoroughly explored. As a lidar, CALIOP can be leveraged for this task, with the capability of determining trends in aerosol layers nearest the surface, the segment of the atmospheric profile in which we are concerned about PM_{2.5} pollution.

Therefore, this doctoral dissertation research aims to increase the current understanding of aerosol extinction and optical thickness data derived from CALIOP for AQ applications. Through the use of active and passive remotely-sensed aerosol data, and in situ PM_{2.5} observations, the following research topics and questions are explored:

1. How does the quality of passive satellite AOT retrievals impact their relationship with PM_{2.5}?
2. How representative are surface-based measurements to aerosol particle presence within the full atmospheric column as observed by CALIOP?
3. What issues should be considered when working with CALIOP aerosol data, particularly the impact of undetectable aerosol in an atmospheric profile (the RFV issue)?
4. Through a bulk-mass-modeling-based method, can near-surface CALIOP-derived aerosol extinction be directly used for estimating surface PM_{2.5} concentrations from a 2-year mean perspective?
5. What are the temporal variations of CALIOP-based aerosol vertical distribution, especially those of near-surface aerosol loading?

This dissertation is comprised of seven chapters. In Chapter II, the datasets used in this research are discussed. Chapter III focuses on the first two questions, while the third question is explored in Chapter IV. The findings of the study concerning the fourth

question are shown in Chapter V, and Chapter VI highlights the answers to the fifth question. The overall results of this dissertation are summarized in Chapter VII.

CHAPTER II

DATASETS

The topics of this research are explored through a variety of ground-based and satellite remotely-sensed data. These measurements can be broadly categorized as either active (i.e., using energy from the instrument) or passive (i.e., using naturally available energy). The active analyses include those of the CALIOP instrument, while the passive remote sensors are comprised of MODIS, MISR, and AERONET sun photometers. Additionally, filter and laser-based instruments provide in situ concentrations of surface-based PM_{2.5}. The active and passive datasets are employed synergistically, along with the PM_{2.5} datasets, to accomplish the research tasks of this dissertation. In this section, overviews of each instrument/dataset and their overall operating principles are provided. Due to different versions and collections of data available throughout the course of this doctoral study, various products and parameters were used. Therefore, each chapter contains its own description of the specific products used for each respective study.

2.1 CALIOP

The Cloud-Aerosol Lidar with Orthogonal Polarization (CALIOP) is a multi-wavelength (0.532 and 1.064 μm) elastic backscatter polarization lidar flown aboard the Cloud-Aerosol Lidar and Infrared Pathfinder Satellite Observations (CALIPSO) platform within the NASA “A-Train” constellation (Stephens et al., 2002). Since June 2006, CALIOP has provided global range-resolved measurements of the vertical distribution of

aerosols and clouds in the atmosphere. The Level 2 CALIOP aerosol retrieval is comprised of several advanced algorithms, and includes the following general steps. First, a feature detection scheme is implemented to locate areas of the CALIOP profile with backscatter greater than the expected background molecular signal (Young and Vaughan, 2009). Next, features are classified as aerosols or clouds (and corresponding subtypes) using the cloud and aerosol discrimination (CAD) algorithm (Liu et al., 2009). Lastly, an extinction retrieval is performed during which aerosol backscatter is obtained through inversion of the lidar equation, after which aerosol extinction is derived using an assumed lidar ratio (extinction-to-backscatter ratio) based on aerosol type (Omar et al., 2009; Young and Vaughan, 2009). Integrating the retrieved aerosol extinction profiles results in column AOT.

For this work, Level 2 datasets are primarily used (Winker et al. 2007), including the aerosol profile (L2_05kmAProf) and aerosol layer (L2_05kmALay) products. Both feature a horizontal resolution of 5 km, with the L2_05kmAProf product exhibiting a 60 m vertical resolution. The L2_05kmALay product provides vertical information for up to 8 aerosol layers. Additionally, the L2 vertical feature mask (L2_VFM) product is used to determine feature classification (i.e., aerosol vs. cloud), with both its vertical and horizontal resolutions dependent upon altitude. The CALIPSO Level 1.5 (CAL_LID_L15) and Level 3 aerosol profile (CAL_LID_L3) products are also used for a few supplemental analyses throughout this work. Uncertainties in CALIOP-derived AOTs are large, mainly due to the assumption of the lidar ratio during the aerosol retrieval process. Past studies report CALIOP AOTs agree within 13-25% of AOTs from AERONET (Schuster et al., 2012; Omar et al., 2013) and within 63% of AOTs from MODIS (Kim et al., 2013). Most of this

work utilizes Version 3 CALIOP data, while Version 4 products will be used for some parts of the dissertation.

2.2 MODIS

Aboard both the NASA Aqua and Terra satellites, the Moderate Resolution Imaging Spectroradiometer (MODIS) is a spectroradiometer with 36 channels (0.41 to 15 μm), seven of which (0.47 to 2.13 μm) are applied for the operational retrieval of aerosol particle optical properties (Remer et al., 2005). The general MODIS aerosol retrieval is a complex process, and involves different algorithms concerning surface characteristics and the atmospheric aerosols found above these surfaces. For example, the Dark Target (DT) algorithm is implemented for vegetated land and oceans. First, the surface type is determined, after which bad pixels are filtered out (e.g., contamination by clouds, snow/ice, etc.). Corrections are then completed for atmospheric gaseous absorption (e.g., ozone and water vapor). From what remains, the mean top-of-atmosphere (TOA) reflectance from MODIS is matched with reflectances computed from a radiative transfer model through a look up table (LUT) approach. The model computes reflectances for each of the seven wavelengths using predetermined aerosol models that assume particular aerosol size distributions. AOT is then derived using the calculated aerosol extinction coefficients from the radiative transfer model (Levy et al., 2013).

This study utilizes Collections 5 and 6 (C5 and C6) Level 2 DT AOT data (at 0.550 μm) from both the Aqua (MYD04_L2) and Terra (MOD04_L2) satellites. Both products are reported at a spatial resolution of 10 x 10 km, with C5 uncertainties of $0.05 \pm 0.15 \cdot \text{AOT}$ over-land and $0.03 \pm 0.05 \cdot \text{AOT}$ over-ocean (Remer et al., 2005). The reported expected error of C6 over-ocean AOTs is (-0.02 - 10%), (+0.04 + 10%) (Levy et al., 2013).

2.3 MISR

Aboard the Terra satellite, the Multiangle Imaging Spectroradiometer (MISR) is a unique spectroradiometer able to collect observations at nine different viewing angles, providing a means for studying aerosol particle size and shape (Diner et al., 1998). The instrument features four spectral bands (0.446, 0.558, 0.672, and 0.867 μm) and a swath width of 360 km. Different from the DT MODIS aerosol products, the MISR aerosol product also includes AOT retrievals over bright surfaces, like desert regions. Kahn et al., (2005; 2010) suggest that about 70% of MISR AOT data are within 0.05 (or 20%*AOT) of sun-photometer measured AOT values. The MISR AOT retrieval is based upon a LUT approach (similar to that of MODIS), that involves preprocessing (filtering out bad pixels, e.g., due to clouds), determination of surface type (i.e., land vs. water), and inversion of radiance observations (Martonchik et al., 1998). This study utilizes AOT derived from Version 22 (Level 2) MISR retrievals (at 0.558 μm ; spatial resolution of 17.6 km; Martonchik et al., 2009).

2.4 DA MODIS and MISR

Existing uncertainties in passive satellite AOT retrievals are optimally suppressed before application for data assimilation (DA) activities involving operational aerosol forecast models (e.g., Zhang et al., 2008). Through rigid QA (including cloud screening, snow filter, and albedo and regional slope bias corrections), reduced AOT uncertainties have been characterized and DA-quality AOT datasets have been created for both over-land (Hyer et al., 2011) and over-ocean MODIS DT products (Shi et al., 2011a), as well as MISR aerosol products (Shi et al., 2011c; 2012). Available at 6-hourly $1^\circ \times 1^\circ$ resolution, both DA-quality MODIS and MISR AOT products are used in this work.

2.5 AERONET

Developed for the purpose of furthering aerosol research and validating satellite retrievals, NASA's Aerosol Robotic Network (AERONET) program is a federated worldwide system of ground-based sun photometers that collect measurements of aerosol optical and radiative properties (Holben et al., 1998). To derive AOT from AERONET observations, the sun photometer first takes measurements in its direct sun scanning mode, during which the instrument points directly at the sun and measures solar radiation in 15 minute intervals. After consideration of the Rayleigh component of the measurement and correcting for gaseous absorption, AOT is then derived using Beer's Law (Holben et al., 1998). With a reported uncertainty of ± 0.01 - 0.02 , AOTs are derived at several wavelengths (0.34-1.64 μm ; Eck et al., 1999). Due to the lack of retrievals at the CALIOP wavelength, AOTs at 0.532 μm are computed from interpolation of those derived at the 0.5 and 0.675 μm channels using an Ångström relationship (e.g., Shi et al., 2011a; Toth et al., 2013), which is the dependency of AOT on wavelength. The highest quality AERONET data (L2.0) are used in this work, as these are both rigorously cloud-screened and quality-assured (Smirnov et al., 2000).

2.6 $\text{PM}_{2.5}$

The U.S. Environmental Protection Agency (EPA) has collected observations of surface-based particulate matter since the passage of the Clean Air Act in 1970 (Greenstone, 2002) and began specifically monitoring particulate matter less than 2.5 μm ($\text{PM}_{2.5}$) concentrations in 1997 (Federal Register, 2006). There are a few methods that can be used to obtain in situ PM mass concentrations. For one, the Federal Reference Method (FRM), a gravimetric method, is used to measure concentration over a continuous 24-hour

period. The filter is weighed prior to and after the sample collection interval, and $\text{PM}_{2.5}$ mass concentration (in units of $\mu\text{g}/\text{m}^3$) is calculated by division of the total mass of $\text{PM}_{2.5}$ particles by the volume of air sampled (Federal Register, 1997; Noble et al., 2001). Another method involves inertial mass measurement through the use of a Tapered Element Oscillating Microbalance (TEOM) monitor, for which PM mass concentration is determined by the reduction of the frequency of an oscillating filter due to the accumulation of particles (Amaral et al., 2015). Optical methods can also be employed to measure PM concentration, involving the scattering and absorption of radiation, via optical particle counters (OPCs) and beta gauge samplers (Park et al., 2001; Amaral et al., 2015). For this work, both daily and hourly $\text{PM}_{2.5}$ Local Conditions (EPA Parameter Code 88101) data are used, as these are collected from either FRM or Federal Equivalent Method (FEM) instruments and are subject to quality control/quality assurance (QC/QA) procedures.

CHAPTER III

IMPACT OF DATA QUALITY AND SURFACE-TO-COLUMN REPRESENTATIVENESS ON THE PM_{2.5}/SATELLITE AOT RELATIONSHIP FOR THE CONTIGUOUS UNITED STATES

3.1 Introduction

3.1.1 Rationale

As mentioned in Chapter I, past studies have used satellite-derived passive aerosol optical thickness (AOT) retrievals to infer concentrations of particulate matter (PM) with diameters smaller than 2.5 μm (PM_{2.5}) near the surface (e.g., Hoff and Christopher, 2009). One of the potential limitations of those studies, however, is the representativeness of column-integrated AOT values to surface PM_{2.5} concentrations. Therefore, as a first step for this doctoral study, this chapter explores the impact of this issue on the PM_{2.5}/AOT relationship.

3.1.2 Background

PM, especially PM_{2.5}, contributes greatly to regional air pollution and can pose a threat to human health (e.g., Schwartz and Neas, 2000; Pope et al., 2002). Traditionally, the U.S. EPA has monitored surface-based PM_{2.5} concentrations using either a gravimetric-based method at ground stations with 24-hour filter samplers or hourly Tapered Element Oscillating Microbalance (TEOM) and beta gauge samplers. (Federal Register, 1997). A number of studies have attempted estimates of surface-based PM_{2.5} concentrations using satellite-retrieved AOT data (e.g., Wang and Christopher, 2003; Engel-Cox et al., 2004; Kumar et al., 2007; Liu et al., 2007; Hutchison et al., 2008; Hoff and Christopher, 2009).

The advantages of estimating surface-based $PM_{2.5}$ concentrations using satellite-derived AOT data are obvious, as satellites, including both polar orbiting and geostationary satellites, typically provide a much larger spatial coverage than what can be inferred from ground stations over a broad surface footprint. However, data are limited to daylight cloud free conditions with once per day collection by polar orbiters (Diner et al., 1998; Remer et al., 2005) or multiple images in morning or afternoon from geostationary satellites (Zhang et al., 2001; Prados et al., 2007).

Previous research efforts have focused on algorithm development for solving PM proxies based on AOT. For example, Chu et al., (2003) compare PM with diameters smaller than $10\ \mu m$ (PM_{10}) concentrations with surface AOT measurements from the Aerosol Robotic Network (AERONET) in northern Italy and highlight the potential of using Moderate Resolution Imaging Spectroradiometer (MODIS; Remer et al., 2005) AOT as an estimate for PM_{10} concentration. Several studies have focused on correlating satellite AOT observations and $PM_{2.5}$ concentrations (e.g., Wang and Christopher, 2003; Liu et al., 2004), and advances have been made improving correlation between the two by considering other meteorological and environmental parameters, such as the surface mixed-layer height (Engel-Cox et al., 2006; Gupta et al., 2006) and relative humidity (Shinozuka et al., 2007; Van Donkelaar et al., 2010). Simulated vertical structure from chemical transport models (e.g., Van Donkelaar et al., 2006; 2010) has also been used to help improve the $PM_{2.5}$ /satellite AOT relationship.

There are important issues, however, that need be considered when applying satellite-based observations in general, much less as a proxy for $PM_{2.5}$ estimates. First, uncertainties exist in satellite-retrieved AOT values due to issues such as cloud contamination, inaccurate optical models used in the retrieval process, and heterogeneous surface boundary

conditions (e.g., Zhang and Reid, 2006; Shi et al., 2011a; Toth et al., 2013). Even today, convergence has not yet been reached for retrieved AOT values found among the most widely used satellite aerosol products, such as the Dark Target (DT)/DeepBlue (DB) MODIS and Multi-angle Imaging Spectroradiometer (MISR; Diner et al., 1998; Kahn et al., 2010) aerosol products (e.g., Shi et al., 2011b). Any estimate of $PM_{2.5}$ derived from satellite AOT data cannot be more accurate than the AOT data themselves. Thus, relationships between AOT and $PM_{2.5}$ are likely to be highly sensor product specific. Second, AOT derived from passive sensors is a column-integrated value, and $PM_{2.5}$ concentration is a surface measurement. Under conditions where aerosol particles are concentrated primarily within the surface/boundary layer, AOT is presumably a likelier proxy for $PM_{2.5}$ concentration. Conversely, in conditions where aerosol plumes are transported above the boundary layer, AOT will likely prove a weaker one. Finally, AOT is a column-integrated sum of total ambient particle extinction, whereas $PM_{2.5}$ is measured with respect to dried particle ingested for analysis by corresponding instruments. Thus, hygroscopicity and mass extinction efficiency corrections are further required to accurately characterize any relationship present between the two parameters.

While some studies have attempted to use chemical transport models and ground-based lidars to investigate a relationship between aerosol particle structure, column-integrated AOT and surface-based $PM_{2.5}$ (Liu et al., 2004; Van Donkelaar et al., 2006; Boyouk et al., 2010; Hyer and Chew, 2010), a measurement-based analysis using the Cloud-Aerosol Lidar with Orthogonal Polarization (CALIOP; Winker et al., 2007; Hunt et al., 2009) would allow for such a study over relatively-broad spatial and temporal scales, for which more tenable proxies between AOT and $PM_{2.5}$ may be realized and thus applied on more representative scales. Range-resolved information collected with CALIOP

provides the critical perspective for relating the depth and vertical extent of aerosol particle presence to both surface-based $\text{PM}_{2.5}$ measurements and passive retrievals of column-integrated AOT.

This study differs from past research efforts in several aspects. For one, the impact of passive satellite AOT data quality on the $\text{PM}_{2.5}$ /satellite AOT relationship has yet to be investigated. Secondly, while other studies have considered the aerosol vertical distribution during estimation of $\text{PM}_{2.5}$ from satellite AOT retrievals, this has not been examined over large spatial and temporal domains. Lastly, near-surface aerosol extinction from CALIOP has never been evaluated as a potential proxy for surface $\text{PM}_{2.5}$ concentrations. Therefore, through the use of MODIS, MISR, and CALIOP observations, the following research questions are considered:

1. How does the quality of passive satellite AOT retrievals impact the $\text{PM}_{2.5}$ /AOT relationship?
2. Based on CALIOP data, how representative are surface-based measurements to aerosol particle presence within the full column?
3. Can near surface observations from CALIOP be used as a better proxy for $\text{PM}_{2.5}$ concentration?

This chapter has been designed to discuss each component sequentially, thus building off the previous step. In Sec. 3.2 of this chapter, the various satellite and surface-based datasets used are described. In Sec. 3.3, the $\text{PM}_{2.5}$ /AOT relationship is first examined at an hourly timescale, followed by a daily analysis in which the impact of AOT quality on this relationship is explored. In Sec. 3.4, the representativeness of satellite-derived surface aerosol concentration to that of the entire column, and how well surface AOT correlates with total column AOT, is investigated. Lastly in Sec. 3.5, results comparing surface-based

PM_{2.5} and CALIOP aerosol extinction near the lower bounds of the satellite profile are provided to investigate the potential use of CALIOP data for air quality applications.

3.2 Datasets

3.2.1 MODIS, MISR, and CALIOP Data

Aboard both the NASA Aqua and Terra satellites, MODIS is a spectroradiometer with 36 channels (0.41 to 15 μm), seven of which (0.47 to 2.13 μm) are applied operationally for the retrieval of aerosol particle optical properties. The DT Level 2 products created from these retrievals are reported at a spatial resolution of 10 x 10 km², with over-land uncertainties of $0.05 \pm 0.15 \cdot \text{AOT}$ (Remer et al., 2005). This study utilizes the Corrected_Optical_Depth_Land (0.550 μm) parameter of DT Level 2 Collection 5.1 retrievals from Aqua (MYD04_L2) and Terra (MOD04) MODIS (2008-2009, operational), with quality assurance (QA) limiting the analysis to only those retrievals with Quality_Assurance_Land parameter flags of “very good”. Although the DB MODIS aerosol products also provide aerosol retrievals over land, the Collection 5.1 Aqua/Terra DB MODIS aerosol products are not available for the study period and are thus not included in the study.

MISR, aboard the Terra satellite, is a unique spectroradiometer, able to collect observations at nine different viewing angles, providing a means for studying aerosol particle size and shape (Diner et al., 1998). MISR features four spectral bands, located at 0.446, 0.558, 0.672, and 0.867 μm . Different from the DT MODIS aerosol products, the MISR aerosol product also includes AOT retrievals over bright surfaces such as desert regions. Kahn et al. (2005) suggested that 70% of MISR AOT data are within 0.05 (or $20\% \times \text{AOT}$) of sun-photometer measured AOT values. This study utilizes the same two

years (2008-2009) of AOT derived from Version 22 MISR retrievals (0.558 μm), flagged through QA screening as “successful”.

CALIOP is a multi-wavelength (0.532 and 1.064 μm) polarization lidar flown aboard the Cloud-Aerosol Lidar and Infrared Pathfinder Satellite Observations (CALIPSO) platform within the NASA “A-Train” constellation (e.g., Stephens et al., 2002). To gain an understanding of aerosol particle distribution over the CONUS for 2008-2009, this study utilizes the Version 3.01 CALIOP Level 2 5 km Aerosol Profile (L2_05kmAProf) (Winker et al., 2007; 2012) product. The Version 3.01 Level 2 Vertical Feature Mask (L2_VFM) product is also used to restrict the analysis to those 5 km AOT and total extinction (at 0.532 μm) profile retrievals that are cloud-free, in a manner consistent with that of Toth et al. (2013). Additionally, only daytime CALIOP data are used in this study.

3.2.2 Quality-Assured MODIS and MISR Subsets

Existing uncertainties in passive satellite AOT retrievals, such as those for MODIS and MISR, are optimally suppressed before being considered and applied for data assimilation (DA) activities involving operational aerosol forecast models (e.g., Zhang et al., 2008). Through rigid QA, reduced AOT uncertainties have been characterized and DA-quality AOT datasets have been created for both over land (Hyer et al., 2011) and over ocean MODIS DT products (Shi et al., 2011a), as well as the MISR aerosol products (Shi et al., 2011b; 2012). In this study, DA-quality MODIS and MISR AOT products are used as control datasets for comparison with operational MODIS and MISR products.

Available at 6-hourly $1^\circ \times 1^\circ$ resolution, DA-quality AOT data are converted to daily averages and then compared with daily $\text{PM}_{2.5}$ concentrations. For comparison

purposes with the $PM_{2.5}$ data available (described further below), daily-averaged “Level 3” AOT data have been constructed using operational MODIS and MISR aerosol products after applying first-order QA as described in Sec. 3.2.1. DA-quality MODIS aerosol products are available from the Global Ocean Data Assimilation Experiment (GODAE) server (<http://www.usgodae.org/>). However, no quality-assured hourly DA-quality aerosol products are currently available, and no comparisons were therefore made between the DA-quality products and hourly $PM_{2.5}$ measurements.

3.2.3 Surface $PM_{2.5}$

The U.S. EPA has collected observations of surface-based PM since the passage of the Clean Air Act in 1970 (<http://www.epa.gov/air/caa/>). In 1997, the EPA began specifically monitoring $PM_{2.5}$ concentrations (Federal Register, 2006). The Federal Reference Method (FRM), a filter-based method, is used to measure concentration over a continuous 24-hr period. The filter is weighed before and after the sample collection interval and $PM_{2.5}$ mass concentration ($\mu\text{g}/\text{m}^3$) is calculated by dividing the total mass of $PM_{2.5}$ particles by the volume of air sampled (Federal Register, 1997). Some EPA sites also report hourly (continuous) $PM_{2.5}$ measurements. For this study, two years (2008-2009) of daily and hourly $PM_{2.5}$ Local Conditions (EPA Parameter Code 88101) data were used and obtained from the EPA Air Quality System (AQS).

3.2.4 AERONET AOT

AERONET is a worldwide ground-based network of sun photometers that provides measurements of aerosol optical properties, and is currently used as the benchmark for validation of satellite AOT retrievals. AERONET AOT is reported at eight channels (0.34

to 1.64 μm), and has an uncertainty of 0.01 to 0.015 (Holben et al., 1998). For the purposes of this study, AOT derived at 0.67 μm is used.

3.3 How Does the Quality of Passive Satellite AOT Retrievals Impact their Linear Correlation with Surface-Based $\text{PM}_{2.5}$?

As a first step, linear correlations between passive satellite AOT retrievals and $\text{PM}_{2.5}$ observations in the CONUS are derived. The impact of data quality to the AOT/ $\text{PM}_{2.5}$ relationship is investigated through a daily analysis using both daily-averaged operational and DA-Quality AOT datasets, as well as daily $\text{PM}_{2.5}$ data. No hourly DA-quality AOT retrievals are currently available, and therefore the impact of data quality to the AOT/ $\text{PM}_{2.5}$ correlations are not specifically characterized on this temporal scale. Still, an hourly analysis is first considered, using only operational AOT data and hourly $\text{PM}_{2.5}$ data, for comparison purposes and for establishing a relevant context for the relationship between AOT and $\text{PM}_{2.5}$.

Figure 1 depicts those $\text{PM}_{2.5}$ monitoring sites for the 2008-2009 period that reported hourly (Fig. 1a) and daily-averaged (Fig. 1b) $\text{PM}_{2.5}$ observations. A total of 102 sites reported hourly data, while 991 sites collected daily data (see figure caption for color scheme). Note that some sites feature multiple instruments observing $\text{PM}_{2.5}$ concentration; one routine/primary, regular measurement and a secondary measurement that is only available sporadically. Both types of $\text{PM}_{2.5}$ data are included for this analysis.

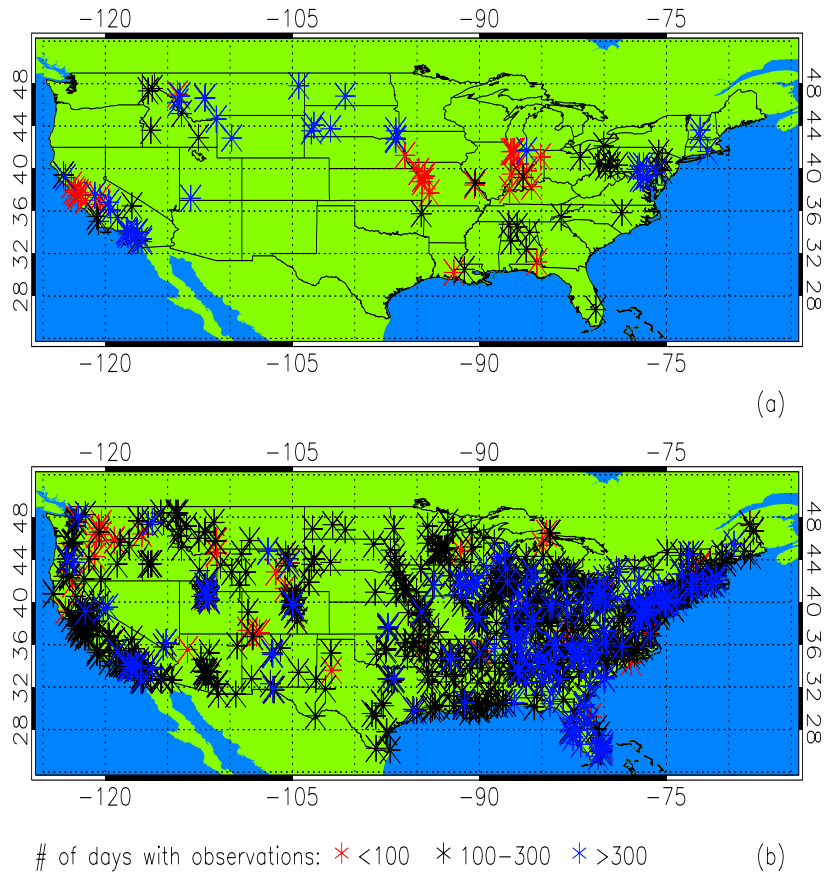


Figure 1. For the period 2008-2009, U.S. Environmental Protection Agency (EPA) sites with available $PM_{2.5}$ measurements at (a) hourly and (b) daily intervals, respectively. The sites are color-coded based on number of days with observations, as red (fewer than 100), black (between 100 and 300), or blue (greater than 300).

3.3.1 Hourly Analysis

For the period 2008-2009, the operational Level 2 AOT datasets are spatially and temporally collocated with available $PM_{2.5}$ observations. After these AOT data are filtered through basic QA screening (Sec. 3.2.1), each hourly $PM_{2.5}$ observation is matched with those Level 2 AOT retrievals meeting the QA criteria and found within 40 km and 1 hr of the $PM_{2.5}$ observation. All remaining AOT values are then averaged for a single comparison with the $PM_{2.5}$ observation. 40 km was chosen as the averaging range for the

satellite data after assuming a mean wind speed of 10 m/s influencing aerosol plumes transport (approximately 40 km/hr). AOT autocorrelation at or exceeding 0.8 has been reported for a distance of 40 km (on average) (Anderson et al., 2003; Zhang et al., 2011), making this a reasonable constraint.

Table 1. Correlation coefficients and data counts of the 40 km average operational Aqua/Terra MODIS and MISR AOT/hourly PM_{2.5} collocation analyses for the Eastern, Central, Mountain, and Pacific time zones and contiguous United States total for the entire two-year (2008-2009) study period, December through May 2008-2009 (DJFMAM), and June through November 2008-2009 (JJASON).

Dataset		Operational Aqua MODIS		Operational Terra MODIS		Operational MISR	
		R value	Data Count	R value	Data count	R value	Data count
Eastern	All	0.57	2081	0.47	2748	0.42	614
	DJFMAM	0.49	477	0.39	566	0.11	154
	JJASON	0.57	1551	0.50	2001	0.50	408
Central	All	0.27	1765	0.22	2005	0.22	447
	DJFMAM	0.11	335	0.14	346	0.16	112
	JJASON	0.38	1330	0.28	1511	0.26	304
Mountain	All	0.19	1369	0.12	1632	0.10	391
	DJFMAM	-0.08	215	0.09	250	0.16	95
	JJASON	0.30	1136	0.17	1354	0.20	277
Pacific	All	0.15	3832	0.22	3873	0.11	903
	DJFMAM	0.08	1064	0.21	1047	0.15	269
	JJASON	0.26	2560	0.21	2564	0.29	539
Contiguous U.S.	All	0.19	9047	0.22	10258	0.15	2355
	DJFMAM	0.03	2091	0.12	2209	0.07	630
	JJASON	0.34	6577	0.25	7430	0.27	1528

Table 1 summarizes the results of the hourly collocation of 40 km/1 hr average MODIS/MISR AOT with corresponding ground-based PM_{2.5} measurements over the two-year study, including linear correlation coefficients and data counts for the CONUS divided into its four respective time zones: Eastern (UTC-5), Central (UTC-6), Mountain (UTC-7), and Pacific (UTC-8). Relatively low correlations are found for the CONUS, as

a whole. However, a regional dependence of the relationship between the two parameters is also apparent. The Eastern CONUS region exhibits higher correlation than does the Pacific CONUS by a factor of nearly two (0.2 vs. 0.4). This is consistent with several studies that have shown similar regional effects. For example, Hu (2009) reports average $PM_{2.5}/AOT$ correlations of 0.67 (Eastern U.S.) and 0.22 (Western U.S.), with Engel-Cox et al. (2004) and Paciorek et al. (2008) reporting similar correlations of 0.6-0.8 (Eastern U.S.) and 0.2-0.4 (Western U.S.). It has been suggested that this regional variability in the $PM_{2.5}/AOT$ relationship is due to differences in topography, surface albedo, and boundary layer depth between the Eastern and Western U.S. (Engel-Cox et al., 2006).

In Fig. 2, regional differences of $PM_{2.5}/AOT$ correlation are also evident from scatterplots for the Eastern (Fig. 2a) and Pacific (Fig. 2b) time zones, with greater linearity observed in the Eastern CONUS compared to the west. Also, $PM_{2.5}$ concentration averages were computed for each 0.1 bin of AOT, and shown with respect to both Terra MODIS and MISR. Note that although both Aqua and Terra MODIS are listed in Table 1, only the Terra MODIS/MISR analyses are shown in Fig. 2 because of their common satellite-observing platform. In general, a better correlation is found for the bin averages, which is consistent with that reported by Gupta et al. (2006).

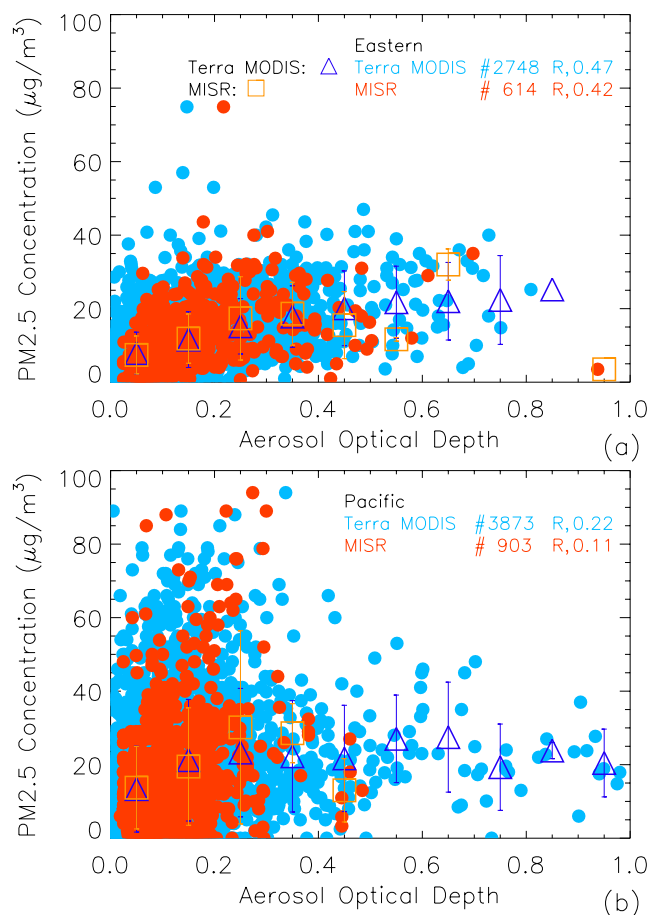


Figure 2. Two-year (2008-2009) scatterplots of operational Terra MODIS (in light blue) and MISR (in red) AOT, averaged within 40 km of each respective $\text{PM}_{2.5}$ -monitoring site, versus hourly $\text{PM}_{2.5}$ concentrations for the (a) Eastern and (b) Pacific U.S. time zones. Also plotted are averages of $\text{PM}_{2.5}$ for each 0.1 AOT bin, represented with triangles (in dark blue) for Terra MODIS and squares (in orange) for MISR. Error bars (± 1 standard deviation) for the bin averages are also shown.

Seasonally, each of the hourly $\text{PM}_{2.5}$ /AOT correlations coefficients shown in Table 1 are recomputed for December through May (Table 1; DJFMAM) and June through November (Table 1; JJASON). There are fewer data points for DJFMAM than JJASON ($\sim 68\%$ decrease), enhanced by the absence of December 2007 in the dataset (this month was not included in the analysis due to the lack of $\text{PM}_{2.5}$ Local Conditions data, EPA Parameter Code 88101, before 2008). Overall, however, lower correlations are found

during this season compared with the annual mean. The opposite is thus true for JJASON. Although not shown here, further analysis reveals that higher correlations of JJASON may be due to a significant number of cases of relatively high $\text{PM}_{2.5}$ (greater than $35 \mu\text{g}/\text{m}^3$) and high satellite AOT (greater than 0.3) that occur during this season, relative to DJFMAM, which may positively influence the regression compared with JJASON.

3.3.2 Daily Analysis

Next, how the relationship between AOT and $\text{PM}_{2.5}$ is affected by the perceived data quality of the operational satellite AOT datasets is investigated, using only basic QA, versus the DA-quality Level 3 AOT data. As discussed above, these latter data are subject to more advanced screening, with filtering, correction, and spatial aggregation applied. Each available daily ground-based $\text{PM}_{2.5}$ observation is matched with both the operational and DA-quality AOT retrievals found within 1° latitude/longitude and the day of the $\text{PM}_{2.5}$ observation. Results of the daily $1^\circ \times 1^\circ$ operational and DA-quality MODIS/MISR AOT analyses are shown for the CONUS and each respective time zone in Table 2.

Distinct increases are found for $\text{PM}_{2.5}/\text{AOT}$ correlation using the DA-quality satellite AOT products versus the operational satellite AOT datasets (Table 2). For example, $\text{PM}_{2.5}/\text{AOT}$ correlations for the CONUS increase by about 0.12 (Aqua MODIS), 0.16 (Terra MODIS), and 0.14 (MISR) from each respective operational to DA-quality dataset. Note that data counts for each DA-quality AOT analysis decrease relative to each corresponding operational AOT analysis, indicative of fewer available collocations from the Level 3 AOT datasets from increased data rejection. It is believed that such a pronounced pattern reflects the influence of AOT retrieval quality from the passive satellites on their relationship with surface-based $\text{PM}_{2.5}$ measurements.

Table 2. Correlation coefficients and data counts of the daily $1^\circ \times 1^\circ$ average operational/DA Aqua/Terra MODIS and MISR AOT/daily $PM_{2.5}$ collocation analyses for the Eastern, Central, Mountain, and Pacific time zones and contiguous United States total for the entire two-year (2008-2009) study period, December through May 2008-2009 (DJFMAM), and June through November 2008-2009 (JJASON).

Dataset	Aqua MODIS						Terra MODIS						MISR						
	Operational			DA			Operational			DA			Operational			DA			
	R value	Data Count		R value	Data Count		R value	Data Count		R value	Data Count		R value	Data Count		R value	Data Count		
Eastern	All	0.40	76194	0.50	29682		0.38	80810	0.51	38725		0.32	15526	0.50	10949				
	DJFMAM	0.23	30615	0.31	12180		0.23	32492	0.35	15166		0.20	6819	0.37	4829				
	JJASON	0.45	43837	0.56	17123		0.44	45839	0.55	22723		0.37	8194	0.55	5750				
Central	All	0.39	39942	0.47	18584		0.36	40824	0.51	21084		0.30	8396	0.46	6256				
	DJFMAM	0.27	15892	0.31	7507		0.22	15853	0.29	8130		0.23	3536	0.35	2549				
	JJASON	0.45	23217	0.55	10708		0.44	23979	0.57	12506		0.33	4649	0.53	3551				
Mountain	All	0.09	14160	0.21	5007		0.07	15597	0.13	6313		0.04	3455	0.06	2489				
	DJFMAM	0.06	4788	0.00	1180		0.04	5258	-0.04	1463		-0.01	1385	-0.05	782				
	JJASON	0.13	9178	0.30	3775		0.13	10078	0.29	4793		0.12	1974	0.16	1659				
Pacific	All	0.13	21871	0.33	11446		0.12	22405	0.33	11470		0.16	4639	0.27	3625				
	DJFMAM	0.00	9110	0.08	4218		-0.03	9308	0.08	4265		0.06	2047	0.16	1509				
	JJASON	0.24	12310	0.44	7107		0.24	12470	0.43	7011		0.27	2431	0.37	2025				
Contiguous U.S.	All	0.31	152167	0.43	64719		0.29	159636	0.45	77592		0.26	32016	0.40	23319				
	DJFMAM	0.15	60405	0.21	25085		0.12	62911	0.22	29024		0.15	13787	0.26	9669				
	JJASON	0.40	88542	0.52	38713		0.39	92366	0.52	47033		0.34	17248	0.48	12985				

Also shown in Table 2, the Eastern sample exhibits greater linearity (i.e., correlation) overall compared with the Western one. Figure 3 further illustrates the regional variation in $PM_{2.5}$ /DA AOT correlation, through corresponding scatterplots for

the Eastern (Fig. 3a) and Pacific (Fig. 3b) time zones. As in Fig. 2, only the Terra MODIS/MISR analyses are shown because of their common platform. Also, averages of $PM_{2.5}$ concentrations are shown for each 0.1 bin of DA TERRA and MISR AOT.

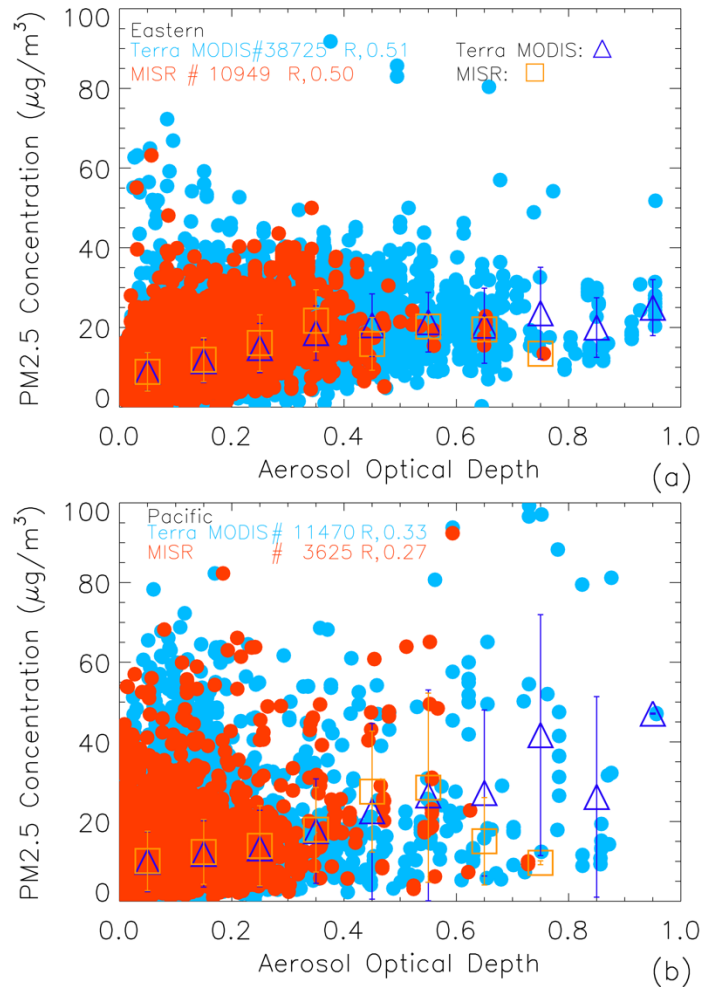


Figure 3. Two-year (2008-2009) scatterplots of daily $1^\circ \times 1^\circ$ DA Terra MODIS (in light blue) and daily $1^\circ \times 1^\circ$ MISR (in red) AOT versus daily $PM_{2.5}$ concentrations for the (a) Eastern and (b) Pacific U.S. time zones. Averages of $PM_{2.5}$ are plotted for each 0.1 AOT bin, represented with triangles (in dark blue) for Terra MODIS and squares (in orange) for MISR. Error bars (± 1 standard deviation) for the bin averages are also shown.

The seasonality of the $\text{PM}_{2.5}/\text{AOT}$ relationship for the daily analysis is investigated in Table 2. As encountered above for Table 1, there are fewer data points for DJFMAM than JJASON (~32% decrease). Likewise, lower $\text{PM}_{2.5}/\text{AOT}$ correlations are found during DJFMAM, and higher correlations are found from JJASON, as compared to the mean annual results presented in Table 2. Again, this pattern may be due to a larger number of high $\text{PM}_{2.5}$ (greater than $35 \mu\text{g}/\text{m}^3$) and high satellite AOT (greater than 0.3) values that are found from JJASON, as compared to DJFMAM. However, a longer study period is likely needed to more appropriately understand the seasonal dependence of the $\text{PM}_{2.5}/\text{AOT}$ relationship.

Figure 4 consists of two maps depicting daily $\text{PM}_{2.5}$ sites used in this analysis, color-coded with respect to $\text{PM}_{2.5}/\text{AOT}$ correlation coefficient. Figure 4a reflects the $\text{PM}_{2.5}/\text{daily}$ operational Terra MODIS AOT relationship, with generally higher correlations in the Eastern CONUS than the Pacific CONUS. Figure 4b illustrates a clear increase in $\text{PM}_{2.5}/\text{AOT}$ correlation for the daily DA Terra MODIS AOT analysis, with again still higher correlations for the Eastern CONUS compared to those results found in the west. Similar regional and operational-to-DA AOT patterns in the $\text{PM}_{2.5}/\text{AOT}$ relationship are shown in Fig. 5 for the operational MISR AOT (Fig. 5a) and DA MISR AOT (Fig. 5b) daily analyses.

In order to strengthen the results obtained in the hourly and daily analyses, a common point filter is applied to the data. The common point filter refers to the requirement of valid points from all four data sources (i.e., hourly/daily $\text{PM}_{2.5}$ and operational/DA AOT). As such, for common $\text{PM}_{2.5}$ sites, correlations between hourly $\text{PM}_{2.5}$ and 40 km average operational AOT, and daily $\text{PM}_{2.5}$ and $1^\circ \times 1^\circ$ average DA AOT, were computed (Table 3). Regional variations in the $\text{PM}_{2.5}/\text{AOT}$ relationship found here

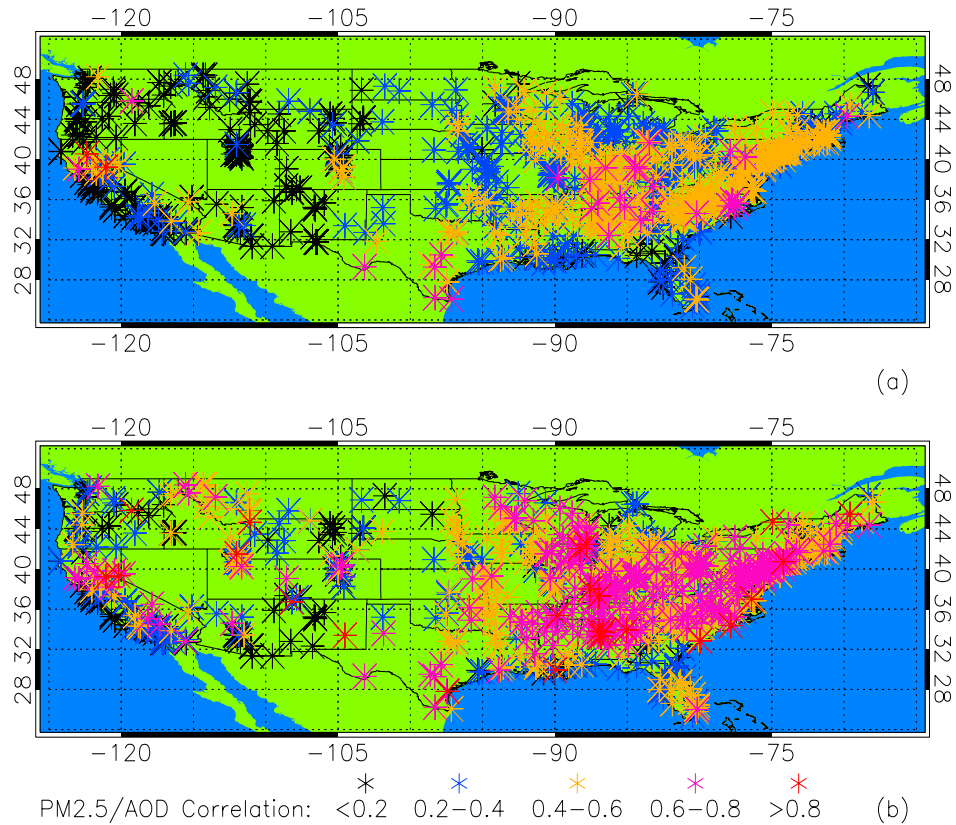


Figure 4. For the period 2008-2009, the U.S. Environmental Protection Agency (EPA) daily $\text{PM}_{2.5}$ sites used in this study. Sites are color-coded based on the correlation between daily $\text{PM}_{2.5}$ observations and daily $1^\circ \times 1^\circ$ (a) operational and (b) DA Terra MODIS AOT.

are similar to those in earlier analyses presented in this study, with higher correlations for the east than for the west. Also, the correlations from the hourly analysis are generally higher than those from the daily analysis, but with some dependency on region and satellite sensor. While this common point study implies that operational AOT may be a better estimate of $\text{PM}_{2.5}$ than DA AOT, note here that when only daily data are used (Table 2), there exists a distinct improvement in $\text{PM}_{2.5}$ estimation from the operational to DA AOT datasets. Thus, it is reasonable to expect further improvement in the $\text{PM}_{2.5}$ /passive satellite

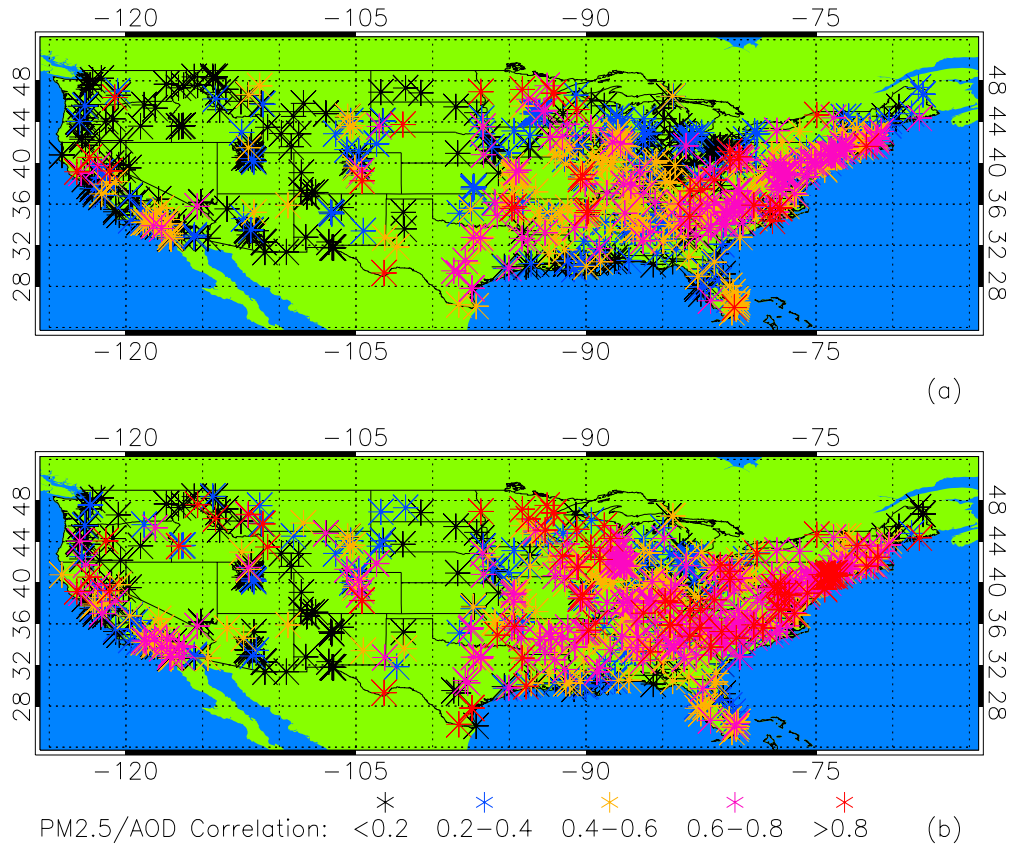


Figure 5. For the period 2008-2009, the U.S. Environmental Protection Agency (EPA) daily PM_{2.5} sites used in this study. Sites are color-coded based on the correlation between daily PM_{2.5} observations and daily 1° x 1° (a) operational and (b) DA MISR AOT.

AOT relationship through the use of hourly DA-quality AOT datasets. These data are currently not readily available, however, so this topic is left for a future study.

As a final step for Sect. 3.3, the hourly PM_{2.5}/AERONET AOT relationship for the CONUS is examined. AERONET AOT (0.67 μm) measurements found within 0.3° latitude/longitude and the hour of an hourly PM_{2.5} observation were first averaged, and hourly PM_{2.5}/AERONET AOT correlations and data counts were then computed (Table

4). Similar to the results from the PM_{2.5}/satellite AOT analyses, a higher correlation is found for the Eastern time zone (0.61) compared to the Pacific time zone (0.54). Also, the

Table 3. Correlation coefficients and data counts for the hourly PM_{2.5}/40 km average operational AOT and daily PM_{2.5}/1° x 1° average DA AOT common point analyses for the Eastern, Central, Mountain, and Pacific time zones and contiguous United States total for the two-year (2008-2009) study period.

Dataset	Aqua MODIS			Terra MODIS			MISR		
	Hourly R value	Daily R value	Data Count	Hourly R value	Daily R value	Data Count	Hourly R value	Daily R value	Data Count
Eastern	0.63	0.54	369	0.52	0.58	543	0.56	0.49	138
Central	0.29	0.2	305	0.25	0.28	362	0.20	0.12	93
Mountain	0.52	0.56	108	0.35	0.55	119	0.39	-0.08	21
Pacific	0.32	0.16	916	0.25	0.21	874	0.25	0.15	270
Contiguous US	0.36	0.20	1698	0.30	0.25	1898	0.30	0.22	522

hourly PM_{2.5}/AERONET AOT correlations are generally higher than those between hourly PM_{2.5}/satellite AOT (Table 1). These findings are not surprising, as AERONET is considered the benchmark for validation of satellite AOT retrievals.

Table 4. Correlation coefficients and data counts for the hourly PM_{2.5}/average AERONET AOT (0.670 μm) collocation analysis (AERONET AOT averaged within the hour and 0.3° latitude/longitude of an hourly PM_{2.5} measurement) for the Eastern, Central, Mountain, and Pacific time zones and contiguous United States total for the two-year (2008-2009) study period.

Dataset	R value	Data Count
Eastern	0.61	6596
Central	0.36	613
Mountain	0.16	2438
Pacific	0.54	512
Contiguous US	0.51	10159

3.4 How Representative is the Surface Layer Aerosol Particle Presence to the Atmospheric Column?

It was demonstrated that the quality of the AOT datasets investigated impacts any linear correlation apparent with ground-based $\text{PM}_{2.5}$ measurements. Next, the representativeness of aerosol particle presence near the surface to that of the atmospheric column is explored. The CALIOP L2_05kmAProf product is used, featuring a vertical resolution of 60 m for altitudes below 20.2 km above mean sea level (MSL). Using the corresponding mean surface elevation reported with each profile, values of extinction coefficient and AOT ($0.532 \mu\text{m}$) are re-gridded linearly at 100 m resolution vertically from the surface (above ground level, or a.g.l.) to 8.2 km after a robust QA screening procedure takes place. The details of this QA process are documented in past studies (Kittaka et al., 2011; Campbell et al., 2012; Winker et al., 2013; Toth et al., 2013). Only cloud-free profiles are considered.

Shown in Fig. 6 are $1^\circ \times 1^\circ$ averages (relative to the number of cloud free 5 km CALIOP profiles in each $1^\circ \times 1^\circ$ regional bin) of $0.532 \mu\text{m}$ aerosol extinction coefficient for the 0.0 to 0.5 km layer (Fig. 6a), 0.5-1.5 km (Fig. 6b), 1.5-2.5 km (Fig. 6c) and 2.5-3.5 km a.g.l. (Fig. 6d), respectively. In general, extinction values observed in the lower atmospheric layers (Figs. 6a and b) are larger than those observed in the elevated atmospheric layers (Figs. 6c and d). However, higher mean values are found nearer the surface in the eastern region (particularly the southeastern CONUS; Figs. 6a and b), while higher values are found at elevated heights in the west (Figs. 6c and d). These data indicate that, on average, aerosol particle distributions tend to be more concentrated near the surface in the east and more diffuse vertically in the west.

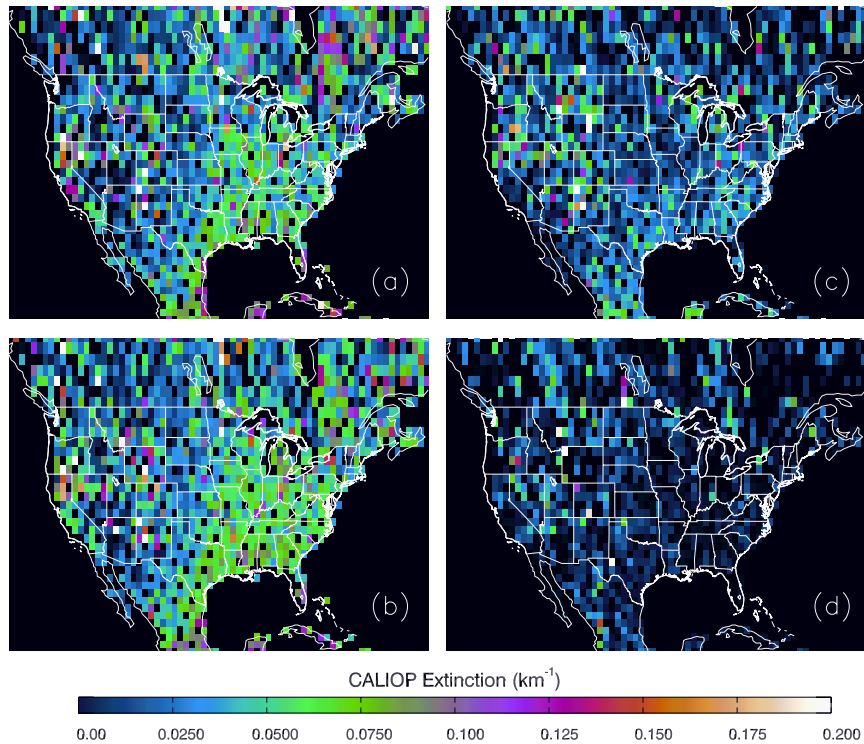


Figure 6. Two-year (2008-2009) $1^\circ \times 1^\circ$ average CALIOP $0.532 \mu\text{m}$ extinction, relative to the number of cloud-free 5 km CALIOP profiles in each $1^\circ \times 1^\circ$ bin, for atmospheric layers a.g.l. of (a) 0-500 m, (b) 500-1500 m, (c) 1500-2500 m, and (d) 2500-3500 m.

Corresponding with Fig. 6a, Fig. 7 is a plot of the average percentage of surface layer-integrated extinction (altitudes lower than 500 m a.g.l.) to total column AOT. The average of the lower 500 m a.g.l. is used to represent the surface layer so as to minimize ground flash contamination in the CALIOP data when observations are near the ground (e.g., Campbell et al., 2013). Values are generally below 40% across the CONUS, with higher values more concentrated in the eastern part of the country. The distribution is noisy, however, and thus to better interpret these data, a five-year assessment (2006-2011) of CALIOP data is presented (Fig. 8). Common patterns emerge, though more distinctly,

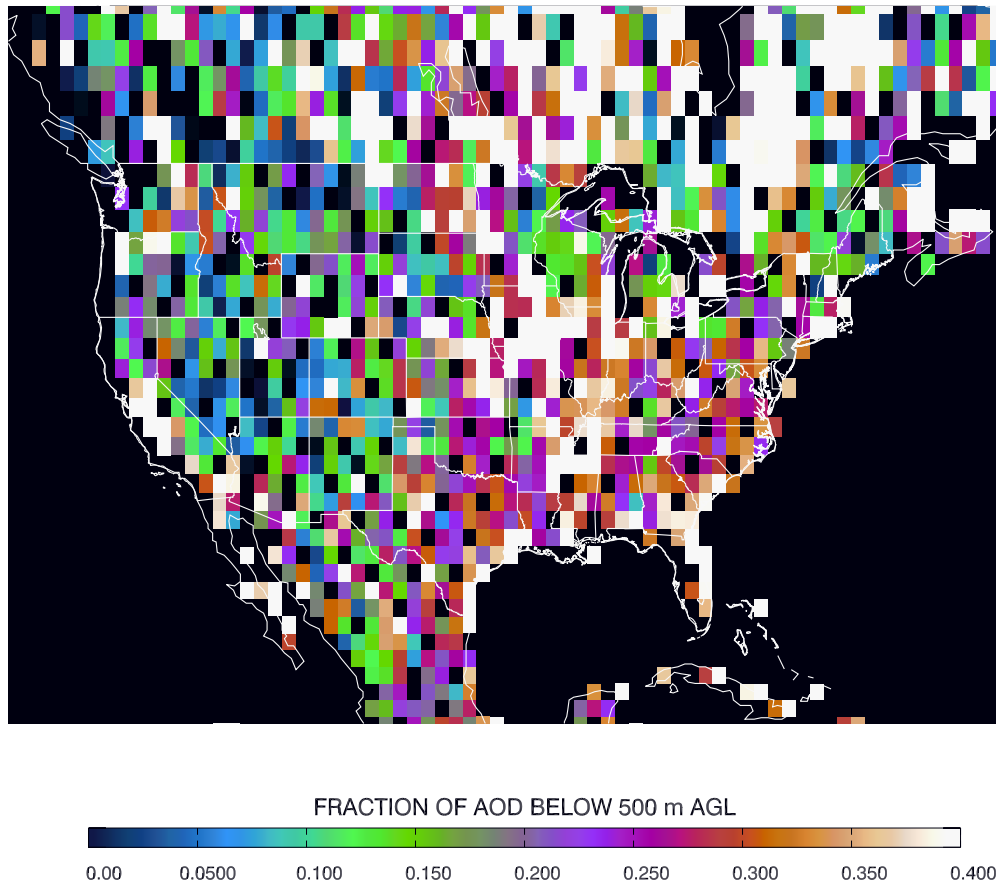


Figure 7. Two-year (2008-2009) $1^\circ \times 1^\circ$ average contribution percentage of 0 to 500 m a.g.l. integrated CALIOP extinction to total column AOT (at $0.532 \mu\text{m}$) relative to the number of cloud-free CALIOP profiles in each $1^\circ \times 1^\circ$ bin, for the contiguous United States.

as higher percentages are again found over the east versus the west. In general, however, AOT below 500 m a.g.l. accounts for only 30% or less of the total column AOT across the CONUS. This indicates that it is necessary to have a priori knowledge of the ratio between near-surface integrated extinction to column-integrated AOT in order to better characterize the likely representativeness of applying satellite AOT as a proxy for surface $\text{PM}_{2.5}$ concentration.

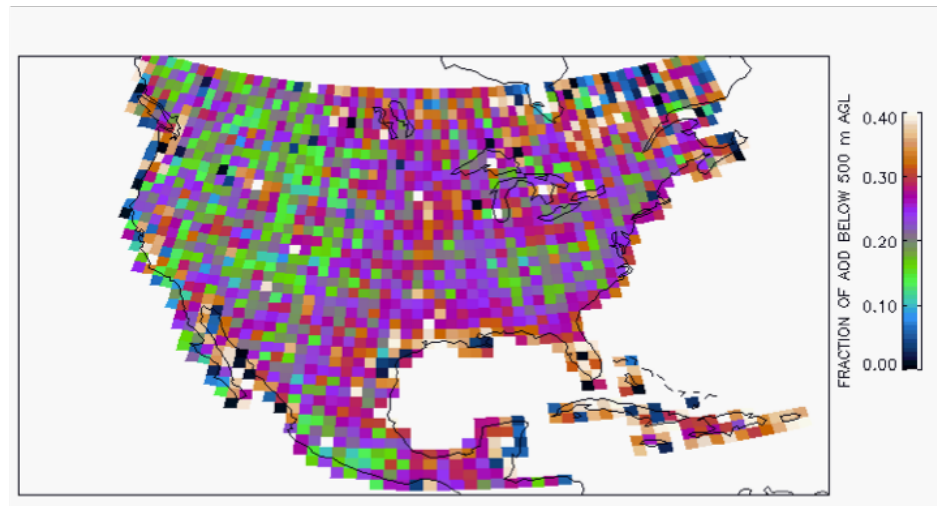


Figure 8. From 2006 to 2011, fraction of CALIOP-integrated $0.532\ \mu\text{m}$ extinction below 500 m a.g.l. for the contiguous United States.

Note that although integrated extinction over the lowest 500 m a.g.l. may not be representative of the total column AOT, it is possible that the correlation between the two could be high, and thus useful for satellite AOT/ $\text{PM}_{2.5}$ studies. Although not shown here, the $1^\circ \times 1^\circ$ average correlation between integrated extinction from the lowest 500 m a.g.l. and total column AOT is computed. Globally over land, an average correlation of 0.61 is found. For the CONUS, a similar value of 0.62 is calculated, with values of 0.61 for the Eastern time zone and 0.57 for the Pacific. Importantly, the lack of significant regional variability in these relationships indicates that although the Eastern and Pacific time zones may exhibit different AOT surface contribution percentages, integrated surface extinction correlates relatively consistently with total column AOT. Still, given a perfect possible correlation of 1 between integrated surface level extinction and $\text{PM}_{2.5}$ concentration, the correlation value of ~ 0.6 between the former with column-integrated AOT might represent the best-case scenario, on a regional average, that one could derive presently for the satellite

AOT to $PM_{2.5}$ concentration relationship. This agrees well with the findings reported in Hoff and Christopher (2009).

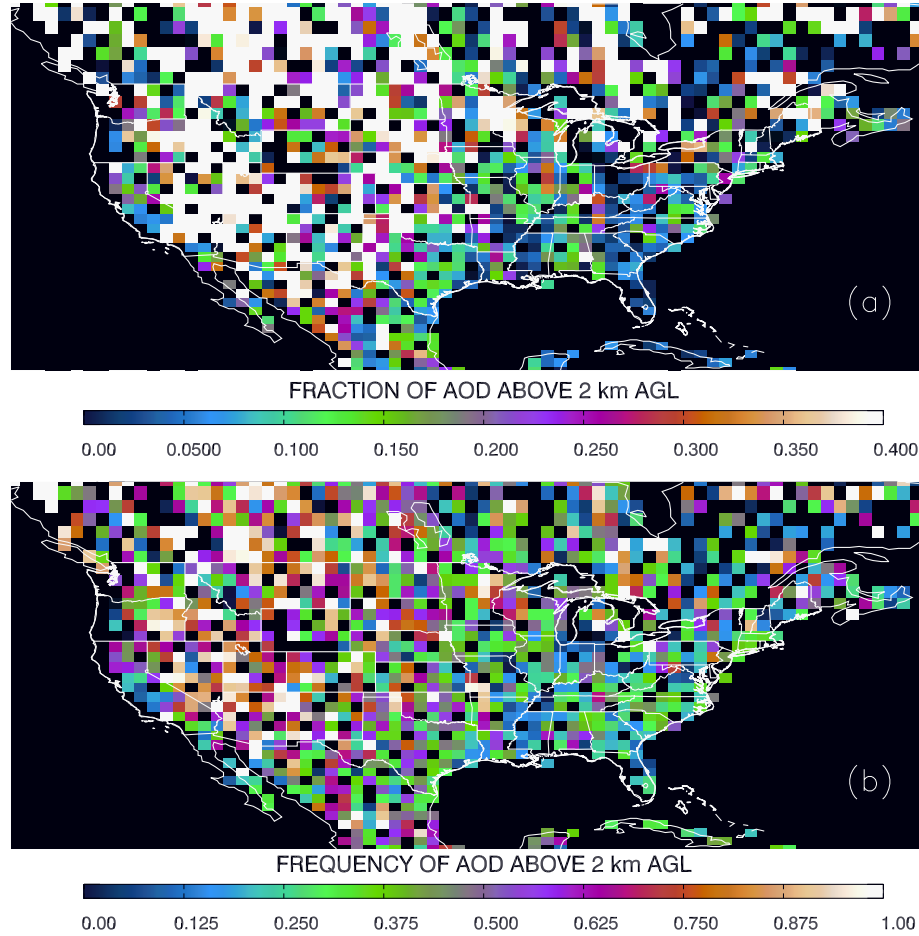


Figure 9. Two-year (2008-2009) $1^\circ \times 1^\circ$ average (a) contribution percentage of above 2 km a.g.l. CALIOP AOT to total column AOT (at $0.532 \mu\text{m}$) and (b) frequency of occurrence of AOT above 2 km a.g.l., both relative to the number of cloud-free CALIOP profiles in each $1^\circ \times 1^\circ$ bin, for the contiguous United States.

To evaluate the influence of aerosol particle presence at elevated levels, in Fig. 9a the fraction of CALIOP-retrieved column-integrated AOT found above an arbitrary standard height of 2 km a.g.l. is shown, thus segregating mostly boundary layer particle presence versus those propagating within the free troposphere. It is evident that regional variations in the fraction of AOT above 2 km exist, as the western half of the CONUS

exhibits at least double the amount of particle extinction above 2 km than does the eastern CONUS. However, note that many areas in California, where a relatively dense array of Pacific U.S. $PM_{2.5}$ sites are located, exhibit relatively low contributions comparable to that of the east (usually below 30%). Consistent with the findings shown in Fig. 9a, regional variations in the frequency of occurrence of AOT above 2 km a.g.l. are also observed (Fig. 9b), with generally higher frequencies in the west as compared to the east. The average frequency of occurrence of aerosol particle presence (as measured by CALIOP total column AOT) above 2 km a.g.l for the U.S. is $\sim 40\%$ (Fig. 9b). Also, about 20% of data records (not shown) have at least 50% of aerosol particle presence above 2 km a.g.l. This indicates a significant number of elevated aerosol plumes occurred over the CONUS during the 2008-2009 period, and thus will not be recognized by surface-based $PM_{2.5}$ measurements.

3.5 Can Near Surface Observations from CALIOP Be Used As a Better Proxy for $PM_{2.5}$ Concentration?

Taking advantage of an active-profiling aerosol particle sensor like CALIOP, the relationship between hourly $PM_{2.5}$ concentration and CALIOP 532 μm extinction coefficient values near the surface is investigated. The temporal/spatial collocation and 40 km AOT averaging process here is the same as described in Sect. 3.3. Recall that $PM_{2.5}$ is a dry particle mass measurement. However, satellite-retrieved AOT values include the effects of aerosol particle growth as a function of vapor pressure. To compute the CALIOP extinction and $PM_{2.5}$ relationship, a sensitivity study was performed for which the hygroscopic growth of aerosol particles was accounted for. It is approximated that aerosol particles over the CONUS are sulfate aerosols, and apply the sulfate aerosol hygroscopic growth factor (Hanel, 1976; Hegg et al., 1993; Anderson et al., 1994) to compute dry

aerosol extinction and AOT using Goddard Modeling and Assimilation Office (GMAO) relative humidity values included as metadata in the NASA-disseminated CALIOP files. No correction is made to extinction coefficient values when relative humidity is less than 30% or above 95%. Further, the sensitivity of the CALIOP value chosen to compare with is investigated by varying the height of the retrieval used between 0 and 500 m a.g.l. in 100 m segments.

Table 5. Two-year (2008-2009) correlation coefficients of hourly $PM_{2.5}$ observations and 40 km average CALIOP extinction (both uncorrected and dry mass) at various 100 m a.g.l. atmospheric layers.

CALIOP Extinction Layer	Uncorrected CALIOP Extinction		Dry Mass CALIOP Extinction	
	Eastern	Pacific	Eastern	Pacific
0 - 100 m	0.35	0.72	0.33	0.71
100 - 200 m	0.62	0.73	0.66	0.72
200 - 300 m	0.57	0.72	0.69	0.74
300 - 400 m	0.54	0.61	0.63	0.59
400 - 500 m	0.69	0.58	0.70	0.56

Results, including the level of CALIOP extinction used, are summarized in Table 5. For both the Eastern and Pacific U.S. time zones, altering the level of the reported CALIOP extinction from 200 to 500 m a.g.l. has little effect on correlation. Relatively low correlation is observed using the CALIOP extinction values at the 0-100 m level, however, suggesting the likely impacts of ground contamination of the backscatter signal. When hygroscopic growth of aerosol particles is considered, modest improvements are found for the eastern CONUS but not the climatologically drier Pacific region.

Next, the relationship between CALIOP extinction near the surface and $PM_{2.5}$ concentrations when collocated Aqua MODIS operational retrievals are available is investigated. This $PM_{2.5}$ /CALIOP/Aqua MODIS dataset was constructed for both hourly and daily analyses during the 2008-2009 period. For the hourly study, both CALIOP and

operational Aqua MODIS observations are again averaged within 40 km and 1 hr of the $PM_{2.5}$ measurements. For the daily comparison, observations from CALIOP are averaged within 100 km along-track (approximately 1°), and those from operational Aqua MODIS are averaged within 1° latitude/longitude and the day of each $PM_{2.5}$ measurement.

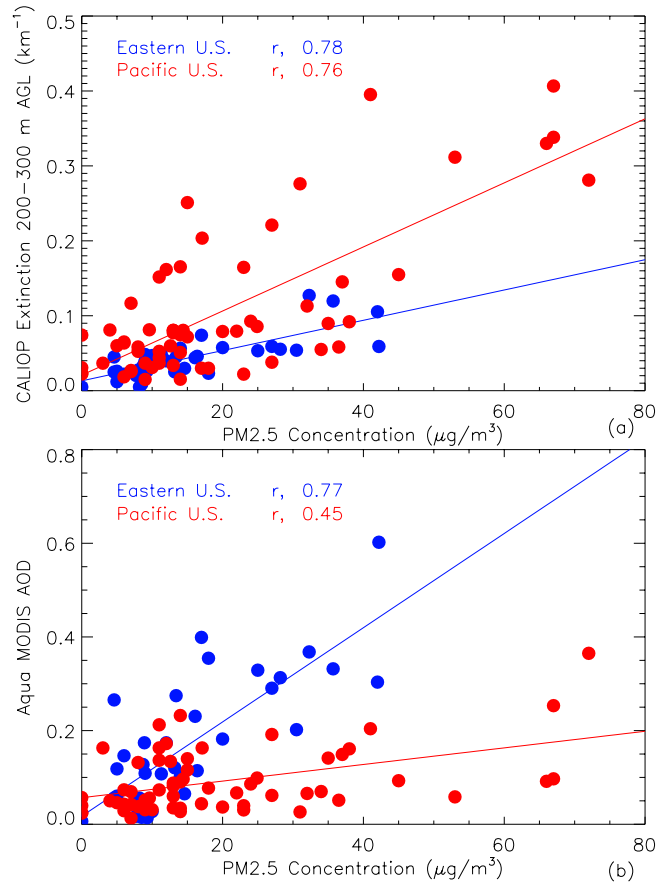


Figure 10. For the Eastern (in blue) and Pacific (in red) U.S. Time zones, two-year (2008-2009) scatterplots of hourly $PM_{2.5}$ concentrations versus (a) cloud-free 5 km CALIOP dry mass $0.532 \mu m$ extinction at the 200-300 m a.g.l. layer, and (b) operational Aqua MODIS AOT, both averaged within 40 km and the hour of each respective $PM_{2.5}$ measurement.

Figure 10 shows hourly analysis results for dry mass-adjusted CALIOP extinction at 200-300 m a.g.l. (Fig. 10a) and operational Aqua MODIS AOT (Fig. 10b). The 200-300 m layer was used because the lowest 200 m a.g.l. of retrieved extinction is considered subject to ground contamination (e.g., Schuster et al., 2012; Omar et al., 2013). Reasonably high correlations of ~ 0.8 are found for CALIOP/PM_{2.5} for both the Eastern and Pacific time zones. A difference exists between these two regions for Aqua MODIS, however. The Eastern CONUS exhibits similar correlation compared with that found above from CALIOP, but drops off to about ~ 0.5 for the Pacific CONUS. Clearly, CALIOP and Aqua MODIS retrievals behave similarly for the Eastern CONUS, but CALIOP performance is much better than Aqua MODIS over the Pacific. However, the correlations between PM_{2.5} and CALIOP/Aqua MODIS observations computed in this analysis should be considered with caution, as the low data count (fewer than 100 data points) make these findings tenuous.

Figures 11a and b depict the same analyses as in Fig. 10, but now for the daily analysis of PM_{2.5}/CALIOP/Aqua MODIS. Correlations are reduced for each time zone, compared with the hourly results. As was shown in Fig. 10, CALIOP and Aqua MODIS exhibit similar correlations with daily PM_{2.5} for the Eastern U.S., but daily PM_{2.5}/CALIOP correlations are better than daily PM_{2.5}/Aqua MODIS correlations for the Pacific CONUS.

CALIOP near-surface extinction/hourly PM_{2.5} relationships represent the most consistent correlations solved in this study. However, more research is necessary to advance the understanding of the relationship between actively-profiled aerosol optical properties and PM_{2.5}. This is particularly important since studies have reported significant uncertainties in CALIOP AOT and extinction data (e.g., Schuster et al., 2012; Omar et

al., 2013), especially for values lower than 200 m a.g.l., which are clearly critical to resolving the most optimal CALIOP extinction/ $PM_{2.5}$ relationship. Note, however, that aside from

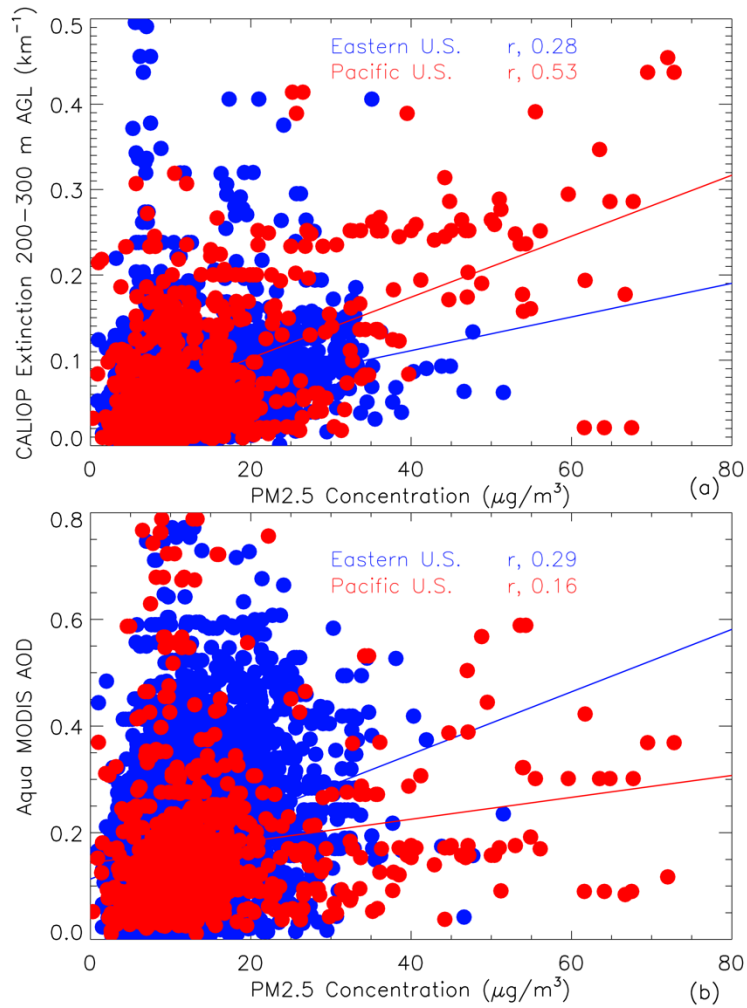


Figure 11. For the Eastern (blue) and Pacific (red) U.S. Time zones, two-year (2008-2009) scatterplots of daily $PM_{2.5}$ concentrations versus (a) cloud-free 5 km CALIOP dry mass $0.532 \mu m$ extinction at the 200-300 m a.g.l. layer (averaged within 100 km), and (b) operational Aqua MODIS AOT (averaged within 1°) and the day of each respective $PM_{2.5}$ measurement.

ground contamination issues described above, Campbell et al. (2012; 2013) argue for an additional QA step of removing CALIOP profiles from bulk averages where no aerosol

extinction is retrieved below 200 m to limit the effects of signal pulse attenuation. This effect may be further contributing to lower skill at these heights. Further, additional analysis can be further explored where the top height of the surface-detached mixed aerosol layer is known. This constraint was not considered here, and is outside the general scope of this investigation.

3.6 Conclusions

Surface measurements of particulate matter with diameters less than 2.5 μm ($\text{PM}_{2.5}$) are a frequent tool used to evaluate air quality in urban areas. Past studies have investigated the ability of using aerosol optical thickness (AOT) retrievals from passive satellite sensors as proxies for $\text{PM}_{2.5}$ concentrations. Extending from past efforts, this study explores the impact of passive satellite AOT data quality and satellite-derived surface-to-column aerosol representativeness on the $\text{PM}_{2.5}$ /AOT relationship for a two-year period (2008-2009). With a focus on the contiguous United States (CONUS), passive AOT operational Level-2 retrievals from Aqua/Terra Collection 5.1 Moderate Resolution Imaging Spectroradiometer (MODIS) and Version 22 Multi-angle Imaging Spectroradiometer (MISR) are temporally and spatially collocated for an hourly comparison with $\text{PM}_{2.5}$ measurements. Next, operational and data assimilation (DA) quality Aqua/Terra MODIS and MISR AOT datasets are analyzed against $\text{PM}_{2.5}$ on a daily temporal scale to reveal the effects that AOT data quality can exhibit with respect to $\text{PM}_{2.5}$ /AOT correlations. The representativeness of surface aerosol particle concentration to that of the entire column, as well as the correlation between surface AOT and total column AOT, are investigated using observations from Cloud-Aerosol Lidar with Orthogonal Polarization (CALIOP). CALIOP is then used to examine the relationship between near surface aerosol extinction and $\text{PM}_{2.5}$.

The conclusions of this study are summarized as follows:

- (1) Application of aggressive quality assurance (QA) procedures to passive satellite AOT retrievals increases their correlation with $PM_{2.5}$ for all of the CONUS, but significantly decreases data counts by a factor of about 2.
- (2) Correlations remain low even with aggressive QA.
- (3) Aerosol particle distributions tend to be more concentrated near the surface in the eastern CONUS and more diffuse vertically in the western CONUS. This regional variability in aerosol vertical distribution across the CONUS confirms one reason for the higher $PM_{2.5}$ /satellite AOT correlations observed in the east compared to the west.
- (4) Near-surface extinction (below 500 m a.g.l.), as measured by CALIOP, is not well representative of total column-integrated extinction (i.e., AOT). Regionally, near-surface aerosols are more representative of total column AOT in the eastern CONUS than in the western CONUS.
- (5) Correlations between near-surface CALIOP $0.532\ \mu\text{m}$ extinction and hourly $PM_{2.5}$ observations are better than can be achieved with passive AOT retrievals. However, with fewer than 100 pairs of collocated $PM_{2.5}$ and CALIOP extinction data points used, such a finding is tenuous. Additional studies are needed to further explore the possibility of accurately estimating $PM_{2.5}$ concentrations from surface extinction derived from active sensors.

In this study, it was demonstrated that estimation of $PM_{2.5}$ concentrations from satellite retrieved AOT is limited by both the quality of satellite AOT retrievals as well as the representativeness of column-integrated AOT to near surface AOT. Also, some of the past studies have shown that passive satellite AOT may be used to accurately estimate

PM_{2.5} for particular sites. However, this study shows that, even with the use of higher-quality DA AOT observations, column-integrated AOT derived from passive satellite sensors may not be used directly as accurate proxies for surface-based PM_{2.5} over broad spatial domains. As discussed earlier, this is partly attributed to differences in the aerosol surface-to-column representativeness across the CONUS. Therefore, the direct use of passive satellite AOT observations for PM_{2.5} estimation over large areas is cautioned, especially in regions where elevated aerosol plumes exist.

Additionally, as this initial study has shown, the use of near surface extinction measurements from active sensors, such as CALIOP, may provide a better PM_{2.5} estimation over broad spatial scales than column-integrated passive satellite AOT. However, ground contamination for near-surface CALIOP measurements and the effects of humidity on aerosol optical properties need further investigation. Still, satellite derived aerosol properties are of much value to PM_{2.5} studies, especially with the synergistic use of passive and active aerosol-sensitive observations, and through assimilating these quality-assured data into air-quality focused numerical models for future PM_{2.5} monitoring and forecasts.

CHAPTER IV

MINIMUM AEROSOL LAYER DETECTION SENSITIVITIES AND THEIR SUBSEQUENT IMPACTS ON AEROSOL OPTICAL THICKNESS RETRIEVALS IN CALIPSO LEVEL 2 DATA PRODUCTS

4.1 Introduction

4.1.1 Rationale

While aerosol optical thickness (AOT) may not be a good proxy for surface-based particulate matter with diameters less than 2.5 μm ($\text{PM}_{2.5}$) concentrations due to the surface-to-column representativeness issue, as explored in the previous chapter, it is natural and reasonable to investigate whether or not observations from active-based observations, like those from Cloud-Aerosol Lidar with Orthogonal Polarization (CALIOP), can be used for near surface $\text{PM}_{2.5}$ concentrations estimates. This is because CALIOP can directly observe near surface aerosol properties, which bypasses the surface-to-column representativeness issue. Still, prior to analysis, issues with CALIOP aerosol extinction retrievals need to be carefully considered. One such issue is the occurrence of retrieval fill values (RFVs) found within the CALIOP datasets, resulting from minimum aerosol layer detection sensitivities. This is important for air quality studies because the treatment of RFVs will impact the mean values of aerosol extinction, subsequently affecting their relationship with $\text{PM}_{2.5}$. Thus, in this chapter, the RFV issue is investigated through comparisons with passive satellite aerosol data.

4.1.2 Background

CALIOP measurements provide critical information on aerosol vertical distribution for studies involving aerosol modeling (e.g., Campbell et al., 2010; Sekiyama et al., 2010; Yu et al., 2010; Zhang et al., 2011; 2014), air quality (e.g., Martin, 2008; Prados et al., 2010; Toth et al., 2014), aerosol climatic effects (e.g., Huang et al., 2007; Chand et al., 2009; Tesche et al., 2014; Thorsen and Fu, 2015; Alfaro-Contreras et al., 2016;), and aerosol climatologies (Pappalardo et al., 2010; Wandinger et al., 2011; Amiridis et al., 2015; Toth et al., 2016). In addition, the column-integrated AOT derived from Level 2 (L2) CALIOP 532 nm observations is also widely used, in comparing and combining with passive-based L2 aerosol retrievals, for a comprehensive understanding of regional and global aerosol optical properties (e.g., Redemann et al., 2012). Two such passive-based systems are Aqua Moderate Resolution Imaging Spectroradiometer (MODIS), due to its proximity to CALIOP in the “A-Train” satellite constellation (Levy et al., 2013), and Aerosol Robotic Network (AERONET) sun photometers, which is the primary means for validation of satellite AOT retrievals (Holben et al., 1998).

It is well-documented that a discrepancy exists between CALIOP-derived AOTs and those from MODIS data (i.e., CALIOP retrievals lower than MODIS counterparts), albeit invoking varying quality-assurance (QA)/quality control (QC) procedures across different timeframes and spatial domains (e.g., Kacenelenbogen et al., 2011; Kittaka et al., 2011; Redemann et al., 2012; Kim et al., 2013; Ma et al., 2013). These studies tend to attribute the AOT differences to either uncertainties/cloud contamination in the MODIS retrieval, or incorrect selection of the lidar ratio (extinction-to-backscatter ratio; Campbell et al., 2013) when deriving CALIOP aerosol extinction, and subsequent AOT. In a similar fashion, CALIOP AOTs have been evaluated against AERONET-derived AOTs, with the

disparities (CALIOP lower) attributed to incorrect CALIOP lidar ratio assumptions, cloud contamination, and differences in instrument viewing angles (Schuster et al., 2012; Omar et al., 2013).

While some studies cite the failure to detect tenuous aerosol layers as a possible factor in the aforementioned AOT discrepancy (Kacenelenbogen et al., 2011; Rogers et al., 2014), the extent to which these layer detection failures contribute to the AOT differences between multiple sensors has not been fully quantified. For L2 CALIOP profiles, an extinction coefficient retrieval is performed only for those range bins where aerosol backscatter is detected above the algorithm noise floor. Otherwise, the bins are assigned fill values (RFVs) within the corresponding profile (i.e., -9999.00s; Vaughan et al., 2009; Winker et al., 2013). In fact, all L2 CALIOP extinction profiles contain a non-zero percentage of RFVs. It is thus critical to recognize that since lidar-derived AOTs reflect the integration of range-resolved extinction retrievals, in the absence of multi-spectral instruments (i.e., Raman and high spectral resolution lidars [HSRLs]), there will always be range bins where aerosol is present below the detection thresholds of the instrument. Indeed, even in relatively “clean conditions”, low extinction but geometrically deep aerosol loadings can integrate to significant AOT contributions (Reid et al., 2017).

For a fairly large subset of CALIOP daytime measurements, no aerosol is detected anywhere within a column and hence no aerosol extinction retrieved. This results in an aerosol extinction profile consisting entirely of RFVs (defined as CALIOP all-RFV profiles in this study). Assigning aerosol extinction coefficients to 0.0 km^{-1} to replace fill values during integration of the extinction coefficient profile results in a corresponding column AOT equal to zero. Note that this scenario further includes those profiles reduced to fill values in the process of applying QA procedures on a per-bin basis (e.g., Campbell et al.,

2012; Winker et al., 2013). Thus, it is plausible that a column exhibiting significant AOT may be underestimated in those cases where the aerosol backscatter is both highly diffuse and unusually deep, and thus consistently falls below the algorithm detection threshold.

The RFV issue is essentially a layer detectability problem, which has been previously investigated in regional validation studies. For example, Rogers et al. (2014) evaluated CALIOP layer and total-column AOT with the use of collocated HSRL data. Minimum detection thresholds for aerosol extinction were estimated as 0.012 km^{-1} at night and 0.067 km^{-1} during daytime (in a layer median context). From a column-integrated perspective, CALIOP algorithms were found to underestimate AOT by about 0.02 during nighttime (attributed to tenuous aerosol layers in the free troposphere). During daytime, due to the influence of the solar background signal, CALIOP algorithms were unable to detect about half of weak ($\text{AOT} < 0.1$) aerosol profiles.

At first glance, the RFV issue may seem superfluous, and one easily resolved in a subsequent study. In fact, the issue has already caused some confusion within the literature. For example, some studies (e.g., Redemann et al., 2012; Kim et al., 2013; and Winker et al., 2013) include all-RFV profiles (i.e., $\text{AOT} = 0$) for analysis when evaluating climatological AOT characteristics. Campbell et al. (2012; 2013) and Toth et al. (2013; 2016), on the other hand, do not include all-RFV profiles while generating climatological averages. Clearly, the first approach introduces an artificial underestimation of mean AOT by including profiles where AOT was not retrieved. The latter, however, presumably leads to an overestimation, since it is likely that all-RFV profiles reflect relatively low AOT cases (i.e., lower than any apparent mean sample value) where CALIOP layer detection exhibits a lack of sensitivity to diffuse aerosol presence that caused nothing to be reported within the column. As a result, Kim et al. (2013) and Winker et al. (2013) report global mean

CALIOP AOTs lower than those from Campbell et al. (2012) that does not include the profiles. Other factors (e.g., different temporal domains and QA metrics invoked) also contribute to the observed disparity in these global mean AOT computations. This state of affairs indicates a clear need to carefully quantify the occurrence frequency of all-RFV profiles on a global scale, and, if possible, derive representative column-integrated AOT values for RFV profiles.

Further, and as introduced above, for non-all-RFV profiles there remain range bins with RFVs where low aerosol extinction is likely present (the sum of which, however, can result in a relatively significant AOT). Though some QA can filter obvious cases of attenuation-limited profiles (e.g., require aerosol presence within 250 m of the surface as in Campbell et al., 2012; 2013), the only current remedy otherwise is to accept RFV bins as equal to zero extinction, then integrating to obtain a column AOT estimate. It is compelling to investigate, in a manner similar to Rogers et al. (2014), what this quantitative effect is for climatological analysis.

In this study, using four years (2007-2008 and 2010-2011) of daytime observations from CALIOP, Aqua MODIS, and AERONET, the RFV issue is investigated with an emphasis on the following questions:

- (1) What is the frequency of occurrence of all-RFV profiles in the daytime cloud-free CALIOP data set?
- (2) By collocating MODIS and AERONET AOTs with CALIOP cloud-free all-RFV profiles, what is the modal AOT associated with this phenomenon and how randomly are the data distributed as a function of passive-derived AOT?
- (3) What is the quantitative underestimation in CALIOP AOT due to RFVs in profiles where extinction is retrieved?

- (4) How much of the discrepancy between MODIS and CALIOP L2 over-ocean AOT retrievals can be explained by RFVs and all-RFV profiles?

Note that the primary CALIOP laser failed in March 2009, forcing the Cloud-Aerosol Lidar and Infrared Pathfinder Satellite Observations (CALIPSO) mission team to switch to a secondary laser. Therefore, two years of CALIOP aerosol data are analyzed prior to, and after, the switch to investigate any discernible difference in RFV statistics between the two lidar profiles.

4.2 Datasets

4.2.1 CALIOP

Orbiting aboard the CALIPSO satellite within the “A-Train” constellation (Stephens et al., 2002), CALIOP is a two-wavelength (532 and 1064 nm) polarization-sensitive (at 532 nm) elastic backscatter lidar, observing the vertical distribution of aerosols and clouds in Earth’s atmosphere since June 2006 (Winker et al., 2010). The 532 nm backscatter profiles measured by CALIOP are used to detect aerosol and cloud features and then retrieve corresponding particle extinction and subsequent AOTs (i.e., column-integrated extinction; Young and Vaughan, 2009) within layer boundaries determined by a multi-resolution layer detection scheme (Vaughan et al., 2009) and the assumption of a lidar ratio based upon aerosol or cloud type (Omar et al., 2005; 2009). For this study, 532 nm aerosol extinction coefficient data from the Version 3 (V3) CALIPSO L2 5 km Aerosol Profile (L2_05kmAProf) product are utilized (Winker et al., 2009; hereafter in this chapter, all references to CALIOP data imply the 532 nm channel/product). These aerosol profiles are reported in 5 km segments and feature a vertical resolution of 60 m below an altitude of 20.2 km above mean sea level (AMSL). Only CALIOP data collected during daytime

conditions are considered for this study, such that comparison with aerosol observations from MODIS and AERONET can be accomplished.

Prior to analysis, advanced QA procedures are performed on the L2_05kmAProf product. This QA scheme is similar to that employed in Campbell et al. (2012) and Winker et al. (2013), and involves several parameters included in the L2_05kmAProf product: Extinction_Coefficient_532 (≥ 0 and $\leq 1.25 \text{ km}^{-1}$), Extinction_QC_532 (= 0, 1, 2, 16, or 18), CAD_Score (≥ -100 and ≤ -20), and Extinction_Coefficient_Uncertainty_532 ($\leq 10 \text{ km}^{-1}$). The Integrated_Attenuated_Backscatter_532 ($\leq 0.01 \text{ sr}^{-1}$) parameter from the L2 5 km Aerosol Layer (L2_05kmALay) product is also used as a QA metric. A detailed description of these QA checks is also outlined in a recent CALIOP-based study (Toth et al., 2016; Chapter VI of this dissertation). Extinction retrievals reported in the CALIOP data products that do not pass the full suite of QA tests are converted to RFVs. To limit the influence of clouds on this analysis (i.e., in order to ensure that the RFV issue is occurring due to layer detection sensitivity and not because of attenuation effects caused by cloud presence), each aerosol profile is cloud-screened using the Atmospheric Volume Description (AVD) parameter. The strictest cloud-screening possible is implemented, as profiles are flagged “cloudy” if any of the bins within the CALIOP column are classified as cloud.

4.2.2 Aqua MODIS

As an integral part of the payloads for NASA’s Terra and Aqua satellites, MODIS is a 36 channel spectroradiometer with wavelengths ranging from 0.41 microns to 15 microns. Seven of these channels (0.47-2.13 microns) are used to retrieve aerosol optical properties,

such as AOT (e.g., Levy et al., 2013). MODIS L2 aerosol products are reported at a spatial resolution of $10 \times 10 \text{ km}^2$ at nadir, with a reported over-ocean expected error of $(-0.02 - 10\%)$, $(+0.04 + 10\%)$ (Levy et al., 2013). However, uncertainties for individual retrievals may be larger (Shi et al., 2011c). Also, thin cirrus contamination may exist in the MODIS aerosol products (e.g., Toth et al., 2013). In this study, the Effective_Optical_Depth_Best_Ocean (550 nm) parameter in the L2 Collection 6 (C6) Aqua MODIS aerosol product (MYD04_L2; Levy et al., 2013) is utilized. Only those retrievals flagged as “Good” and “Very Good” are considered for analysis, as determined by the Quality_Assurance_Ocean parameter within the MYD04_L2 files.

4.2.3 AERONET

Developed for the purpose of furthering aerosol research and validating satellite retrievals, NASA’s AERONET program is a federated worldwide system of ground-based sun photometers that collect measurements of aerosol optical and radiative properties (Holben et al., 1998). With a reported uncertainty of $\pm 0.01 - 0.02$ (although this estimate is low in the presence of unscreened cirrus clouds; e.g., Chew et al., 2011), AOTs are derived at several wavelengths ranging from 340 nm to 1640 nm. Due to the lack of retrievals at the CALIOP wavelength, AOTs at 532 nm are computed from interpolation of those derived at the 500 and 675 nm channels using an Ångström relationship (e.g., Shi et al., 2011c; Toth et al., 2013). The highest quality V2.0 AERONET data (Level 2.0) are used in this study, as these are both cloud-screened and quality-assured (Smirnov et al., 2000). Also, only observations from coastal/island AERONET sites are considered for comparison with over-ocean CALIOP profiles, despite the potential overestimation of

CALIOP AOT in coastal regions due to the CALIPSO aerosol typing algorithms (e.g., Kanitz et al., 2014).

4.3 Results and Discussion

4.3.1 Demonstrating how CALIOP backscatter distribution can render profiles of all RFVs

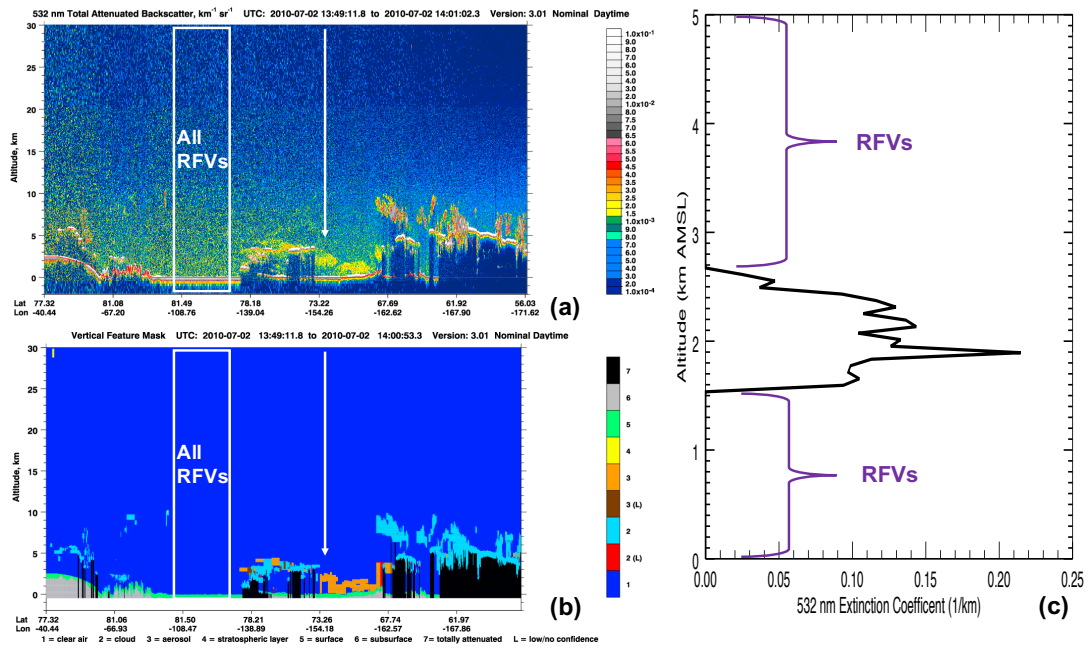


Figure 12. For data collected during daytime on July 2nd, 2010 over the Arctic, browse image curtain plots of CALIPSO (a) 532 nm total attenuated backscatter ($\text{km}^{-1} \text{sr}^{-1}$) and (b) corresponding vertical feature mask (VFM). The white box represents an example segment of the granule for which range bins in the associated Level 2 (L2) aerosol extinction coefficient profile are all retrieval fill values (RFVs), as the VFM classified these bins as either surface (green) or clear air (blue) features. The white arrow indicates a column in which some aerosol has been detected (orange), and the resultant L2 aerosol extinction profile for this column is shown in (c).

To demonstrate the nature of the RFV problem, Fig. 12 shows an example of cloud free all-RFV CALIOP profiles embedded within curtain plots of total attenuated backscatter (TAB; Fig. 12a) and matching vertical feature mask (VFM; Fig. 12b). Both plots were obtained from the CALIPSO Browse Images website (<https://www->

calipso.larc.nasa.gov/products/lidar/browse_images/production/), and the data were collected from CALIOP during daytime on July 2nd, 2010 over the Arctic. The VFM shows that the range bins within the white box are classified as either surface or clear air features, and thus the corresponding L2 aerosol extinction coefficient profiles (not shown) are all-RFVs (i.e., the AOT=0 scenario).

However, even under pristine conditions, aerosol particles are still present in the atmosphere. For example, the baseline maritime AOT is estimated to be 0.06 ± 0.01 (Kaufman et al., 2005; Smirnov et al., 2011). Thus, aerosol particles are likely present and yet undetected for the all-RFV cases shown in Fig. 12. Similar issues can also exist for profiles for which some aerosol is detected. This scenario is represented by the white arrow in the TAB and VFM plots, and the associated L2 aerosol extinction coefficient profile is depicted in Fig. 12c. An aerosol layer is evident from about 1.5 to 2.5 km AMSL, leaving the remainder of the column as RFVs.

To further demonstrate the RFV phenomenon in the CALIOP dataset, differences in TAB found in profiles where all-RFV were reported and those where some extinction was retrieved are next examined. The CALIPSO Lidar Level 1.5 data product (L1.5) is specifically leveraged for this task, as TAB for the all-RFVs class of data is not included in L2 datasets. The L1.5 product is a merging of the L1 and L2 products, cloud-cleared, screened for non-aerosol features (e.g., surface, subsurface, totally attenuated, invalid, etc.), and available at 20 km (horizontal) and 60 m (vertical) resolutions (Vaughan et al., 2011). One month (February 2008) of daytime L1.5 TAB profiles over all global oceans were collocated with CALIOP AOTs derived from the L2_05kmAProf product. The data were limited to only those L1.5 averages that contain either four contiguous 5 km L2 all-RFV profiles, or, conversely, four contiguous profiles where extinction was retrieved in each.

The selected TAB profiles were then averaged to a 20 km resolution for each altitude range (i.e., to obtain over global ocean mean TAB profiles).

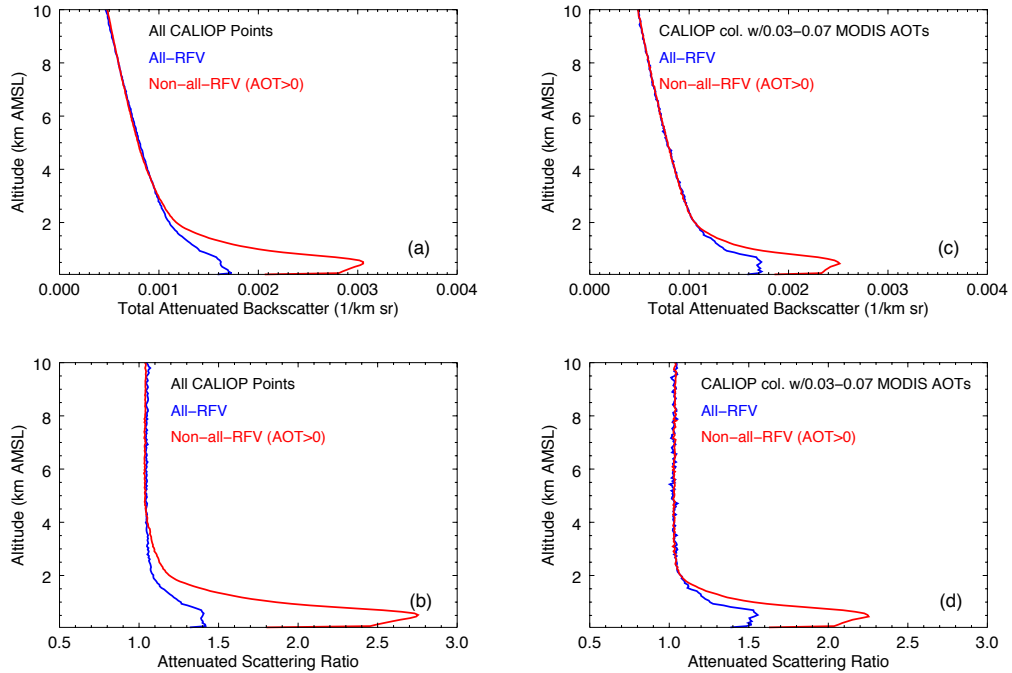


Figure 13. For February 2008, mean profiles of (a, c) Level 1.5 total attenuated backscatter (TAB) and (b, d) attenuated scattering ratio (TAB/molecular attenuated backscatter) over global oceans, corresponding to Level 2 all-RFV (in blue) and non-all-RFV (AOT > 0; in red) profiles. The left column is from an analysis of all cloud-free CALIOP points over global oceans and the right column represents only those collocated with MODIS AOTs between 0.03 and 0.07.

The results of this analysis are shown in Fig. 13. Profiles of mean TAB over global oceans for February 2008 are shown in Fig. 13a; blue lines show all-RFV profiles and red lines show those where some extinction was retrieved (i.e., non-all-RFVs). For most of the troposphere, little difference is observed between the two profiles (i.e., “clear sky” in the aggregate). However, the profiles begin to deviate below 3 km AMSL, as larger TAB are found for the extinction-retrieved sample (peak TAB is $\sim 0.0031 \text{ km}^{-1} \text{ sr}^{-1}$) compared to those profiles consisting of all-RFVs (peak TAB value is $\sim 0.0017 \text{ km}^{-1} \text{ sr}^{-1}$). An additional

analysis was conducted (not shown) using data over the Pacific Ocean to check for influences of geographic sampling (i.e., aerosol distribution) on the mean TAB profiles. Both the all-RFV and non-all-RFV mean TAB profiles increase at similar magnitudes after implementing this restriction, thus resulting in only a minor difference between the profiles.

Figure 13c shows a second pair of mean TAB profiles, but now restricted to only those L2 CALIOP profiles collocated with MODIS AOTs between 0.03 and 0.07 (i.e., arbitrarily selected for low aerosol loading scenarios). The collocation method applied here is the same as the one used by Toth et al. (2013), where the midpoint of a 10 x 10 km² (at nadir) over-ocean MODIS AOT pixel is required to be within 8 km of the temporal midpoint of a 5 km L2 CALIOP aerosol profile. Observations outside this range are not considered. Whereas below, the modal MODIS AOT for passive retrievals collocated with all-RFV CALIOP profiles is about 0.05, this restriction (i.e., 0.03-0.07 MODIS AOTs) is meant to investigate a more nuanced question. The presence of all-RFV profiles is the result of several processes that can work either independently or in tandem. The dominant cause is, as described above, detection failure. RFVs also occur when the cloud-aerosol discrimination algorithm mistakenly classifies an aerosol layer as a cloud, and again when the extinction coefficients retrieved for a detected aerosol layer fail any of the QA metrics (e.g., an out-of-range extinction QC flag). This restriction is meant to limit the influence of layer misclassifications and occasional QA failures, and in particular relatively high AOT cases where unusually high TAB could influence the mean profile. Including such samples would degrade the accuracy of the TAB noise floor estimate that will be used in subsequent analyses described in Sec. 4.3.5. Relatively speaking, though, the profiles in Fig. 13c are fairly similar to those of Fig. 13a. However, the relative deviation between the two samples now occurs below 2 km AMSL, and the peak value of TAB for non-all-RFVs lowers to

around $0.0025 \text{ km}^{-1} \text{ sr}^{-1}$ (illustrating the effect of the MODIS AOT restriction). Also, for context, corresponding profiles of attenuated scattering ratio (TAB/molecular attenuated backscatter) are included for both analyses in Figs. 13b and 13d.

The initial point of this comparison is that the mean TAB for all-RFV profiles is, as expected, lower than in those profiles where extinction is retrieved above and within the planetary boundary layer. Thus, the figures represent a simple conceptual model of how profiles consisting of all-RFV cases arise with respect to diffuse aerosol backscatter structure and inherently lower signal-to-noise ratios (SNRs). While there are several possible strategies for mitigating this issue for future global satellite lidar missions (discussed in the concluding remarks), the goal for this initial part of the study is to simply depict how the situation is manifested in the base backscatter product measured by the sensor.

4.3.2 Frequency of occurrence for L2 CALIOP all-RFV aerosol profiles

The next step of the analysis is to determine the frequency of occurrence of all-RFV profiles in the daytime CALIOP L2_05kmAProf archive. As these data will be collocated with both MODIS and AERONET data for subsequent analysis, no nighttime data are considered here. Table 6 summarizes the statistics of this analysis. For the 2010-2011 period, all-RFV profiles make up about 71% (66%) of all daytime CALIOP L2_05kmAProf profiles globally (global oceans-only). However, these statistics include those profiles for which the CALIOP signal was totally attenuated (e.g., by an opaque cloud layer), thus inhibiting aerosol detection near the surface. For context, the 2010-2011 occurrence frequencies of CALIOP not detecting the surface are 39.9% (46.1%) globally (global oceans-only). Roughly 30% of the full archive corresponds with cloud-free conditions (where again, as described in Sec. 4.2.1, “cloud-free” refers to the implementation of the

strictest CALIOP cloud-screening possible where no clouds are classified in the entire profile). Approximately 45% of all cloud-free profiles, and 25% of cloud-free over ocean profiles, are also all-RFV profiles (~15% and 8%, respectively, in absolute terms). The over-ocean sample is next considered below, given the relatively higher fidelity expected in the collocated MODIS AOT data (e.g., Levy et al., 2013).

Note that due to the primary CALIOP laser failing in 2009, Table 6 also includes results from a two-year period (2007-2008) before the laser switch to examine any differences in the statistics of the RFV issue between the two lasers. The global frequency of occurrence of all-RFV profiles is consistent for both time periods (i.e., 70.4% for 2007-2008 and 71.1% for 2010-2011), and thus the remainder of this study focuses on the 2010-2011 analysis alone. No evidence is found to suggest that laser performance exhibits any significant influence on the occurrence of per-range bin RFVs and all-RFV profiles within the L2 archive.

Table 6. Statistical summary of the results for this study, for the 2007-2008 and 2010-2011 periods, both globally and for global oceans only. The values in bold and parentheses represent the percentages of each category relative to the entire CALIOP aerosol profile archive for each respective period.

Number of 5 km CALIOP Profiles	Globe		Global Oceans	
	2007-2008	2010-2011	2007-2008	2010-2011
Total	41,929,328	41,188,208	27,742,947	27,198,000
All-RFV	29,503,781 (70.4%)	29,297,919 (71.1%)	18,190,188 (65.6%)	18,026,930 (66.3%)
Cloud-free	13,317,918 (31.8%)	13,190,530 (32.0%)	8,006,719 (28.9%)	7,812,682 (28.7%)
Cloud-free & all-RFV	5,764,098 (13.7%)	5,899,221 (14.3%)	2,089,865 (7.5%)	2,101,155 (7.7%)
Cloud-free, all-RFV, & MODIS AOT \geq 0	791,570 (1.9%)	814,514 (2.0%)	781,983 (2.8%)	803,546 (3.0%)

The spatial distribution of daytime over-ocean cloud-free all-RFV profiles is shown in Fig. 14. The percentage of cloud-free CALIOP all-RFV aerosol profiles relative to all

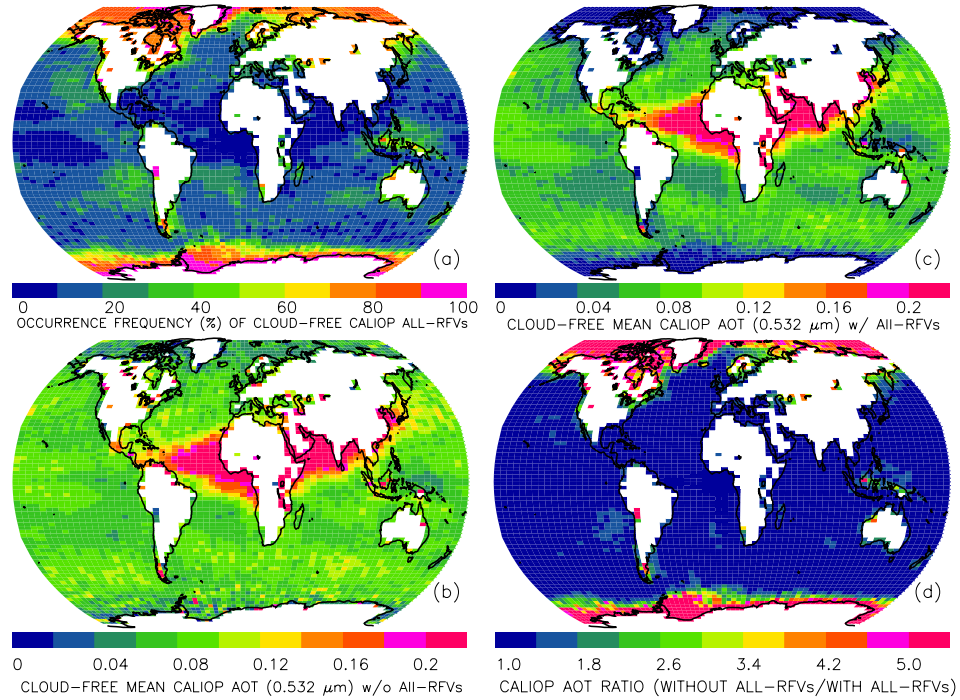


Figure 14. For 2010-2011, (a) the frequency of occurrence (%) of cloud-free CALIOP profiles at $2^\circ \times 5^\circ$ latitude/longitude grid spacing. Also shown are the corresponding cloud-free mean CALIOP column AOTs (b) without and (c) with all-RFV profiles, and (d) the ratio of (b) to (c).

cloud-free CALIOP aerosol profiles is computed and presented on a $2^\circ \times 5^\circ$ latitude/longitude grid (Fig. 14a). Here again the analysis is restricted to cloud-free scenes to avoid ambiguities in RFV occurrence that are introduced by the presence of clouds. Regions with the largest occurrence frequencies of all-RFV profiles ($>75\%$) include the high latitudes of both the Northern and Southern Hemispheres (NH and SH, respectively). In fact, over snow surfaces, over 80% of CALIOP aerosol profiles are all-RFVs. Over permanent ice (e.g., Greenland), $\sim 99\%$ are all-RFVs. In contrast, the Tropics exhibit the lowest RFV profile occurrence frequencies ($<25\%$). The CALIOP archive contains a significant fraction of all-RFV profiles in polar regions, which is an important result with

many ramifications for NASA Earth Observing System science. It is likely that all-RFVs correlate with both low aerosol loading scenarios and high albedo surfaces (e.g., snow and sea ice).

Figure 14 also includes the spatial distribution of mean cloud-free CALIOP-derived AOT ($2^\circ \times 5^\circ$ latitude/longitude resolution) without (Fig. 14b) and with (Fig. 14c) all-RFV profiles, demonstrating the quantitative impact of adding all-RFV AOT=0 profiles to the relative analysis. As mentioned above, both approaches have been implemented in past studies. Comparison of the plots reveals that including the all-RFV profiles in the average naturally lowers the mean AOT. To determine the areas for which mean AOTs are most impacted by all-RFVs, the ratio of mean AOT without and with all-RFV profiles (i.e., the ratio of Fig. 14b to 14c) is shown in Fig. 14d. Little change in mean AOT is found for most of the oceans, with the exception of the high latitudes of each hemisphere. Overall, global ocean cloud-free mean AOT values of ~ 0.09 and ~ 0.07 are found, without and with all-RFV profiles, respectively. Such decrease of mean AOT is expected, as 27% of CALIOP L2 over-ocean cloud-free aerosol profiles are all-RFVs. Also, regions with the largest all-RFV occurrence frequencies (i.e., high latitudes of both the NH and SH) correspond with a greater lowering of mean AOT, compared with those regions (i.e., the Tropics) where small all-RFV occurrence frequencies dominate.

4.3.3 Collocation of MODIS AOT for over-ocean CALIOP all-RFV cases

By collocating MODIS over-ocean AOT retrievals with CALIOP all-RFV profiles, the distribution of AOT when algorithm detection/retrieval performance has been compromised can be estimated. After collocation was performed (as described in Sec. 4.3.1), the number of all cloud-free CALIOP all-RFV profiles were binned by MODIS

AOT in 0.01 increments (as depicted in Fig. 15), and separated into three latitude bands: the NH mid-latitudes (30° to 60° N; Fig. 15a), the Tropics (-30° to 30° N; Fig. 15b), and the SH mid-latitudes (-60° to -30° N; Fig. 15c) where coincident data densities are reasonably sufficient. For example, see Fig. 16a for numbers of valid MODIS over-ocean AOT data points available for collocation at $2^{\circ} \times 5^{\circ}$ latitude/longitude, based on “Good” or “Very Good” over-ocean L2 MODIS AOT retrievals, relative to all corresponding retrievals. For context, Fig. 16b shows the associated spatial distribution of mean L2 MODIS AOT. Note that this includes only those MODIS points collocated with CALIOP,

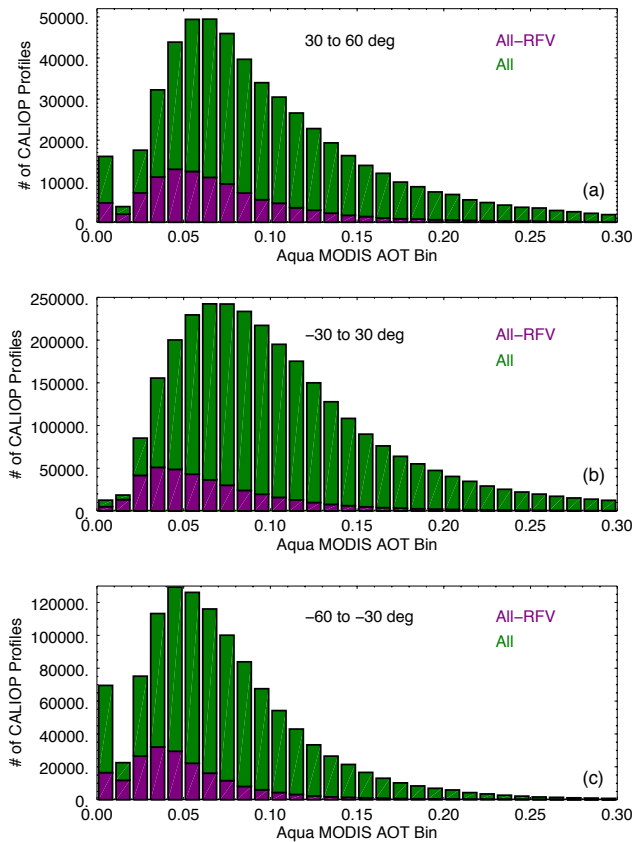


Figure 15. For 2010-2011, histograms of all over-ocean cloud-free CALIOP profiles (in green) and all-RFV profiles (in purple) as a function of collocated Aqua MODIS AOT (0.01 bins), for (a) 30° to 60° N, (b) -30° to 30° N, and (c) -60° to -30° N.

and thus the AOT distributions shown in Fig. 16b are likely different from distributions derived using the full MODIS data record (e.g., Levy et al., 2013). Also note, for the reference of the reader, that histograms of C6 MODIS AOT (not collocated with CALIOP) are provided in Levy et al. (2013).

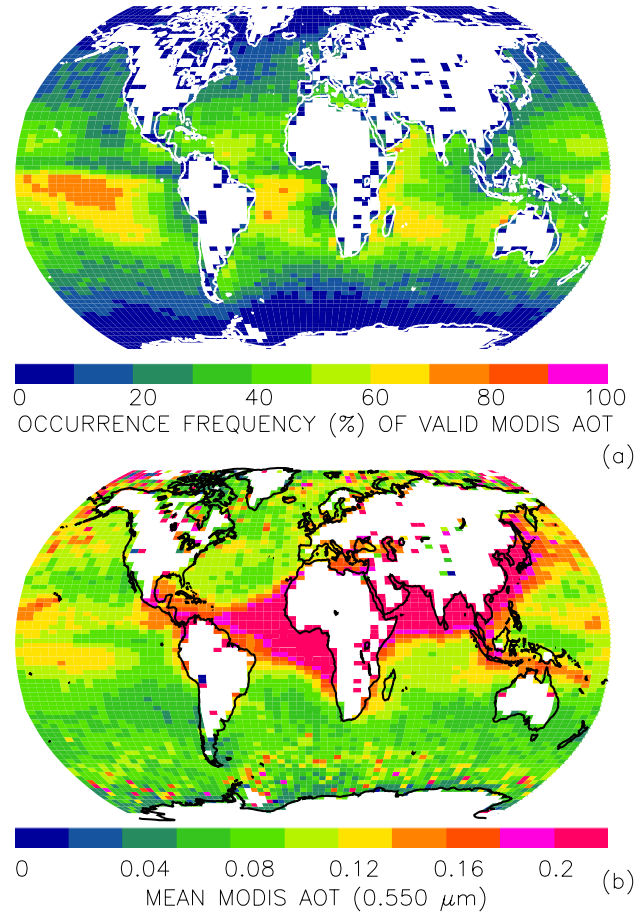


Figure 16. For 2010-2011, (a) frequency of occurrence (%) of valid (“Good” or “Very Good”) over-ocean Level 2 (L2) MODIS AOT retrievals, relative to all over-ocean L2 MODIS AOT retrievals, for every $2^\circ \times 5^\circ$ latitude/longitude grid box. Also shown is (b) the corresponding spatial distribution of mean L2 MODIS AOT for the same time period. This analysis includes only those MODIS points collocated with CALIOP.

Modal values of MODIS AOT for all-RFV profiles are found between 0.03 and 0.04, with the exception of the 30° to 60° N band for which the greatest number of all-RFV

profiles coincide with MODIS AOTs between 0.04 and 0.05. Thus, the primary mode of CALIOP RFV profiles is 0.03-0.05 from the perspective of MODIS. Corresponding mean and median MODIS AOTs for collocated CALIOP all-RFV profiles are presented in Table 7, with a mean value of 0.07 for the Tropics and NH mid-latitudes, and 0.05 for the SH mid-latitudes band (global mean of 0.06). Median AOTs are similar, though slightly lower, with a global median of 0.05, reflecting the impact of the tail toward higher AOT in the sample distributions. Several modes of algorithm response contributing to these distributions are expected, which are borne out in the CALIOP data: layer detection failures due to sensitivity limits, random noise in the attenuated backscatter measurement, and extinction retrieval failures.

Table 7. Mean, median, and standard deviation of AOTs derived from Aqua MODIS (2010-2011) and AERONET (2007-2008; 2010-2011), both independently collocated with CALIOP all-RFV profiles.

Region	MODIS			AERONET		
	Mean	Median	Standard Deviation	Mean	Median	Standard Deviation
90°S to 60°S	0.05	0.04	0.10	-	-	-
60°S to 30°S	0.05	0.04	0.11	0.04	0.04	0.01
30°S to 30°N	0.07	0.06	0.11	0.10	0.10	0.19
30°N to 60°N	0.07	0.06	0.13	0.09	0.08	0.07
60°N to 90°N	0.07	0.06	0.17	0.05	0.04	0.04
Globe	0.06	0.05	0.12	0.08	0.07	0.11

While a similar distribution is exhibited for each region, the number of total observations for the Tropics is much greater than that of the other two regions. Thus, the results of Fig. 15b are more robust, which is primarily due to MODIS AOT data availability and collocation (Fig. 16a). Total MODIS occurrence frequencies are greatest

in the Tropics (generally >50%), decreasing poleward. The mid-latitude regions exhibit occurrence frequencies less than 25%, with near-zero frequencies observed in the high latitudes of the NH and SH. Note the low number of valid MODIS AOT retrievals in the high Northern and Southern latitudes, due at least partly to sea ice extent in these regions, presents a limitation for this study. That is, the areas for which all-RFV profiles occur most frequently (Fig. 14a) are the same areas with the least numbers of valid MODIS AOT retrievals. Note that in these regions, even for valid MODIS AOT retrievals, biases due to sub-pixel sea ice contamination may still exist.

All-RFV profile occurrence frequencies are computed as a function of MODIS AOT, in order to quantify the amount of CALIOP-derived AOT underestimation at a given MODIS-based AOT. Achieved by division of corresponding data counts in Fig. 15, this underestimation (expressed as a percentage) is shown in line plots in Fig. 17. The same regional sorting and MODIS AOT binning procedures from Fig. 15 are applied. A similar distribution is found for all three latitude bands, with the 0.01-0.02 MODIS AOT bin exhibiting the largest underestimation percentage that gradually lowers toward higher MODIS AOT. CALIOP all-RFV underestimation near 50% is found for the NH and SH mid-latitude regions (the red and black curves, respectively, of Fig. 17), respectively, for MODIS AOTs between 0.01 to 0.02, and this value increases to about 70% for the Tropics (the blue curve of Fig. 17). This implies that 70% of all CALIOP aerosol profiles in this MODIS AOT range are underestimated (i.e., CALIOP reports all-RFV profiles 70% of the time for MODIS AOTs between 0.01 and 0.02).

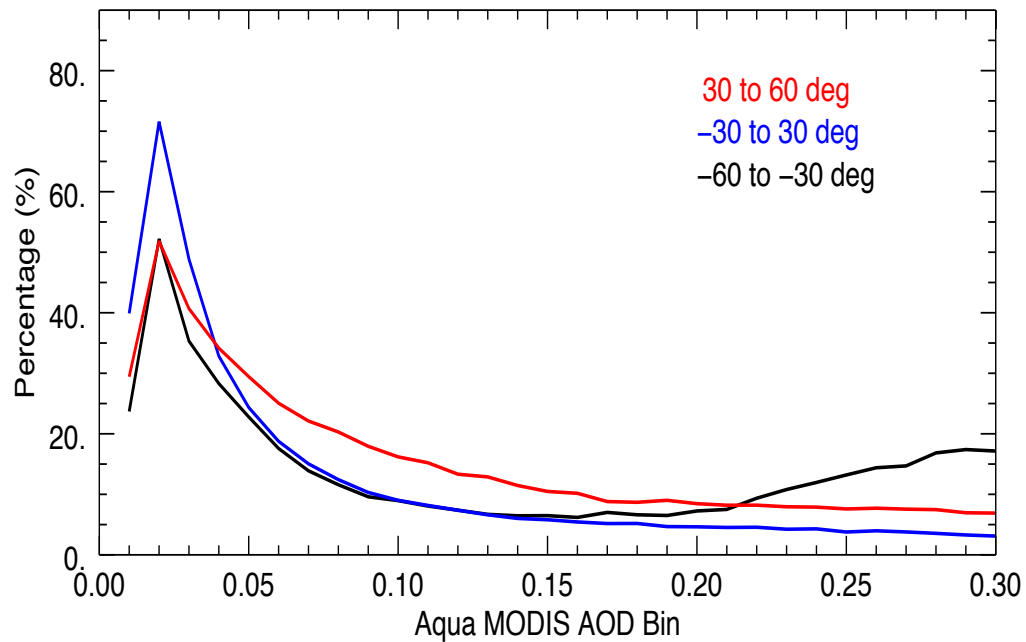


Figure 17. 2010-2011 frequency of occurrence (%) of over-ocean cloud-free CALIOP all-RFV profiles, relative to all cloud-free CALIOP profiles, as a function of collocated Aqua MODIS AOT (0.01 bins), for 30° to 60° N (in red), -30° to 30° N (in blue), and -60° to -30° N (in black).

While the distribution for the Tropics is considered most robust, due to MODIS AOT availability in this region, it is important to note that increasingly lower AOTs (i.e., below ~0.03) are within the uncertainty range of MODIS AOT retrievals, and thus these results should be interpreted within the context of this caveat. Also, the relatively low underestimation percentages corresponding with MODIS AOTs less than 0.02 are believed to be an error, likely resulting from an artifact in the MODIS AOT retrievals/products.

4.3.4 Collocation of CALIOP all-RFV Profiles with AERONET

AERONET data are considered the benchmark for satellite AOT retrievals (Holben et al., 1998). Thus, similar to the over-ocean MODIS analysis above, CALIOP AOT and all-RFV profiles are examined using collocated AOTs derived from measurements collected at coastal and island AERONET sites. Ninety-three sites are used, the locations of which are depicted globally in Fig. 18. Similar to Sec. 4.3.2, CALIOP L2_05kmAProf data are spatially (within 0.4° latitude/longitude) and temporally (within 30 minutes) collocated with Level 2.0 AERONET data. Note that all four years (2007-2008 and 2010-2011) are included for this analysis, as there are far fewer AERONET data points available in contrast to MODIS (e.g., Omar et al., 2013).

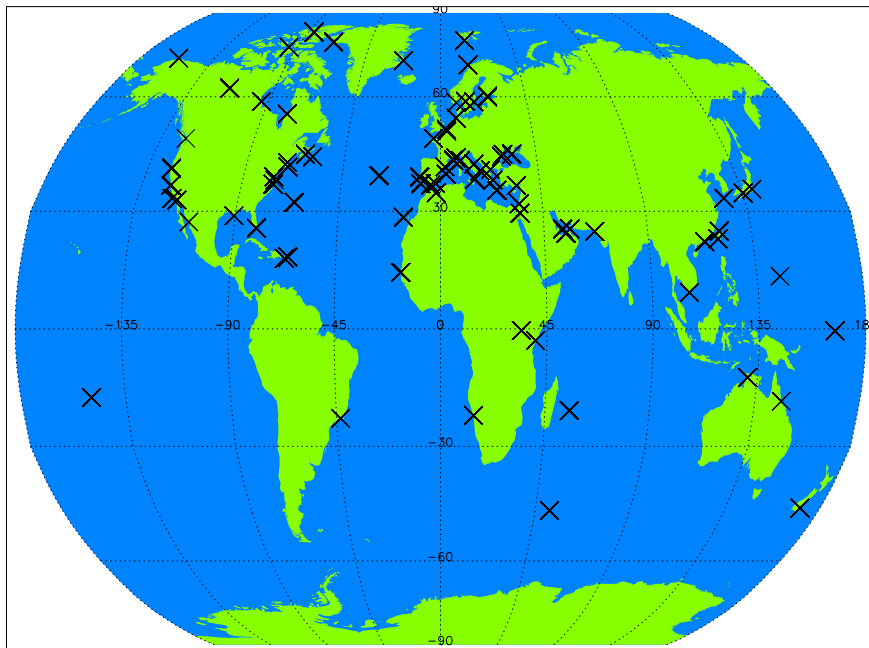


Figure 18. Map of the ninety-three coastal/island AERONET sites with Level 2.0 data, for the 2007-2008 and 2010-2011 periods, used for collocation with over-ocean CALIOP aerosol observations.

Figure 19 summarizes the results of the CALIOP/AERONET collocation. In a similar manner as Fig. 15, Fig. 19a is a histogram of the number of cloud-free CALIOP aerosol profiles (all-RFV profiles and all available) for each 0.01 AERONET AOT bin. The overall distribution observed here is comparable to that from MODIS (Fig. 15), but noticeably noisier due to the limited AERONET data sample size. However, peak counts of all-RFV profiles occur for AERONET AOTs between 0.04 and 0.05, which is roughly consistent with the MODIS comparisons. The corresponding mean AERONET AOTs of collocated CALIOP all-RFV profiles are generally higher than those found from MODIS, with values of 0.1 and 0.09 for the Tropics and NH mid-latitudes, respectively (Table 7), and a global mean (median) value of 0.08 (0.07). Note that this analysis may be influenced by residual cloud contamination of subvisible cirrus in the AERONET dataset (e.g., Chew et al., 2011; Huang et al., 2012). Also note that histograms of sun photometer derived AOT from Maritime Aerosol Network (MAN) observations (i.e., over-ocean component of AERONET; not collocated with CALIOP data) are shown in Smirnov et al. (2011).

Figure 19b shows all-RFV profile occurrence frequencies as a function of AERONET AOT, computed by dividing the respective counts in Fig. 19a. Again, a noisier overall distribution is found compared with the line plots of Fig. 17. As expected, the 0.01-0.02 bin exhibits the largest underestimation percentage. However, while this value is 70% for the MODIS analysis (the blue curve of Fig. 17), it increases to 100% for AERONET, and again it is concluded that an artifact is likely present in the MODIS retrievals for very low aerosol loading cases. While the sample size is small, in the 4-year data set examined in this study, whenever AERONET measured an AOT lower than 0.02 the collocated CALIOP aerosol profiles contained only RFVs.

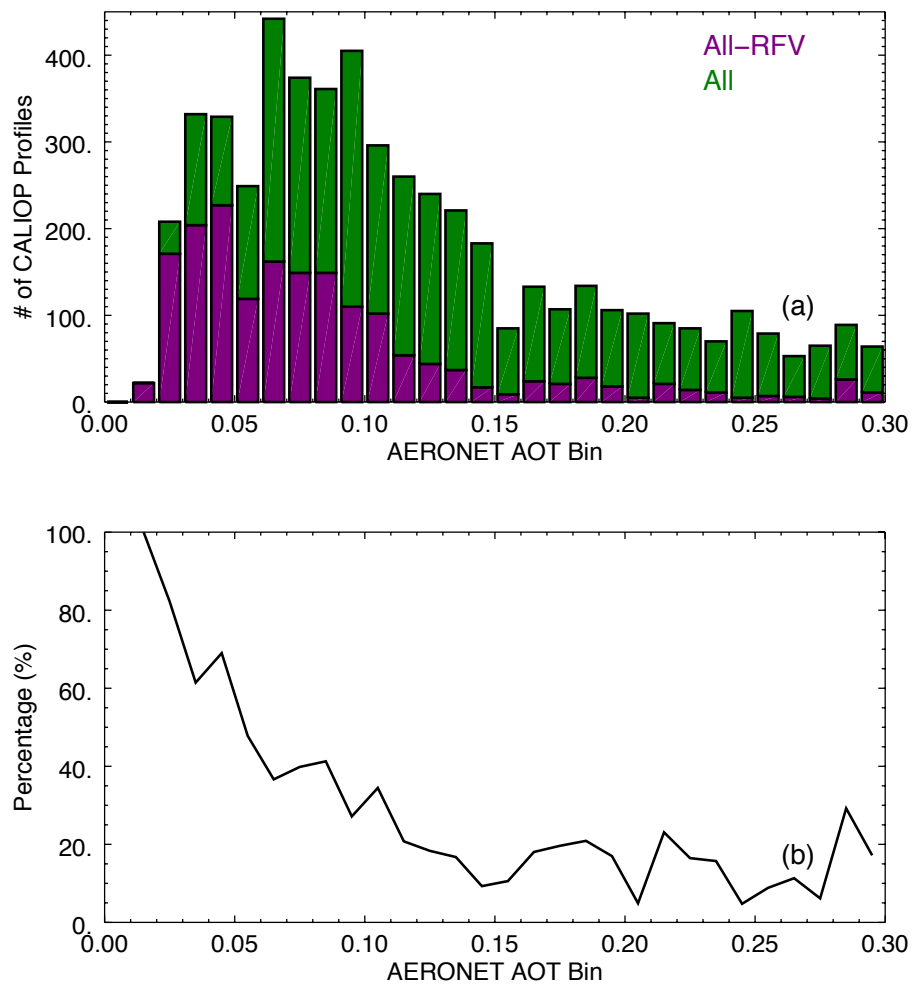


Figure 19. For the 2007-2008 and 2010-2011 periods, (a) histograms of all cloud-free CALIOP profiles (in green) and all-RFV profiles (in purple), and (b) corresponding frequency of occurrence (%) of cloud-free CALIOP all-RFV profiles, relative to all cloud-free CALIOP profiles, both as a function of collocated coastal/island AERONET AOT (0.01 bins).

4.3.5 Reconciling CALIOP AOT Underestimation

In this part of the study, a proof-of-concept analysis is described, that uses one-month of data with the same spatio-temporal domain and conditions introduced in Sec. 4.3.1 to estimate the nominal underestimation of CALIOP AOT due to RFVs in otherwise high-fidelity L2 retrievals (i.e., those where extinction is derived and the profile passes all

QA/QC tests). This is achieved by retrieving extinction profiles from the mean global TAB profiles previously constructed from all-RFV profiles (i.e., as presented in Fig. 13). Characterizing these profiles, including those derived for all corresponding/collocated MODIS AOT (Fig. 13a, with an average MODIS AOT of 0.067) and MODIS AOT between 0.03 and 0.07 (Fig. 13c, with an average MODIS AOT of 0.045) to suppress the influence of random algorithm failure events at relatively high AOT, as TAB “noise floors”, RFV bins with corresponding extinction are then replaced and column-integrated AOT is calculated. The premise here assumes that the distribution of aerosol depicted in the TAB noise floors is constant globally. This is highly uncertain, and it is strongly cautioned that the purpose is to provide an initial demonstration of a practical way to correct RFVs in the CALIOP archive.

The aerosol extinction profiles for all-RFVs are derived in two steps. First, using an assumed lidar ratio of 29 sr (standard deviation of 10 sr; derived from constrained lidar ratios over ocean and represents background aerosols for the entire atmospheric column; Kim et al., 2017), an unconstrained extinction solution is generated from 20 km to the top of the surface-attached layer (3.5 km). In this step, the molecular and aerosol attenuation in the measured backscatter is accounted for at each range bin (from a top-down approach) by taking into account the overlying molecular and aerosol loading. The aerosol backscatter is then calculated by subtracting the unattenuated molecular backscatter from the newly derived aerosol-and-molecular-attenuation-corrected backscatter, from which the aerosol extinction is derived by multiplication of the lidar ratio. The top of surface-attached layer is determined by inspection of the ratio between the measured backscatter and the modeled molecular attenuated backscatter, as provided in the CALIPSO L1.5 product. Integrating this extinction profile provides an estimate of the AOT overlying the

surface-attached layer (AOT_{upper}). The derived AOT_{upper} values are ~ 0.015 and ~ 0.01 for the total all-RFV sample and AOT-limited sample, respectively. These values are not surprising, as they are in agreement with AERONET measurements obtained at the Mauna Loa site (elevation of ~ 3.5 km AMSL; Alfaro-Contreras et al., 2016).

Next, a constrained extinction solution and optimized estimate of the lidar ratio are generated from 3.5 km to the surface using the AOT of this layer (i.e., column AOT – AOT_{upper}). This step is similar to the above-mentioned approach, except now an iterative process is implemented to derive a lidar ratio for the layer. Resulting surface-attached layer lidar ratios are 43 sr and 30 sr, for the first and second case respectively, with the latter value comparing reasonably well with the coastal marine lidar ratio of ~ 28 derived from AERONET analyses (Sayer et al., 2012). However, the lidar ratio solved for the all-RFV sample case is higher than that typical of marine aerosols (i.e., ~ 26 ; Dawson et al., 2015), which may be a result of uncertainties in both MODIS and CALIOP datasets. For example, the uncertainty of the lower end of MODIS AOT retrievals is on the order of 0.02 - 0.04 (Levy et al., 2013). These lidar ratios are also likely biased high due to biases in the daytime CALIOP V3 calibration scheme: the V3 daytime calibration coefficients are typically 10% to as much as 30% higher than their V4 counterparts, depending on location and season (Getzewich et al., 2016). Additionally, some all-RFV profiles may include non-marine aerosols, which would further contribute to the high biases in the retrieved lidar ratios.

Despite these caveats, the resultant all-RFV extinction profiles are shown in Fig. 20, with values peaking near the surface and decreasing exponentially with height. These are thus considered the corresponding/approximated CALIOP extinction-based noise floors. Next, for those cloud-free, over-ocean, L2_05kmAProf CALIOP profiles from the same

month (February 2008), RFV bins for profiles where some measure of extinction has been observed and passed QA/QC were replaced with the corresponding extinction noise-floor values solved for the two TAB samples. Profiles were then reintegrated to yield RFV-corrected AOTs.

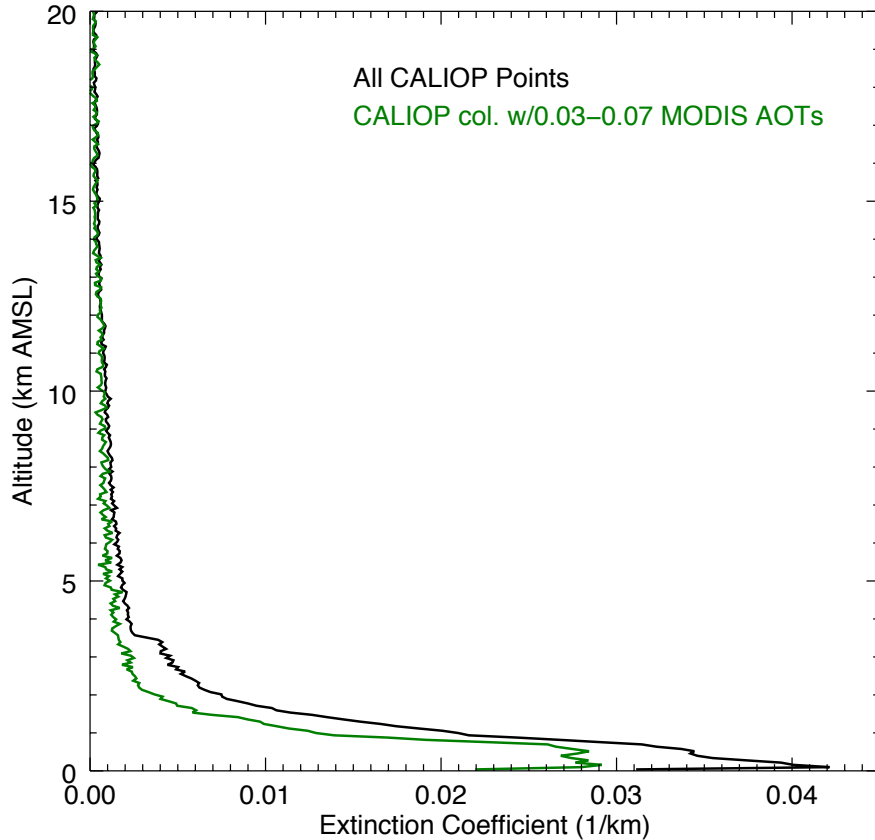


Figure 20. For February 2008 over cloud-free global oceans, the all-RFV aerosol extinction coefficient profiles derived from the inversion algorithm. The black curve represents all cloud-free CALIOP profiles over global oceans, while the green curve is from an analysis restricted to only those CALIOP points collocated with MODIS AOTs between 0.03 and 0.07.

The results of this exercise are summarized in Table 8. The first result, representing the inclusion of all-RFV profiles as is within bulk global samples (i.e., adding cases of AOT=0 to a given sample) shows a difference of 0.033 between collocated CALIOP and MODIS AOT. The noise floor correction applied to both all-RFV profiles and those

Table 8. For February 2008 over cloud-free global oceans, the mean and standard deviation of collocated CALIOP and MODIS AOTs for various scenarios related to the treatment of non-all-RFV and all-RFV CALIOP aerosol profiles. For those scenarios that involve correction, [1] refers to analyses including all cloud-free CALIOP profiles over global oceans, while [2] refers to analyses restricted to CALIOP points collocated with MODIS AOTs of 0.03 to 0.07. The corresponding aerosol extinction profiles used for RFV correction are shown in Fig. 20. Key results are highlighted in yellow.

Scenario					CALIOP AOT		MODIS AOT		Δ AOT (MODIS-CALIOP)
Corrected non-All-RFVs?	All-RFVs set to zero?	All-RFVs ignored?	All-RFVs corrected?	Correction Subset	Mean	Standard Deviation	Mean	Standard Deviation	
	✓				0.084	0.113	0.117	0.133	0.033
✓			✓	[1]	0.126	0.107	0.117	0.133	-0.009
✓			✓	[2]	0.111	0.109	0.117	0.133	0.006
		✓			0.098	0.116	0.123	0.123	0.025
✓		✓		[1]	0.136	0.112	0.123	0.123	-0.013
✓		✓		[2]	0.122	0.114	0.123	0.123	0.001

where some extinction was solved yields AOT differences (i.e., MODIS-CALIOP) of -0.009 and 0.006, depending on the correction sample, which is an improvement ($\sim 20\%$ in absolute value) in the agreement of CALIOP and MODIS AOTs. If profiles with nominal extinction are not corrected and all-RFV profiles are ignored, a mean AOT difference of 0.025 is found with MODIS. Applying the noise-floor corrections for this scenario results in AOT differences of -0.013 and 0.001, or a $\sim 10\text{-}20\%$ improvement (in absolute value) in the disparity in mean AOT between the two sensors. Lastly, it is emphasized to the reader that this section describes only an initial attempt to resolve the RFV issue, and can likely be improved in future studies. For example, the noise floor extinction profile is derived using data from global oceans, while a regional dependency is possible. Also, longer spatial and temporal averages of CALIOP data would likely increase the SNRs and reduce the frequency of occurrence of the RFV issue.

4.3.6 Case study: Nighttime CALIOP all-RFV profile occurrence frequencies

The analyses in this study use daytime CALIOP data to allow for comparison with passively-sensed aerosol observations from MODIS and AERONET. However, for context, in this section a case study for a two-month (January and February 2008) period is conducted to investigate the occurrence frequencies of CALIOP all-RFV profiles during nighttime conditions. The same CALIOP products and QA procedures as described earlier are used here, and Table 9 summarizes the results of this analysis.

Table 9. All-RFV CALIOP occurrence frequencies for two months (January and February 2008) from various analyses using daytime and nighttime data, as well as their corresponding absolute differences.

Analysis		All Points	Cloud-free
Daytime	Globe	70.7%	46.7%
	Global Oceans	63.4%	21.8%
Nighttime	Globe	53.5%	22.0%
	Global Oceans	52.2%	14.0%
Nighttime - Daytime	Globe	-17.2%	-24.7%
	Global Oceans	-11.2%	-7.8%

During nighttime, about half of all global CALIOP aerosol profiles for this period are all-RFVs, but this statistic decreases to about 22% when restricted to cloud-free conditions. This percentage lowers even further for over-ocean profiles. Depending on the analysis, absolute decreases between daytime and nighttime all-RFV occurrence frequencies range from ~8% to ~25%. These findings are expected, as the lack of solar background signal during nighttime allows for an increased SNR and improves the ability of the CALIOP algorithms to detect aerosol layers.

4.3.7 Anticipating Version 4 CALIOP Aerosol Products

Version 4 (V4) CALIOP L2 aerosol products were publicly released in November

2016. A case study was thus performed to assess changes in RFV impacts using these new products, again considering cloud-free over-global-ocean observations during daytime conditions. Whereas the broader point of the study is a conceptualization of the lower-threshold sensitivity of CALIOP to aerosol presence, and the global distribution and impact on overall archive availability, this analysis is included for general consistency. Specifically, V4 data feature improved calibrations of Level 1 (L1) backscatter, as well as improved cloud-aerosol discrimination and surface detection, that may increase the detection sensitivity of diffuse aerosol layers that are reflected in L2 aerosol extinction retrievals. This may then result in a possible decrease in the occurrence of all-RFV profiles overall.

A two-month (January and February of 2008) V4 analysis using QA aerosol profile data (L2_05kmAPro-Standard-V4-10) reveals a 4% relative decrease (1% absolute decrease) in global all-RFV profile occurrence frequencies between V3 and V4. Without QA screening (Sec. 4.2.1), a 15% relative decrease (2% absolute decrease) is found in the occurrence frequency of all-RFV profiles between versions. A supplemental analysis was also conducted, through the use of the CALIOP aerosol layer product (L2_05kmALay-Standard-V4-10) with alternative cloud screening (i.e., cloud optical depth = 0 instead of the AVD parameter), the results of which are consistent with those from the L2_05kmAPro-Standard-V4-10 test. Though this is an initial look at this important new dataset, it appears that improvements in instrument calibration are likely having some positive influence on retrieval sensitivity, though the broader impact of all-RFV profiles as a limiting factor on the breadth of the CALIOP archive, particularly at the poles, mostly remains.

4.4 Conclusions

Since June 2006, the NASA Cloud-Aerosol Lidar with Orthogonal Polarization (CALIOP) instrument has provided a unique global space-borne view of aerosol vertical distribution in Earth's atmosphere. As indicated by this study, a significant portion of Level 2 (L2) CALIOP 532 nm aerosol profiles consist of retrieval fill values (RFVs) throughout the entire range-resolved column (i.e., all-RFVs), overwhelmingly the result of instrument sensitivity and algorithm layer detection limits. The relevant impact of the all-RFV profile is a subsequent column-integrated aerosol optical thickness (AOT) equal to zero.

Using four years (2007-2008 and 2010-2011) of daytime CALIOP Version 3 L2 aerosol products, the frequency of occurrence of all-RFV profiles within the CALIOP archive is quantified. L2 retrieval underestimation and lower detectability limits of CALIOP-derived AOT are assessed using collocated L2 aerosol retrievals from over-ocean Aqua Moderate Resolution Imaging Spectroradiometer (MODIS) and coastal/island Aerosol Robotic Network (AERONET) measurements. The results are partitioned into three latitude bands: Northern Hemisphere mid-latitudes (30° to 60° N), Tropics (-30° to 30° N), and Southern Hemisphere mid-latitudes (-60° to -30° N). The primary findings of this study are:

1. Analysis of CALIOP Level 1.5 attenuated backscatter data reveals that all-RFV profiles are primarily the result of diffuse aerosol layers with inherently lower signal-to-noise ratios (SNRs) that are below CALIOP layer detection limits.
2. All-RFV profiles make up 71% (66%) of all daytime CALIOP L2 aerosol profiles globally (global oceans-only), although this includes completely attenuated columns. For cloud-free CALIOP L2 aerosol profiles, 45% (27%) globally (global oceans-

only) are all-RFV profiles. The largest relative all-RFV profile occurrence frequencies (>75%) are found in the high latitudes of both hemispheres, and are smallest (<25%) in the Tropics. The results of this study indicate that there is a significant daytime observational gap in CALIOP aerosol products near the poles, which is a critically important finding for community awareness.

3. The primary mode of CALIOP all-RFV profiles corresponds with MODIS AOTs of 0.03-0.05, which is largely consistent with an AERONET-based analysis. Also, a small fraction of AERONET data have AOTs lower than 0.02, of which all collocated CALIOP L2 profiles are all-RFVs. This finding is consistent with the lowest detectable CALIOP aerosol optical depth range of 0.02-0.04, as hypothesized by Kacenelenbogen et al. (2011). Note that this conclusion hints that CALIOP may not detect very thin aerosol layers (i.e., AOTs < 0.05), which account for ~10-20% of the AOT spectrum and are of climatological importance (e.g., Smirnov et al., 2011; Levy et al., 2013). Also, these CALIOP-undetected thin aerosol layers are important for various applications, ranging from data assimilation to aerosol indirect effects.
4. As a preliminary study, aerosol extinction coefficient values for two distinct CALIOP all-RFV profile samples are derived using an inversion algorithm applied to corresponding attenuated backscatter data, and a collection of RFV-corrected mean CALIOP AOTs are estimated for a one-month case study. The mean over-ocean CALIOP AOTs increase 10-20% (in absolute value) after correction, with a closer match to collocated Aqua MODIS mean over-ocean AOT.

5. A small decrease in all-RFV profile occurrence is found from Version 4 CALIOP data, which are undergoing widespread release at the time of this writing. Still, the larger-scale impact of all-RFV profiles remains.

This research demonstrates that all-RFV profiles exert a significant influence on the L2 CALIOP AOT archive, as these data compose nearly half of global cloud-free CALIOP aerosol points. Disagreements exist in the literature on the manner for which to handle all-RFV profiles when generating Level 3 AOT statistics. Some studies have set the integrated AOTs of all-RFV profiles to zero, for instance, and included them. However, analyses with passive-based sensors presented in this study reveal these AOTs are most certainly non-zero (global mean values of 0.06 for MODIS and 0.08 for AERONET). These findings are not surprising, as this is the baseline AOT range expected under clean maritime conditions (Kaufman et al., 2001; 2005).

This research also shows that CALIOP RFVs, caused by lower backscatter threshold sensitivities to highly diffuse aerosols, contribute significantly to the discrepancy between CALIOP AOT and those derived from passive sensors like MODIS. Previous studies have mostly attributed this offset to selection of the CALIOP lidar ratio (extinction-to-backscatter ratio) or errors in passive aerosol retrievals. Multi-spectral lidar measurements can begin to close the gap, but will experience SNR issues of their own.

By characterizing lower detection limits of CALIOP-derived extinction and AOT, the potential exists for innovations in instrumentation design and algorithm development of future lidar missions, such as those affiliated with the NASA Aerosol-Clouds-Ecosystems (ACE) mission or the signal processing effort of Marais et al. (2016). Specifically, increasing the intensity of the lidar signal or implementing larger spatial averaging schemes may help to lower the occurrence frequency of all-RFV profiles and relative RFV occurrence per

range bin in L2 products. Questions, however, arise in terms of developing datasets with sufficient spatial and temporal resolution versus needs for optimal data densities, and which is more significant for a given project. Regardless of the potential solution, science teams of current and future lidar systems should carefully consider the existence of RFVs in project datasets.

CHAPTER V

A BULK-MASS-MODELING-BASED METHOD FOR RETRIEVING PARTICULATE MATTER POLLUTION USING CALIOP OBSERVATIONS

5.1 Introduction

5.1.1 Rationale

As discussed in Chapters I and III, the aerosol optical thickness (AOT)/particulate matter with diameters smaller than 2.5 μm ($\text{PM}_{2.5}$) relationship is empirically-based and the surface-to-column representativeness issue is associated with this approach. To overcome these limitations, in this chapter, the feasibility of using near surface observations from Cloud-Aerosol Lidar with Orthogonal Polarization (CALIOP) to derive $\text{PM}_{2.5}$ concentrations is explored. This is accomplished through a semi-physical-based method using bulk mass parameters.

5.1.2 Background

During the last decade, an extensive number of studies have researched the feasibility of estimating $\text{PM}_{2.5}$ pollution with the use of passive-based satellite derived AOT (e.g., Liu et al., 2007; Hoff and Christopher, 2009; van Donkelaar et al., 2015). Monitoring of PM concentration from space observations is needed, as $\text{PM}_{2.5}$ pollution is one of the known causes of respiratory related diseases as well as other health related issues (e.g., Liu et al., 2005; Hoff and Christopher, 2009; Silva et al., 2013). Yet, ground-based $\text{PM}_{2.5}$ measurements are often inconsistent or have limited availability over much of the globe.

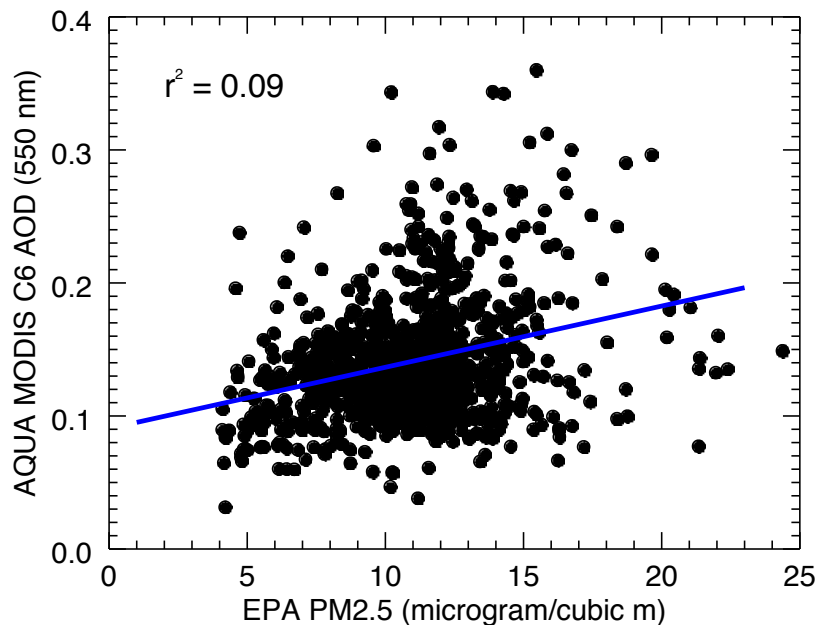


Figure 21. For 2008-2009, scatterplot of mean PM_{2.5} concentration from ground-based U.S. EPA stations and mean column AOT (550 nm) from collocated Collection 6 (C6) Aqua MODIS observations.

In some earlier studies, empirical relationships of PM_{2.5} concentrations and AOTs were developed and used for estimating PM_{2.5} concentrations from passive sensor retrieved AOTs (e.g., Wang and Christopher, 2003; Engel-Cox et al., 2004; Liu et al., 2005; Kumar et al., 2007; Hoff and Christopher, 2009). One of the limitations of this approach is that vertical distributions and thermodynamic state of aerosol particles vary with space and time. Especially for regions with elevated aerosol plumes, deep boundary layer entrainment zones, or strong nighttime inversions, column-integrated AOTs are not a good approximation of surface PM_{2.5} concentrations at specific points and times (e.g., Liu et al., 2004; Toth et al., 2014; Reid et al., 2017). To account for aerosol vertical distribution, several studies have attempted the use of chemical transport models, or CTMs (e.g., van

Donkelaar et al., 2015). Satellite data assimilation of AOT has become commonplace, vastly improving AOT analyses and short term prediction (e.g., Zhang et al., 2014; Sessions et al., 2015). Yet, PM_{2.5} simulations remain poor (e.g., Reid et al., 2016). Uncertainties in such studies are unavoidable due to uncertainties in CTM-based aerosol vertical distributions, and no nighttime AOTs are currently available from passive-based satellite retrievals.

It is arguable that from a climatological/long-term average perspective, the use of AOT as a proxy for PM_{2.5} concentrations has certain qualitative skill (e.g., Toth et al., 2014; Reid et al., 2017) due to the averaging process that suppresses sporadic aerosol events with highly variable vertical distributions. Still, as illustrated in Fig. 21, where 2-year (2008-2009) means of Moderate Resolution Imaging Spectroradiometer (MODIS) AOT are plotted against PM_{2.5} concentrations, although a linear relationship is plausibly shown, a low r^2 value of 0.09 is found. Note that to construct Fig. 21, Aqua MODIS Collection 6 (C6) Optical_Depth_Land_And_Ocean data (0.55 μm), restricted to “Very Good” retrievals as reported by the Land_Ocean_Quality_Flag, are first collocated with daily surface PM_{2.5} measurements over the contiguous United States (CONUS) in both space and time (i.e., within 40 km in distance and the same day), and then collocated daily pairs are averaged into 2-year means (for each PM_{2.5} site). Figure 21 may be indicating that even from a long-term mean perspective, aerosol vertical distributions are not uniform across the CONUS, which is also confirmed by other studies (e.g., Toth et al., 2014). AOT retrievals themselves, with known uncertainties due to cloud contamination and assumptions in the retrieval process (e.g., Levy et al., 2013), may also not be currently up to the task.

On board the Cloud-Aerosol Lidar and Infrared Pathfinder Satellite Observations (CALIPSO) satellite, the CALIOP instrument provides observations of aerosol and cloud vertical distributions at both day and night (Hunt et al., 2009; Winker et al., 2010). Given that near surface aerosol extinction values are available from CALIOP data, it is interesting and reasonable to raise the question: can near surface CALIPSO extinction be used as a better physical quantity than AOT for estimating surface $\text{PM}_{2.5}$ concentrations? This is because unlike AOT, which is a column-integrated value, near surface CALIPSO extinction is, in theory, a more realistic representation of near surface aerosol properties. Yet, in comparing with passive sensors such as MODIS, which has a swath width on the order of ~ 2000 km, CALIOP is a nadir pointing instrument, with a narrow swath of ~ 70 m and a repeat cycle of 16 days (Winker et al., 2009). Thus, the spatial sampling of CALIOP is rather sparse on a daily basis and temporal sampling or other conditional or contextual biases (Zhang and Reid, 2009; Colarco et al., 2014) are unavoidable if CALIOP observations are used to estimate daily $\text{PM}_{2.5}$ concentrations. Also, there are known uncertainties in CALIPSO retrieved extinction values due to uncertainties in the retrieval process, such as the lidar ratio (i.e., extinction-to-backscatter ratio), calibration, and the “retrieval fill value” (RFV) issue (Young et al., 2013; Toth et al., 2018).

Even with these known issues, especially the sampling bias, it is still compelling to investigate if near surface CALIOP extinction can be utilized to retrieve surface $\text{PM}_{2.5}$ concentrations with reasonable accuracy from a long-term (i.e., two-year) mean perspective. To address this question, and to demonstrate a concept, a bulk mass scattering scheme is developed for inferring PM concentrations from near surface aerosol extinction retrievals derived from CALIOP observations. The bulk method used here is based upon the well-established relationship between particle light scattering and $\text{PM}_{2.5}$ aerosol mass

concentration (e.g., Charlson et al., 1968; Waggoner and Weiss, 1980; Liou, 2002; Chow et al., 2006), discussed further, with the relevant equations, in Sect. 5.2.

In this study, using two years (2008-2009) of CALIOP and U.S. Environmental Protection Agency (EPA) data over the fine mode/anthropogenic region of the CONUS, the following questions are asked:

1. Can CALIOP extinction be used effectively for estimating $PM_{2.5}$ concentrations through a bulk mass scattering scheme from a 2-year mean perspective?
2. Can CALIOP extinction be used as a better parameter than AOT for estimating $PM_{2.5}$ concentrations from a 2-year mean perspective?
3. What sampling biases can be expected in CALIOP estimates of $PM_{2.5}$?
4. Are there differences in the CALIOP extinction derived $PM_{2.5}$ concentrations between daytime and nighttime?
5. How do uncertainties in bulk properties compare to overall CALIOP-retrieved $PM_{2.5}$ uncertainty?

Details of the methods and datasets used are described in Sect. 5.2. Section 5.3 shows the preliminary results using two years of EPA $PM_{2.5}$ and CALIOP data, including an uncertainty analysis. The conclusions of this study are summarized in Sect. 5.4.

5.2 Data and Methods

Since 1970, the U.S. EPA has monitored surface-based PM using a gravimetric method, the Federal Reference Method (FRM) or hourly tapered element oscillating microbalance (TEOM) or beta gauge monitors (Federal Register, 1997; Greenstone, 2002).

Two years (2008-2009) of daily $\text{PM}_{2.5}$ Local Conditions (EPA parameter code 88101) were acquired from the EPA Air Quality System (AQS) for use in this investigation, consistent with a previous $\text{PM}_{2.5}$ study (Toth et al., 2014). Note that these data represent $\text{PM}_{2.5}$ concentrations over a 24-hour period and include two scenarios: one sample is taken during the 24-hour duration (i.e., filter-based measurement), or an average is computed from hourly samples within this time period (every hour may not have an available measurement, however).

CALIOP, flying aboard the CALIPSO platform within the A-Train satellite constellation, is a dual wavelength (0.532 and 1.064 μm) lidar that has collected profiles of atmospheric aerosol particles and clouds since summer 2006 (Winker et al., 2007). In this study, daytime and nighttime extinction coefficient (retrieved at 0.532 μm) data from the Version 4.10 CALIOP Level 2 5 km aerosol profile (L2_05kmAPro) product were used. Using parameters included in the L2_05kmAPro product, as well as the corresponding Level 2 5 km aerosol layer (L2_05kmALay) product, a robust quality-assurance (QA) procedure for the aerosol observations was implemented (see Table 10 in Chapter VI). Further information on the QA metrics and screening protocol are discussed in detail in previous studies (Kittaka et al. 2011; Campbell et al. 2012; Toth et al. 2013; 2016). Once the QA procedure was applied, the aerosol profiles were linearly re-gridded from 60 m vertical resolution (above mean sea level) to 100 m segments (i.e., resampled to 100 m resolution) referenced to the local surface (above ground level[AGL]; Toth et al., 2014; 2016). Surface elevation and relative humidity (RH) were taken from collocated model data included in the CALIPSO L2_05kmAPro product (CALIPSO Data Products Catalog (Release 4.20); RH taken from Modern Era Retrospective-Analysis for Research, or MERRA-2 reanalysis product). To limit the effects of signal attenuation and increase the

chances of measuring aerosol presence near the surface, each aerosol profile is cloud-screened using the Atmospheric Volume Description parameter within the L2_05kmAPro dataset in a manner similar to that of Toth et al. (2018).

In this study, near surface PM mass concentration (C_m) is derived from near surface CALIOP extinction based on a bulk formulation, as in Equation 1 (e.g., Liou, 2002; Chow et al., 2006):

$$\beta = C_m(a_{\text{scat}}f_{\text{rh}} + a_{\text{abs}}) \times 1000 \quad (1)$$

where β is CALIOP-derived near surface extinction in km^{-1} , C_m is the PM mass concentration in $\mu\text{g m}^{-3}$, and a_{scat} and a_{abs} are dry mass scattering and absorption efficiencies in $\text{m}^2 \text{g}^{-1}$, and f_{rh} represents the light scattering hygroscopicity, respectively. As a preliminary study, for the purpose of demonstrating this concept, the dominant aerosol type over the contiguous U.S. (CONUS) is assumed to be pollution aerosol (i.e., the most prevalent near-surface aerosol type reported in the CALIOP products is polluted continental) with a_{scat} and a_{abs} values of 3.4 and 0.37 $\text{m}^2 \text{g}^{-1}$ (Hess et al., 1998; Lynch et al., 2016), respectively. These values are similar to those reported in Malm and Hand (2007) and Kaku et al. (2018) but are extrapolated to 0.532 μm . Still, both a_{scat} and a_{abs} have regional and species related dependencies. Also, only 2-year averages are used in this study, and it is assumed that sporadic aerosol plumes are smoothed out in the averaging process, and bulk aerosol properties are similar throughout the study region. The impact of these regional dependencies of bulk aerosol properties on the CALIOP-derived $\text{PM}_{2.5}$ values is left for a future study. Furthermore, the fine mode/anthropogenic aerosol region is focused on in this study and thus the Florida region ($< 32^\circ\text{N}$ and $> 84^\circ\text{W}$) is excluded (with the

exception of the spatial plots), where dust aerosol particles could be transported from the west coast of Africa (Prospero, 1999).

Also, surface PM concentrations are dry mass measurements. To account for the impact of humidity on a_{scat} (it is assumed that a_{abs} is not affected by moisture), the hygroscopic growth factor for pollution aerosol is estimated based on Hanel (1976), as shown in Equation 2:

$$f_{rh} = \left(\frac{1 - RH}{1 - RH_{ref}} \right)^{-\Gamma} \quad (2)$$

where f_{rh} is the hygroscopic growth factor, RH is the relative humidity, and RH_{ref} is the reference relative humidity and is set to 30% in this study (Lynch et al., 2016). Γ is a unitless value and is assumed to be 0.63 (i.e., sulfate aerosol) in this study (Hanel, 1976; Chew et al., 2016; Lynch et al., 2016).

Lastly, the CALIOP-derived PM density is for all particle sizes. To convert from mass concentration of PM (C_m) to mass concentration of $PM_{2.5}$ ($C_{m2.5}$), which represents mass concentration for particle sizes smaller than 2.5 μm , the $PM_{2.5}$ to PM_{10} (PM with diameters less than 10 μm) ratio (ϕ) of 0.6 is adopted, as measured during the Studies of Emissions and Atmospheric Composition, Clouds, and Climate Coupling by Regional Surveys (SEAC⁴RS) campaign over the US (Kaku et al., 2018). Again, the ratio of $PM_{2.5}$ to PM_{10} can also vary spatially, however a regional mean is used to demonstrate the concept. The evaluation of the regional dependencies of the parameters used in this study is left for a future investigation. Here it is assumed that mass concentrations for particle

sizes larger than $10\ \mu\text{m}$ are negligible over the CONUS. Thus, Equation 1 can be rewritten as:

$$C_{m2.5} = \frac{\beta \times \phi}{(a_{\text{scat}} \times f_{\text{rh}} + a_{\text{abs}}) \times 1000} \quad (3)$$

where $C_{m2.5}$ is the CALIOP-derived $\text{PM}_{2.5}$ concentration in units of $\mu\text{g m}^{-3}$.

5.3 Results and Discussion

5.3.1 Regional analysis

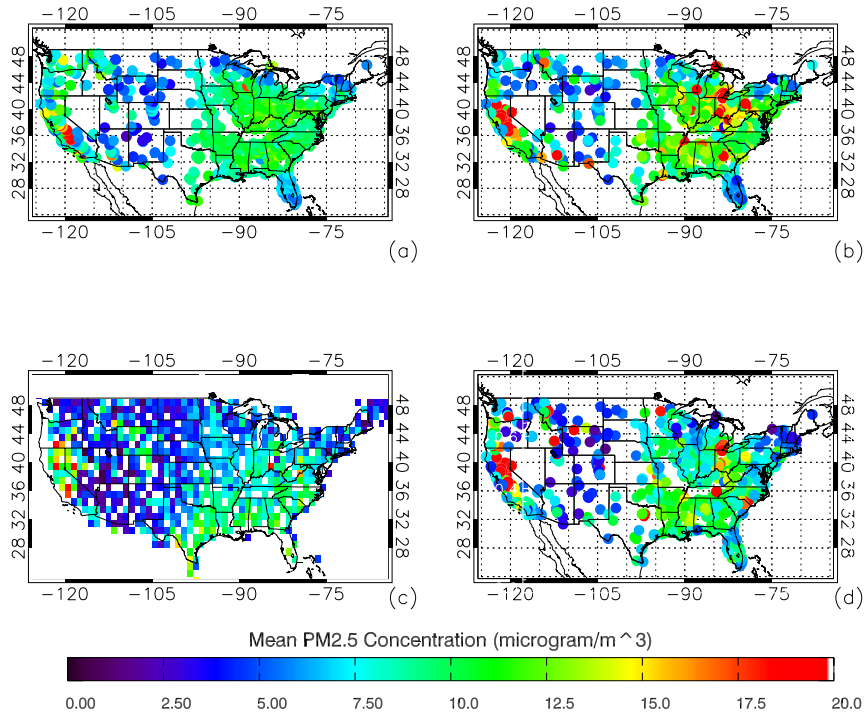


Figure 22. For 2008-2009 over the CONUS, (a) mean $\text{PM}_{2.5}$ concentration ($\mu\text{g m}^{-3}$) for those U.S. EPA stations with reported daily measurements, and (c) $1^\circ \times 1^\circ$ average CALIOP-derived $\text{PM}_{2.5}$ concentrations for the 100–1000 m AGL atmospheric layer, using Equation 3, for combined daytime and nighttime conditions. Also shown are the pairwise $\text{PM}_{2.5}$ concentrations from (b) EPA daily measurements and (d) those derived from CALIOP (day and night combined), both averaged for each EPA station for the 2008-2009 period. For all four plots, values greater than $20\ \mu\text{g m}^{-3}$ are colored red.

Figure 22a shows the mean $\text{PM}_{2.5}$ concentration using two years (2008-2009) of daily surface $\text{PM}_{2.5}$ data from the U.S. EPA ($\text{PM}_{2.5_EPA}$), not collocated with CALIOP observations. A total of 1,091 stations (some operational throughout the entire period; others only partially) are included in the analysis and observations from those stations are further used in evaluating CALOP-derived $\text{PM}_{2.5}$ concentrations ($C_{m2.5}$), as later shown in Fig. 23. $\text{PM}_{2.5}$ concentrations of $\sim 10 \mu\text{g m}^{-3}$ are found over the eastern CONUS. In comparison, much lower $\text{PM}_{2.5}$ concentrations of $\sim 5 \mu\text{g m}^{-3}$ are exhibited for the interior CONUS, over states including Montana, Wyoming, North Dakota, South Dakota, Utah, Colorado, and Arizona. For the west coast of the CONUS, and especially over California, higher $\text{PM}_{2.5}$ concentrations are observed, with the maximum two-year mean near $20 \mu\text{g m}^{-3}$. Note that the spatial distribution of surface $\text{PM}_{2.5}$ concentrations over the CONUS as shown in Fig. 22a is consistent with reported values from several studies (e.g., Hand et al., 2013; Van Donkelaar et al., 2015; Di et al., 2017).

Figure 23a shows the two-year averaged $1^\circ \times 1^\circ$ (latitude/longitude) gridded daytime CALIOP aerosol extinction over the CONUS using CALIOP observations from 100-1000 m, referenced to the number of cloud-free 5 km CALIOP profiles in each $1 \times 1^\circ$ bin. The lower 100 m of CALIOP extinction data are not used in the analysis due to the potential of surface return contamination (e.g., Toth et al., 2014), which has been improved for the Version 4 CALIOP products but may still be present in some cases. Here the averaged extinction from 100-1000 m is used to represent near surface aerosol extinction, as estimated from the mean CALIOP-based aerosol vertical distribution over the CONUS (Toth et al., 2014). As shown in Fig. 23a, higher mean near surface CALIOP extinction of 0.1 km^{-1} are found for the eastern CONUS and over California, while lower values of $0.025\text{-}0.05 \text{ km}^{-1}$ are found for the interior CONUS. Figure 23b shows a similar plot as Fig.

23a but for using nighttime CALIOP observations only. Although similar spatial patterns are found from both day and night, the near surface extinction values are overall lower for nighttime than daytime, and nighttime data are less noisy than daytime. These findings are not surprising, as daytime CALIOP measurements are subject to contamination from background solar radiation (e.g., Omar et al., 2013).

To investigate any diurnal biases in the data, Figs. 23c and 23d show the derived $\text{PM}_{2.5}$ concentration using daytime and nighttime CALIOP data respectively, based on the method described in Sect. 5.2. Both Figs. 23c and 23d suggest a higher $\text{PM}_{2.5}$ concentration of $\sim 10\text{-}12.5 \mu\text{g m}^{-3}$ over the eastern CONUS, and a much lower $\text{PM}_{2.5}$ concentration of $\sim 2.5\text{-}5 \mu\text{g m}^{-3}$ over the interior CONUS. High $\text{PM}_{2.5}$ values of $10\text{-}20 \mu\text{g m}^{-3}$ are also found over the west coast of the CONUS, particularly over California. The spatial distribution of $\text{PM}_{2.5}$ concentrations, as derived using near surface CALIOP data (Figs. 23c and 23d, as well as the combined daytime and nighttime perspective shown in Fig. 22c), is remarkably similar to the spatial distribution of $\text{PM}_{2.5}$ values as estimated based on ground-based observations (Fig. 22a). Still, day and night differences in $\text{PM}_{2.5}$ concentrations are also clearly visible, as higher $\text{PM}_{2.5}$ values are found, in general, during daytime, based on CALIOP observations. The high daytime $\text{PM}_{2.5}$ values, as shown in Fig. 23c, may represent stronger near surface convection and more frequent anthropogenic activities during daytime. However, they may also be partially contributed from solar radiation contamination. Another possibility is that the daytime mean extinction coefficients (from which the mean $\text{PM}_{2.5}$ estimates are derived) appear artificially larger than at night due to high daytime noise limiting the ability of CALIOP to detect fainter aerosol layers during daylight operations.

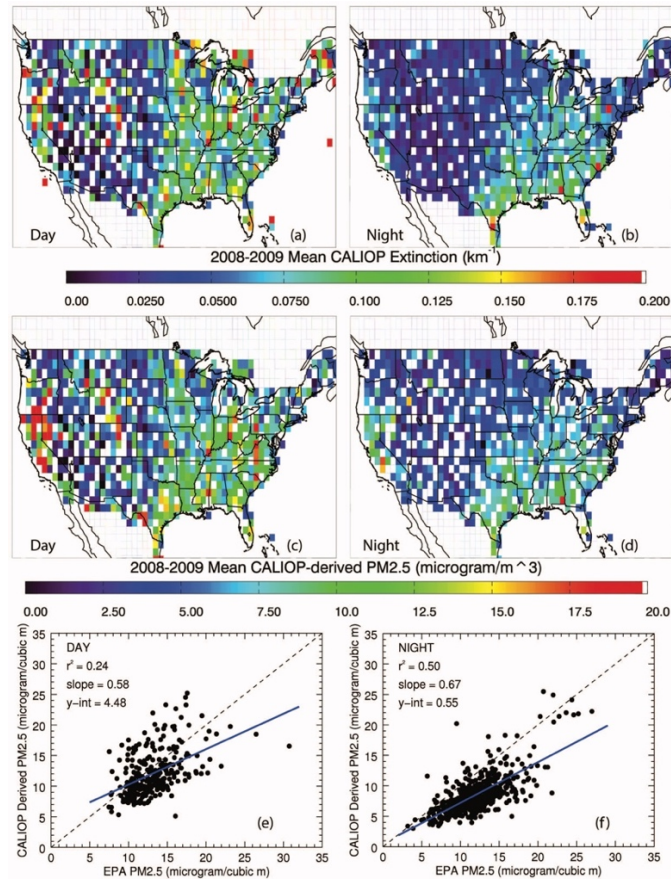


Figure 23. For 2008-2009 over the CONUS, $1^\circ \times 1^\circ$ average CALIOP extinction, relative to the number of cloud-free 5 km CALIOP profiles in each $1^\circ \times 1^\circ$ bin, for the 100 – 1000 m AGL atmospheric layer, for (a) daytime and (b) nighttime measurements. Also shown are the corresponding CALIOP-derived $\text{PM}_{2.5}$ concentrations, using Equation 3 for (c) daytime and (d) nighttime conditions. Values greater than 0.2 km^{-1} and $20 \mu\text{g m}^{-3}$ for (a, b) and (c, d), respectively, are colored red. Scatterplots of mean $\text{PM}_{2.5}$ concentration from ground-based U.S. EPA stations and those derived from collocated near-surface CALIOP observations are shown in the bottom row, using (e) daytime and (f) nighttime CALIOP data.

Figure 23e shows the inter-comparison between $\text{PM}_{2.5_EPA}$ and $\text{PM}_{2.5_CALIOP}$ concentrations. Note that only CALIOP and ground-based $\text{PM}_{2.5}$ data pairs, which are within 100 km of each other and have reported values for the same day (i.e., year, month, and day), are used to generate Fig. 23e. Still, although only spatially and temporally collocated data pairs are used, ground-based $\text{PM}_{2.5}$ data represent 24-hour averages, while CALIOP-derived $\text{PM}_{2.5}$ concentrations are instantaneous values over the CALIOP

overpass. To reduce this temporal bias, two years (2008-2009) of collocated CALIOP-derived and measured $\text{PM}_{2.5}$ concentrations are averaged and only the two-year averages are used in constructing Fig 23e. Also, to minimize the above mentioned temporal sampling bias, ground stations with fewer than 100 collocated pairs are discarded. This leaves a total of 280 stations for constructing Fig. 23e. Note that a seasonality exists in the $\text{PM}_{2.5_EPA}$ and $\text{PM}_{2.5_CALIOP}$ data pairs, with the winter months least represented ($\sim 12\%$ of the total sample). The summer months are the most represented ($\sim 34\%$ of the total sample).

As shown in Fig. 23e, an r^2 value of 0.24 (with a slope of 0.58) is found between CALIOP-derived and measured surface $\text{PM}_{2.5}$ concentrations, with a corresponding mean bias of $-1.1 \mu\text{g m}^{-3}$ ($\text{PM}_{2.5_CALIOP} - \text{PM}_{2.5_EPA}$). Yet from the regression there is a positive y intercept ($\sim 4.5 \mu\text{g m}^{-3}$), suggesting perhaps an elevated CALIOP daytime noise floor (e.g., Toth et al., 2018). In comparison, Fig. 23f shows similar results as Fig. 23e, but for using only nighttime CALIOP data. A much higher r^2 value of 0.50 (with a slope of 0.67) is found between CALIOP-derived and measured $\text{PM}_{2.5}$ values from 535 EPA stations, with a corresponding mean bias of $-3.5 \mu\text{g m}^{-3}$ ($\text{PM}_{2.5_CALIOP} - \text{PM}_{2.5_EPA}$). This may be related to the diurnal variability of $\text{PM}_{2.5}$ concentrations, as the daily mean EPA measurement might be closer to the CALIOP A.M. retrieval than to its P.M. counterpart, as suggested in a later section. Still, data points are more scattered in Fig. 23e in comparison with Fig. 23f, which may suggest that daytime CALIOP data are noisier.

To supplement this analysis, a pairwise $\text{PM}_{2.5_EPA}$ and $\text{PM}_{2.5_CALIOP}$ (day and night CALIOP combined) is presented in the spatial plots of Figs. 22b and 22d. Here, however, the 100 collocated pairs requirement is lifted to increase data samples for better spatial representativeness. The spatial variability of $\text{PM}_{2.5}$ over the CONUS is consistent with the

observed patterns of non-collocated data (i.e., Figs. 22a and 22c), but with generally higher values due to differences in sampling. Also, comparing Figs. 22b and 22d, $PM_{2.5_EPA}$ spatial patterns match well with those of $PM_{2.5_CALIOP}$, yet with larger values for $PM_{2.5_EPA}$ (consistent with the biases discussed above). Lastly, a scatterplot of the pairwise analysis shown in Figs. 22b and 22d is provided in Fig. 24. An r^2 value of 0.39 is found between EPA and CALIOP-derived $PM_{2.5}$ concentrations from a combined daytime and nighttime CALIOP perspective. Overall, Figs. 22, 23, and 24 indicate that near surface CALIOP extinction data can be used to estimate surface $PM_{2.5}$ concentrations with reasonable accuracy.

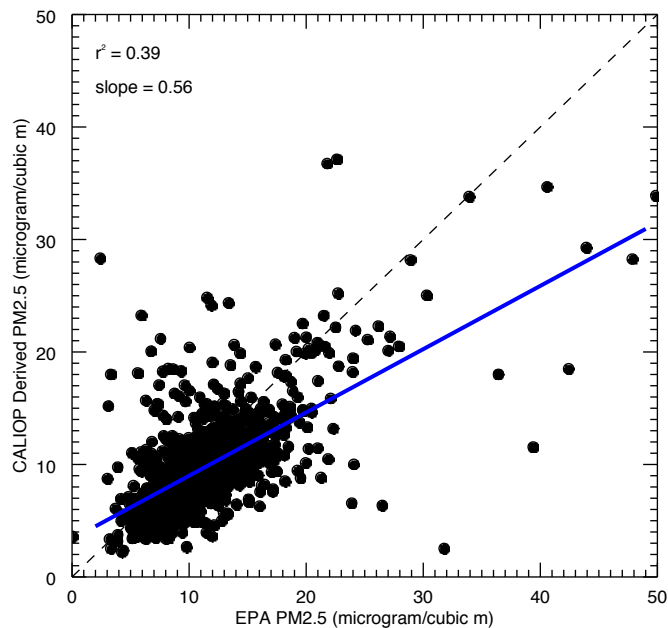


Figure 24. Scatterplot of mean $PM_{2.5}$ concentration from ground-based U.S. EPA stations and those derived from collocated near-surface CALIOP observations using combined daytime and nighttime CALIOP data.

5.3.2 Uncertainty analysis

5.3.2.1 Parameter-related uncertainties and prognostic errors in $C_{m2.5}$.

In this section, the uncertainties in $C_{m2.5}$ values with respect to associated parameters (mass extinction efficiency, hygroscopicity, etc.) are studied, and the prognostic errors of $C_{m2.5}$ are estimated. To study the uncertainties in $C_{m2.5}$ concentrations with respect to the uncertainty from each term in Equation 3, all nighttime (arbitrarily chosen over daytime) all-sky (i.e., not cloud-free) CALIOP aerosol profiles for the two-year (2008-2009) period for the entire CONUS (exact latitudes and longitudes were restricted to 25° to 50° and -125° to -65° , respectively) were used. Keeping all other terms equal, each term in Equation 3 was decreased and increased by 10% to assess the relative change in the derived $PM_{2.5}$ concentration. A percent change in $PM_{2.5}$ was computed for each CALIOP profile, from which a mean percent change was computed. The β and ϕ term exhibited the largest impact, as decreasing and increasing the extinction value by 10% resulted in a -10% and +10% mean change, respectively, in $PM_{2.5}$. The $\sigma_{scat} \times f_{rh}$ term had a large, yet inverse, impact on derived $PM_{2.5}$. That is, decreasing and increasing the σ_{scat} value by 10% resulted in a +10% and -10% mean change, respectively, in the derived values. The α_{abs} term also had an inverse effect on derived $PM_{2.5}$, although of a smaller magnitude (mean of +1% or -1%).

It should be emphasized that the results reported here are only from a simplified and initial uncertainty analysis, and the impact of each parameter on CALIOP-derived $PM_{2.5}$ may differ from this study for instantaneous retrievals. For example, a range of mean σ_{scat} (~ 2 to $5 \text{ m}^2 \text{ g}^{-1}$), dependent upon aerosol species, has been reported in the literature (Hand and Malm, 2007). This range includes values beyond the $\pm 10\%$ bounds of the σ_{scat}

used in this study ($3.4 \text{ m}^2 \text{ g}^{-1}$). Furthermore, for future hourly or daily CALIOP/PM_{2.5} analyses (rather than 2-year means), uncertainties in CALIOP-derived aerosol extinction must be considered, such as those due to assumptions in the lidar ratio based upon aerosol type (Young et al., 2013). Thus, high uncertainties for instantaneous retrievals are expected. Still, this is a semi-physical-based method, and the uncertainties in bulk properties and their subsequent impact on the overall CALIOP-retrieved PM_{2.5} concentrations, can and will be more distinctly quantified in a later paper. Also, since two-year means are used here, it is assumed that random errors are minimized, and the reported errors are mostly due to either sampling or retrieval errors.

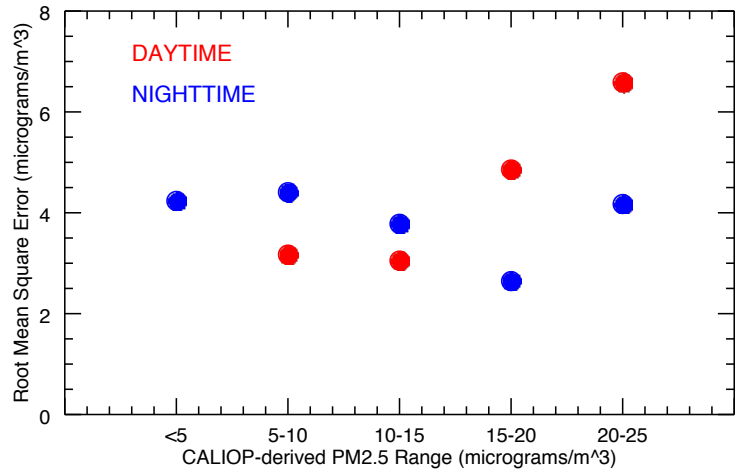


Figure 25. Root-mean-square errors of CALIOP-derived PM_{2.5} against EPA PM_{2.5} as a function of CALIOP-derived PM_{2.5} using both daytime (in red) and nighttime (in blue) CALIOP observations.

The prognostic errors of PM_{2.5,CALIOP} are further estimated as illustrated in Fig. 25. Figure 25 shows the root-mean-square error (RMSE) of CALIOP-based PM_{2.5} concentrations against those from EPA stations as a function of CALIOP-based PM_{2.5} for

the 2008-2009 period over the CONUS. RMSEs were computed in intervals of $5 \mu\text{g m}^{-3}$ from 0 to $25 \mu\text{g m}^{-3}$, with no computations greater than $25 \mu\text{g m}^{-3}$ performed due to very few data points above this $\text{PM}_{2.5}$ concentration level. A mean combined daytime and nighttime minimum error of $\sim 4 \mu\text{g m}^{-3}$ is found, with larger RMSEs for nighttime below $15 \mu\text{g m}^{-3}$, and larger RMSEs for daytime above $15 \mu\text{g m}^{-3}$. However, mean RMSEs are similar for both datasets, $\sim 4.4 \mu\text{g m}^{-3}$ for daytime and $\sim 3.8 \mu\text{g m}^{-3}$ for nighttime. Also, note that while the absolute error for daytime is largest at high $\text{PM}_{2.5}$ concentrations, relative errors are similar (e.g., $3 \mu\text{g m}^{-3}/10 \mu\text{g m}^{-3}$ or 30% for the 5-10 $\mu\text{g m}^{-3}$ bin, versus $7 \mu\text{g m}^{-3}/25 \mu\text{g m}^{-3}$ or 28% for the 20-25 $\mu\text{g m}^{-3}$ bin).

5.3.2.2 Sampling-related biases. As mentioned in the introduction section, a sampling bias, due to the ~ 16 day repeat cycle of CALIOP, can exist while using CALIOP observations for $\text{PM}_{2.5}$ estimates (Zhang and Reid, 2009). This sampling-induced bias is investigated from a 2-year mean perspective by inter-comparing histograms of $\text{PM}_{2.5_EPA}$ and $C_{m2.5}$ concentrations, as shown in Fig. 26. To generate Fig. 26, all available daily EPA $\text{PM}_{2.5}$ are used to represent the “true” 2-year mean spectrum of $\text{PM}_{2.5}$ concentrations over the EPA sites. The aerosol extinction data spatially collocated to the EPA sites (Sect. 5.3.1) but not temporally collocated, are used for estimating the 2-year mean spectrum of $\text{PM}_{2.5}$ concentrations as derived from CALIOP observations. To be consistent with the previous analysis, only cloud-free CALIOP profiles are considered, and Florida is not included. The $\text{PM}_{2.5_EPA}$ concentrations peak at $\sim 9 \mu\text{g m}^{-3}$ (standard deviation of $\sim 3 \mu\text{g m}^{-3}$), and CALIOP-derived $\text{PM}_{2.5}$ peaks at $\sim 8 \mu\text{g m}^{-3}$ (daytime; standard deviation of $\sim 3 \mu\text{g m}^{-3}$) and $\sim 3 \mu\text{g m}^{-3}$ (nighttime; standard deviation of $\sim 2 \mu\text{g m}^{-3}$). The distribution shifts

towards smaller concentrations for CALIOP, more so for nighttime than daytime (possibly due to CALIOP daytime versus nighttime detection differences).

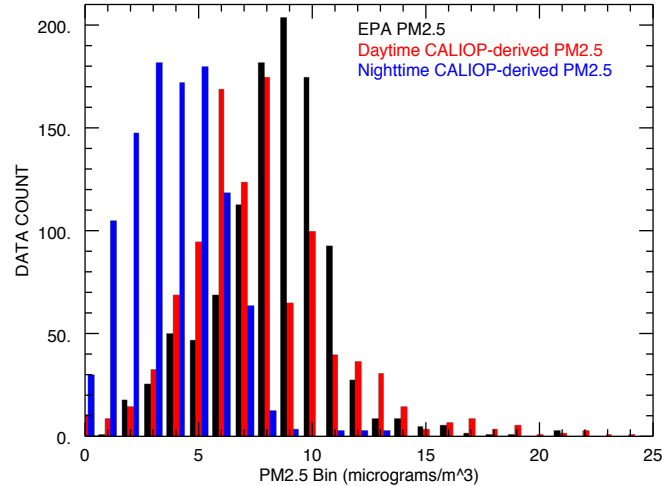


Figure 26. Two-year (2008-2009) histograms of mean $PM_{2.5}$ concentrations from the U.S. EPA (in black) and those derived from aerosol extinction using nighttime (in blue) and daytime (in red) CALIOP data. The U.S. EPA data shown are not collocated, while those derived using CALIOP are spatially (but not temporally) collocated, with EPA station observations.

Still, Fig. 26 may reflect the long-term temporal sampling difference between $PM_{2.5_EPA}$ and $C_{m2.5}$ concentrations. The differences in $PM_{2.5_EPA}$ and $C_{m2.5}$ histograms may also be associated with the diurnal difference in $PM_{2.5}$ concentrations as well as the retrieval bias in $C_{m2.5}$ values. Thus, the exercise shown in Fig. 26 is re-performed using spatially and temporally collocated $PM_{2.5_EPA}$ and $C_{m2.5}$ data as shown in Fig. 27. To construct Fig. 27, $PM_{2.5_EPA}$ and $C_{m2.5}$ data are collocated following the steps mentioned in Sect. 5.3.1, with CALIOP and EPA $PM_{2.5}$ representing 2-year mean values for each EPA station. Again, only cloud-free CALIOP profiles are considered, and Florida is excluded from the analysis. As shown in Fig. 27a, the $PM_{2.5_EPA}$ concentrations peak at $\sim 3 \mu g m^{-3}$

(standard deviation of $\sim 3 \mu\text{g m}^{-3}$), and daytime $C_{\text{m}2.5}$ peaks at $\sim 5 \mu\text{g m}^{-3}$ (standard deviation of $\sim 4 \mu\text{g m}^{-3}$). In comparison, with the use of collocated nighttime $C_{\text{m}2.5}$ and $\text{PM}_{2.5_EPA}$ data as shown in Fig. 27b, the peak $\text{PM}_{2.5_EPA}$ value is about $3 \mu\text{g m}^{-3}$ higher than the peak $C_{\text{m}2.5}$ value (with similar standard deviations as found in the analyses of Fig. 27a). Considering both Figs. 26 and 27, it is likely that the temporal sampling bias seen in Fig. 26 is at least in part due to retrieval bias as well as the difference in $\text{PM}_{2.5}$ concentrations during daytime and nighttime.

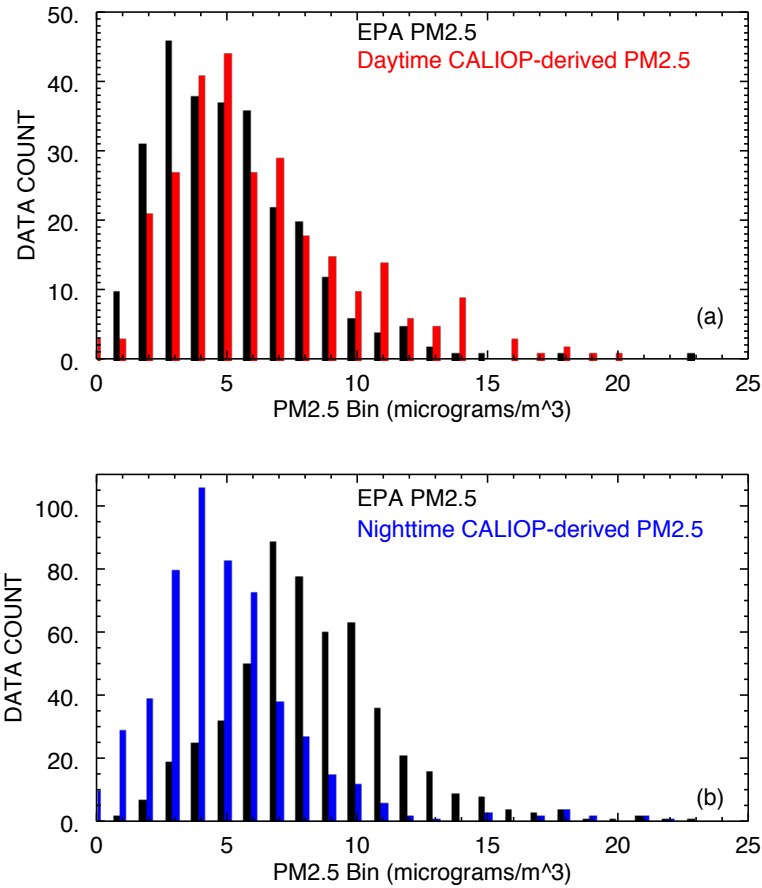


Figure 27. Two-year (2008-2009) histograms of mean $\text{PM}_{2.5}$ concentrations from the U.S. EPA and those derived from spatially and temporally collocated aerosol extinction using (a) daytime and (b) nighttime CALIOP data.

5.3.2.3 CALIOP AOT analysis. Most past studies focused on the use of column AOT as a proxy for surface $PM_{2.5}$ (e.g., Liu et al., 2005; Hoff and Christopher, 2009; van Donkelaar et al., 2015). Therefore, it is interesting to investigate whether near surface CALIOP extinction values can be used as a better physical quantity to estimate surface $PM_{2.5}$ in comparing with column-integrated CALIOP AOT. To achieve this goal, CALIOP column AOT and $PM_{2.5}$ from EPA stations are compared, as shown in Fig. 28. Similar to the scatterplots of Fig. 23, each point represents a two-year mean for each EPA

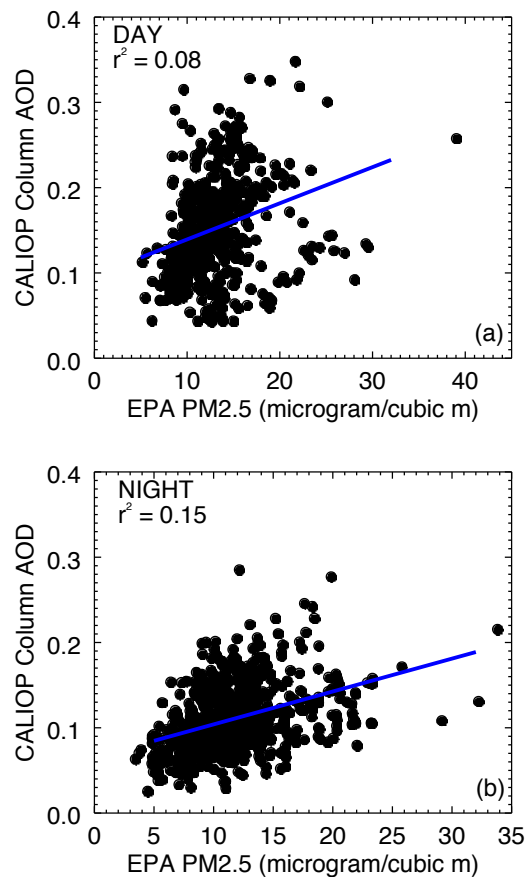


Figure 28. For 2008-2009, scatterplots of mean $PM_{2.5}$ concentration from ground-based U.S. EPA stations and mean column AOT from collocated CALIOP observations, using (a) daytime and (b) nighttime CALIOP data.

site, and was created from a dataset following the same spatial/temporal collocation as described above. As shown in Fig. 28, r^2 values of 0.08 and 0.15 are found for using CALIOP daytime and nighttime AOT data, respectively. This is expected, as elevated aerosol layers will negatively impact the relationship between surface $PM_{2.5}$ and column AOT. Again, the approximation of surface $PM_{2.5}$ from column AOT is indeed an empirical relationship, which may vary with unrealized factors. The derivation of surface $PM_{2.5}$ from near surface CALIOP extinction, as demonstrated from this study however, is a semi-physical based approach, with potential error terms that can be well quantified and minimized in later studies.

5.3.2.4 CALIOP aerosol type analysis. Lastly, for this study, it is assumed that the primary aerosol type over the CONUS is pollution (i.e., sulfate & organic) aerosol, which is generally composed of smaller (fine mode) particles that tend to exhibit mass extinction efficiencies $\sim 4 \text{ m}^2 \text{ g}^{-1}$. However, the study region can also be polluted with dust aerosols, which have a larger particle size and exhibit lower mass extinction efficiencies of $\sim 0.5\text{-}0.7 \text{ m}^2 \text{ g}^{-1}$ (e.g., Hess et al., 1998; Malm and Hand, 2007; Lynch et al., 2016). The use of $PM_{2.5}$ versus PM_{10} somewhat mitigates this size dependency, but nevertheless the coarse mode can dominate $PM_{2.5}$ mass values (e.g., Atwood et al., 2013).

One way in which to infer aerosol type with CALIOP data is through the backscatter color ratio (χ), or the ratio of backscatter coefficients at $1.064 \mu\text{m}$ to $0.532 \mu\text{m}$. A larger $1.064/0.532 \mu\text{m}$ χ could be an indication of a higher percentage of larger particles, such as dust aerosols. The χ was computed from L2_05kmAPro data as the ratio of Backscatter_Coefficient_1064 to Total_Backscatter_Coefficient_532 at 100 m vertical resolution (consistent with the previous analyses). Similar to the method for creating the

scatterplots of Fig. 23 (as described earlier), a mean χ from 100 to 1000 m AGL was computed, followed by a mean χ for each EPA PM_{2.5} site. The collocated EPA PM_{2.5} and CALIOP-derived PM_{2.5} points were then separated based upon the median of the corresponding χ distribution (i.e., 0.78 for daytime and 0.67 for nighttime).

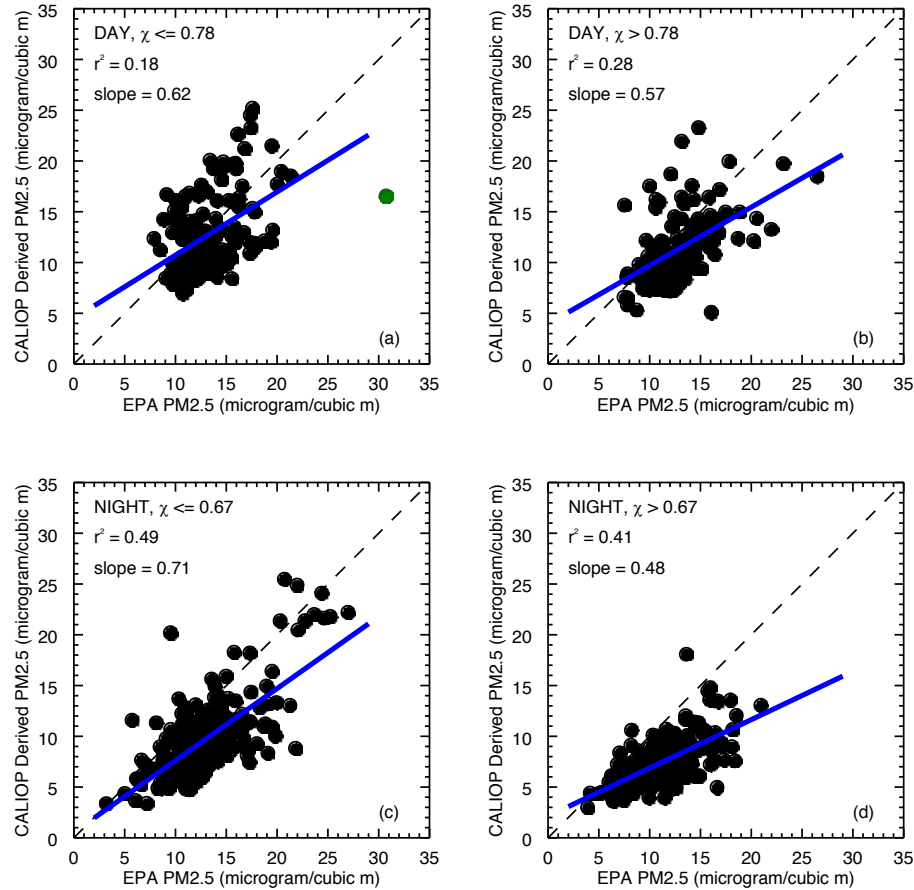


Figure 29. Two-year (2008-2009) scatterplots of mean PM_{2.5} concentration from ground-based U.S. EPA stations and those derived from collocated near-surface CALIOP observations as a function of CALIOP-based backscatter color ratio (1064 nm/532 nm; χ). The results are separated by the median of the χ distribution, i.e., the left (right) column for χ less than or equal to (greater than) the median of each subset. Daytime analyses (a, b) are shown on the top row and nighttime analyses (c, d) are shown in the bottom row. The green circle in (a) represents an outlier and was not included in the computation of the slope.

The results of this exercise are summarized in the scatterplots of Fig. 29. Examining both the daytime (top row) and nighttime (bottom row) analyses, a pattern in the slopes is evident between lower χ values (left column) and higher χ values (right column). Smaller slopes are found for the larger χ subset (Fig. 29b and d) compared to those of the smaller χ subset (Fig. 29a and c). This finding conceptually makes sense, as larger χ values indicate larger particles in general, which may suggest an aerosol mixture with a higher percentage of dust aerosols, thus exhibiting a lower averaged mass extinction efficiency than the pollutant aerosols that are assumed for this study. Therefore, by assuming the aerosol type for the whole study region as pollutant aerosols, mass extinction efficiency values are likely to be overestimated for regions with a higher percentage of dust aerosols, thus (according to Eqn. 3) resulting in an underestimation in the derived mass concentration. Still, no drastic changes in the slopes are found in Fig. 29, which is likely due to the fact that only two-year averages are used in this study, and thus sporadic aerosol events (such as major sporadic dust events) are likely being smoothed out.

Extending from these efforts, the $\text{PM}_{2.5}$ concentrations derived from CALIOP were validated against EPA $\text{PM}_{2.5}$ as a function of CALIOP aerosol type (provided in the aerosol profile product). The most prevalent aerosol type in the 100-1000 m AGL layer over each EPA station for 2008-2009 was first determined, after which the collocated $\text{PM}_{2.5}$ from EPA and CALIOP were separated based upon the two most dominant aerosol types: polluted continental/smoke and polluted dust. The results of this investigation are shown in the scatterplots of Fig. 30. For the daytime analysis (top row of Fig. 30), little change in the slopes are found between the two aerosol regimes. For nighttime (bottom row of Fig. 30), only a slightly higher slope is evident for the polluted dust case compared to polluted

continental/smoke. Thus, no major differences in the EPA/CALIOP-derived $PM_{2.5}$ relationship are found between the two analyses, suggesting our method is reasonable for each of these aerosol types.

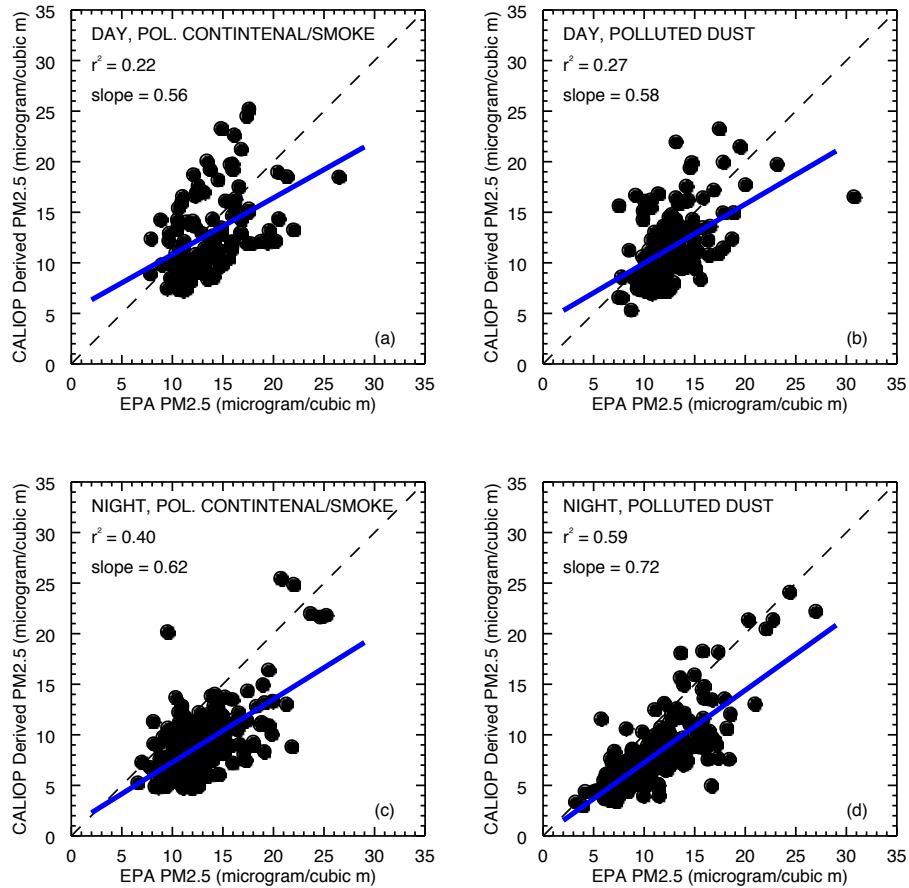


Figure 30. Two-year (2008-2009) scatterplots of mean $PM_{2.5}$ concentration from ground-based U.S. EPA stations and those derived from collocated near-surface CALIOP observations as a function of CALIOP aerosol type. The polluted continental/smoke (polluted dust) analyses are shown in the left (right) column. Daytime analyses (a, b) are shown on the top row and nighttime analyses (c, d) are shown in the bottom row.

As a last step for this initial aerosol type analysis, the performance of our method was checked for pure dust cases. The challenge here, however, is the small amount of pure dust that is found over the CONUS, as determined by the CALIOP aerosol type

algorithms. Only three EPA stations during the study period were found to have pure dust as the most prevalent aerosol type near the surface (i.e., 100-1000 m AGL) for daytime conditions (the latitudes/longitudes of which are: 33.8° N, 118.2° W; 31.8° N, 106.6° W; 39.4° N, 123.4° W). These points are shown in scatterplot form (2-year mean $PM_{2.5}$ for EPA versus derived from CALIOP) in Fig. 31, with no clear relationship found between the two parameters. This finding is expected, as the mass extinction efficiency and aerosol hygroscopic growth factor used for this analysis are for pollution aerosols, which will differ for dust aerosols.

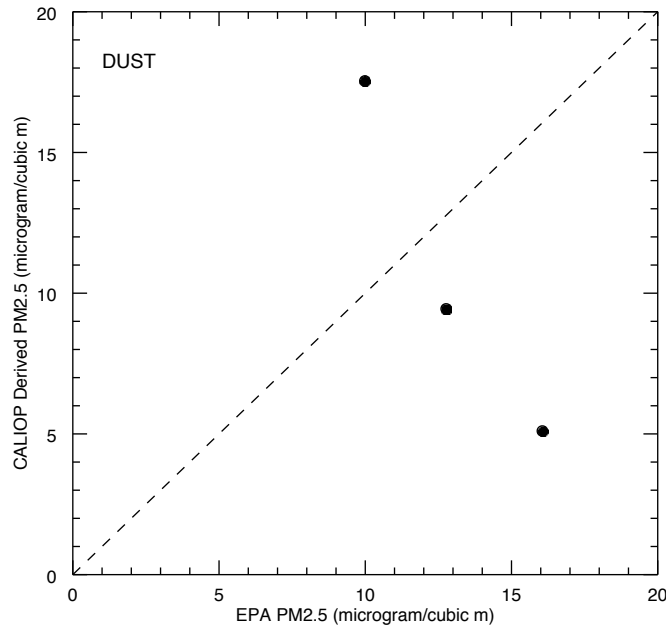


Figure 31. Two-year (2008-2009) scatterplot of mean $PM_{2.5}$ concentration from ground-based U.S. EPA stations and those derived from collocated daytime near-surface CALIOP observations for the dust CALIOP aerosol type.

5.4 Conclusions

In this study, a new bulk-mass-modeling-based method for retrieving surface particulate matter with particle size smaller than 2.5 μm ($PM_{2.5}$) concentrations using

observations from the NASA Cloud-Aerosol Lidar with Orthogonal Polarization (CALIOP) instrument is demonstrated, using averaged data from 2008-2009. For the purposes of demonstrating this concept, only regionally-averaged parameters, such as mass scattering and absorption coefficients, and $\text{PM}_{2.5}$ to PM_{10} (PM with particle size smaller than $10\ \mu\text{m}$) conversion ratio, are used. Also, it is assumed that the dominant type of aerosols over the study region are pollution aerosols (supported by the occurrence frequencies of aerosol types classified by the CALIOP algorithms). Even with the highly-averaged parameters, the results from this study are rather promising and demonstrate a potential for monitoring PM pollution using active-based lidar observations. Specifically, the primary results of this study are as follows:

1. CALIOP-derived $\text{PM}_{2.5}$ concentrations of $\sim 10\text{-}12.5\ \mu\text{g m}^{-3}$ are found over the eastern contiguous United States (CONUS), with lower values of $\sim 2.5\text{-}5\ \mu\text{g m}^{-3}$ over the central CONUS. $\text{PM}_{2.5}$ values of $\sim 10\text{-}20\ \mu\text{g m}^{-3}$ are found over the west coast of the CONUS, primarily California. The spatial distribution of 2-year mean $\text{PM}_{2.5}$ concentrations derived from near surface CALIOP aerosol data compares well to the spatial distribution of in situ $\text{PM}_{2.5}$ measurements collected at the ground-based stations of the U.S. Environmental Protection Agency (EPA). The use of nighttime CALIOP extinction to derive $\text{PM}_{2.5}$ results in a higher correlation ($r^2 = 0.50$; mean bias = $-3.5\ \mu\text{g m}^{-3}$) with EPA $\text{PM}_{2.5}$ than daytime CALIOP extinction data ($r^2 = 0.24$; mean bias = $-1.1\ \mu\text{g m}^{-3}$).
2. Correlations between CALIOP aerosol optical thickness (AOT) and EPA $\text{PM}_{2.5}$ are much lower (r^2 values of 0.08 and 0.15, for daytime and nighttime CALIOP AOT data, respectively) than those obtained from

derived $\text{PM}_{2.5}$ using near-surface CALIOP aerosol extinction. Similar correlations are also found between Moderate Resolution Imaging Spectroradiometer (MODIS) AOT and EPA $\text{PM}_{2.5}$ from two-year (2008-2009) means. This suggests that CALIOP extinction may be used as a better parameter for estimating $\text{PM}_{2.5}$ concentrations from a long-term mean perspective. Also, the algorithm proposed in this study is essentially a semi-physical-based method, and thus the retrieval process can be improved, upon a careful study of the physical parameters used in the process.

3. Spatial and temporal sampling biases, as well as a retrieval bias, are found. In general, these biases result in this method underestimating $\text{PM}_{2.5}$ concentrations using CALIOP. Initial parameter-related uncertainties are provided, and a minimum error of $\sim 4 \mu\text{g m}^{-3}$ is found for combined daytime and nighttime CALIOP analyses.
4. An initial investigation into the relationship between EPA $\text{PM}_{2.5}$ and CALIOP-derived $\text{PM}_{2.5}$ as a function of aerosol type yields no major changes in the results for the two most prevalent aerosol types over the CONUS for the study period (i.e., polluted continental/smoke and polluted dust).

Still, CALIOP observations are rather sparse and there are also issues related to reported CALIOP aerosol extinction values, such as solar and surface contamination (e.g., Toth et al., 2018). Yet, with a new High Spectral Resolution Lidar (HSRL) instrument on board the Earth Cloud Aerosol Radiation Explorer (EarthCARE) satellite on the horizon

(Illingworth et al., 2015), the combined use of several lidar instruments for monitoring regional and global PM pollution is potentially feasible.

CHAPTER VI

TEMPORAL VARIABILITY OF AEROSOL OPTICAL THICKNESS VERTICAL DISTRIBUTION OBSERVED FROM CALIOP

6.1 Introduction

6.1.1 Rationale

In this chapter, column-integrated aerosol optical thickness (AOT) trends as well as AOT trends for selected vertical layers, are investigated using Cloud-Aerosol Lidar with Orthogonal Polarization (CALIOP) observations at both global and regional scales. Note that, as suggested from the previous chapter, near surface CALIOP observations can be linked to particulate matter with diameters smaller than 2.5 μm ($\text{PM}_{2.5}$) concentrations. Thus, near surface AOT trends from this study are a direct indication of trends in $\text{PM}_{2.5}$ concentrations.

6.1.2 Background

Routine monitoring of the global three-dimensional distribution of aerosol particles is fundamental to furthering the scientific understanding of its effects on climate (e.g., Ramanathan et al., 2001) and surface air pollution (e.g., Akimoto, 2003). From satellites, in particular, the growing observational archive is rapidly increasing opportunities for studying aerosol particle physical and optical properties. In this study, temporal variation in the vertical distributions of aerosols is investigated. Such a study is necessary for resolving aerosol-induced circulatory perturbations (e.g., Lau et al., 2006), as well as temporal changes in regional air quality (e.g., Devara et al., 2002).

Several studies have investigated total column AOT trends, based primarily on daytime observations from passive radiometric satellite sensors (e.g., Mishchenko et al., 2007; Zhao et al., 2008; Li et al., 2009; Zhang and Reid, 2010; Yoon et al., 2011; Hsu et al., 2012; Li et al., 2014a; Zhang et al., 2016). In particular, Zhang and Reid (2010) examine decadal (2000-2009) trends in over-ocean AOT derived from the Moderate Resolution Imaging Spectroradiometer (MODIS) and Multi-angle Imaging Spectroradiometer (MISR) instruments. They find a regional dependence in statistically significant AOT trends, with some areas exhibiting positive trends (over Bay of Bengal, east coast of Asia, and Arabian Sea) and others negative (Central America, east coast of North America, and west coast of Africa). They report statistically insignificant MODIS/MISR AOT trends of 0.003 per decade over global oceans. Hsu et al. (2012) follow, investigating thirteen-year (1998-2010) trends in over-land and ocean AOT observed with the Sea-viewing Wide Field-of-view Sensor (SeaWiFS). They report a statistically insignificant positive trend (0.0058 per decade) over global land, and a statistically significant positive trend (0.008 per decade) over global oceans. SeaWiFS AOT trends are identified regionally as well, though discrepancies exist compared with MODIS/MISR (e.g., for Northern Africa, negative trends are found from MODIS/MISR but these are positive from SeaWiFS). Similarly, other studies have investigated AOT trends over a longer term than the NASA Earth Observation System (EOS) era using Advanced Very High Resolution Radiometer (AVHRR) data (e.g., Mishchenko et al., 2007; Zhao et al., 2008; Li et al., 2014a), taking advantage of a much longer data record compared with relatively-recent sensors like MODIS and MISR.

In addition to satellite-based aerosol trend characterization, AOT temporal variations have been investigated using surface-based Aerosol Robotic Network

(AERONET) sun photometer data (e.g., de Meij et al., 2012; Hsu et al., 2012; Yoon et al., 2012; Li et al., 2014b). However, whereas AERONET consists of many hundreds of sites operating simultaneously and continuously at any given time during daylight, there are only a handful of sites where data have been screened for cloud and overall quality assurance over periods long enough for trend study. Still, considering that AERONET data are a benchmark for validating satellite aerosol retrievals (e.g., Holben et al., 1998; Kahn et al., 2005; Levy et al., 2010; Shi et al., 2011c; Hyer et al., 2011), AERONET trend analysis provides valuable insight and perspective from which to intercompare with satellite-based trend analyses for daytime conditions.

Despite the breadth of work and depth of analysis gained from these studies, they are all fundamentally limited in that they provide only a column-integrated perspective of aerosol loading, and thus do not reveal information on the potential for temporal variability in the vertical aerosol distribution. Yet, this knowledge is critical. For instance, only the temporal variation of near-surface aerosol particles affect particulate matter air pollution studies, as aerosol plumes at high altitudes have an insignificant impact on local surface air quality (i.e., total column aerosol measurements include contributions from the free troposphere and above, and thus cannot be used to accurately characterize near-surface variability; Chew et al., 2013). Resolving temporal variability of aerosol particle vertical distribution also has climate radiation budget applications, as longwave aerosol radiative forcing exhibits a strong dependence on altitude (e.g., Zhang and Christopher, 2003; Ban-Weiss et al., 2012). Similarly, knowledge of aerosol vertical distribution is necessary for enhancing the understanding of long-range aerosol particle transport (e.g., Rajeev et al., 2000) and aerosol-induced perturbations to atmospheric circulation (e.g., Chen et al., 2007). More generally, direct, semi-direct, and indirect atmospheric aerosol effects can

only be decoupled from one another, and in contrast to the passive column-integrated viewpoint, when investigating each process from the range-resolved perspective (e.g., Yorks et al., 2009).

The active satellite-based CALIOP instrument provides global range-resolved measurements of the aerosol particle vertical distribution. Orbiting aboard the Cloud-Aerosol Lidar and Infrared Pathfinder Satellite Observations (CALIPSO) platform, CALIOP has continuously profiled aerosols and clouds globally since 2006. This extended data record allows for a qualified study of the vertical distribution of aerosol particle temporal variation. Past studies have used CALIOP data for aerosol trend analyses and climatologies (e.g., Yu et al., 2010; Winker et al., 2013; Amiridis et al., 2015), but focused solely on the mean state (i.e., average AOT) and seasonality of column-integrated aerosol properties. Therefore, using eight and a half years (June 2006 – December 2014) of quality-assured CALIOP aerosol profile data, aerosol temporal variability is investigated here as a function of altitude, with the goal of addressing the following research questions:

- (1) What is the inter-annual variability in aerosol vertical distribution, as observed within the CALIOP record?
- (2) How does the temporal variability in total-column AOT derived from an active remote sensing system like CALIOP compare with those derived from passive-based methods (i.e., MODIS, MISR, SeaWiFS, and AERONET) on both regional and global scales?
- (3) For regions with either positive or negative AOT trends, are the results due to changes in surface-based aerosol concentration or from aerosol plumes aloft?

The remainder of the chapter is organized as follows: Sect. 6.2 provides an overview of CALIOP aerosol retrievals, data screening metrics, and the statistical methods

utilized for trend analysis. In Sect. 6.3, the results of the study are discussed, including the mean state of CALIOP-derived AOT (i.e., average AOT throughout the study period; Sect. 6.3.1) and global AOT temporal variations (Sect. 6.3.2). Section 6.3.3 focuses on findings from regional AOT trend analyses, including a comparison with passive-based AOT trend studies (Sect. 6.3.3.1), nighttime results (Sect. 6.3.3.2), an examination of sources of column-integrated AOT in the vertical domain (Sect. 6.3.3.3), sensitivity studies (Sect. 6.3.3.4), and the temporal variations of collocated CALIOP/Aqua MODIS observations (Sect. 6.3.3.5). The chapter concludes in Sect. 6.4 with a summary of the primary findings of this work.

6.2 Data and Methods

In this study, quality-assured (QA) and above ground level (AGL) corrected monthly-averaged profiles of CALIOP aerosol extinction are created at a vertical resolution of 100 m from the ground to 8.2 km on a $2^\circ \times 5^\circ$ latitude/longitude spatial grid. The construction of this data set is similar to the Level 3.0 (L3) product produced by the CALIPSO project (Winker et al., 2013), albeit with different QA considerations invoked. Like the CALIPSO L3 product, this data set harvests the range-resolved $0.532 \mu\text{m}$ extinction coefficients (km^{-1}) during both daytime and nighttime conditions from the CALIOP Version 3.01, 3.02 and 3.30 Level 2.0 (L2) 5 km Aerosol Profile (L2_05kmAProf) products (Winker et al., 2009). AOTs are then retrieved by integrating these profile data.

The QA process implemented for this study is robust, and involves several checks and parameters. For instance, only extinction coefficients within the nominal range described in the CALIPSO Data Products Catalog (i.e., between 0 and 1.25 km^{-1} , inclusive) are considered, a range adopted by other studies as well (e.g., Redemann et al., 2012).

Negative values are excluded from the analysis, as they represent non-physical aerosol extinction. This also provides a screening metric for the ‘negative surface anomaly’ (i.e., near-surface negative extinction values caused by noise excursions; Amiridis et al., 2013; Winker et al., 2013). A one-month (September 2006) sensitivity test of the extinction range implemented in this study was conducted to determine the number of samples rejected and the corresponding impact on the mean AOT profile. The QA metrics and averaging process (e.g., setting fill values to zero), as described in this section, were used. The test revealed that, on a 60 m profile bin basis, the frequency of occurrence of extinction values outside the accepted range was low ($\sim 1\%$). Further, while including negative values has little impact on the mean AOT profile, those greater than 1.25 km^{-1} increase the mean AOT, particularly near the surface. Note that 1.25 km^{-1} is a practical upper threshold used to assist discrimination between aerosol and cloud layers in CALIOP products. This relates to a reasonable expectation for backscatter measured between the two, which is a function of number concentration, effective particle size, and single scattering albedo. Shi et al. (2015) show how this threshold can break down under cases of unusually dense aerosol propagation. For the purposes here, however, such cases are believed to be extremely rare.

CALIPSO L2_05kmAProf data are also screened based on the quality control (QC) flag (i.e., Extinction_QC_532), extinction coefficient uncertainty, Cloud-Aerosol-Discrimination (CAD) score, and Atmospheric Volume Description (AVD) parameter, similar to Campbell et al. (2012) and Winker et al. (2013). The integrated attenuated backscatter (IAB) parameter from corresponding L2 5 km Aerosol Layer (L2_05kmALay) data is used as an additional QA screening metric. As suggested by Kittaka et al. (2011), profiles containing aerosol layers with a large IAB are not considered. This provides screening for aerosols layers exhibiting anomalously large layer-integrated attenuated

backscatter (most likely due to overcorrection of attenuation of overlying layers; Kittaka et al. 2011). Each metric must be met in order for the aerosol extinction coefficient to be considered QAed. See Table 10 for exact values of these QA screening protocols. Further details of each QA parameter are documented in the CALIPSO Data Users Guide (http://www-calipso.larc.nasa.gov/resources/calipso_users_guide/) and previous studies (Kittaka et al., 2011; Campbell et al., 2012; Toth et al., 2013; Winker et al., 2013).

Table 10. The QA metrics implemented to construct the CALIOP aerosol extinction profiles. The Integrated_Attenuated_Backscatter_532 (L2_05kmALay product) threshold is checked for each aerosol layer within a 5 km CALIOP column, while all other parameters (L2_05kmAProf product) are a function of range within the aerosol profile. Also shown are the values used for construction of aerosol extinction profiles for the official Level 3.0 aerosol profile product (CAL_LID_L3_APro). See Winker et al. (2013) for details on the implementation of these metrics.

Parameter	This Study	Official Level 3 Product
Integrated_Attenuated_Backscatter_532	$\leq 0.01 \text{ sr}^{-1}$	—
Extinction_Coefficient_532	$\geq 0 \text{ and } \leq 1.25 \text{ km}^{-1}$	$\geq -0.2 \text{ km}^{-1}$
Extinction_QC_532	= 0, 1, 2, 16, or 18	= 0, 1, 16, or 18
CAD_Score	$\geq -100 \text{ and } \leq -20$	$\geq -100 \text{ and } \leq -20$
Extinction_Coefficient_Uncertainty_532	$\leq 10 \text{ km}^{-1}$	$< 99.9 \text{ km}^{-1}$
Atmospheric_Volume_Description (Bits 1-3)	= 3	= 3
Atmospheric_Volume_Description (Bits 10-12)	$\neq 0$	—

The presence of aerosol extinction in the lowest 100 m and 200 m bins (binning procedure details are described below) of the aerosol profile is also required, which is designed to limit the negative impact of profile/signal attenuation due to totally-attenuating aerosol layers (e.g., heavy dusts and/or smoke). Campbell et al. (2012) implement a similar, though less restrictive, metric that requires aerosol be present anywhere within 250 m of the surface. All CALIOP profiles that meet this surface aerosol requirement are used. However, clouds may still be present in a small segment of the 5 km aerosol profile (i.e., no

other specific cloud screening aside from attenuation limits through the entire profile). The impact of this is investigated as a sensitivity study in a later section.

The CALIPSO L2_05kmAProf product is reported at 60 m vertical resolution below 20.2 km above mean sea level (AMSL). In order to reference these aerosol profiles to AGL, the mean surface elevation recorded within each 5 km profile is used to linearly regrid the $0.532 \mu\text{m}$ extinction coefficient (and corresponding AOT) profiles in 100 m vertical segments from the ground to 8.2 km (Toth et al., 2014). Extinction coefficients found above this level are used to solve for one AOT value for the 8.2 to 30.1 km AGL layer. The 100 m vertical resolution mean extinction coefficient dataset is then used to construct monthly mean aerosol profiles on a spatial grid of $2^\circ \times 5^\circ$ (latitude/longitude) for June 2006 through December 2014. These averages are computed using only those 5 km profiles with a column AOT greater than zero within each $2^\circ \times 5^\circ$ grid box (Toth et al., 2014). Note that exclusion of AOT-equal-to-zero profiles may cause an under-representation of weakly scattering aerosols (i.e., possibly biasing the monthly mean AOTs high), however the frequency of occurrence of these profiles and their impact on monthly mean AOTs are topics that warrant a separate study.

A significant portion of CALIOP L2 aerosol profile data consists of fill values (i.e., -9999.00), which are inhomogeneously distributed in both the horizontal and vertical domains. It is assumed that most of these fill values reflect relatively weak aerosol signals not detectable by CALIOP algorithms (especially at high altitudes). However, some of these are due to layers that are not classified as aerosol (e.g., cloud) or do not meet the QA criteria (Table 10). For this study, the fill values are set to zero, such that the average column AOT (computed from profiles where binned aerosol extinction coefficient values are larger than zero) for each $2^\circ \times 5^\circ$ grid box is consistent with the sum of the mean

extinction coefficient for each 100 m altitude bin within the corresponding grid box. Note that by setting the fill values to zero, the layer-mean AOTs may be biased low (e.g., misclassification of thick aerosol plumes as clouds). An alternate solution is to set them equal to the layer mean, which has the potential of biasing the layer mean AOTs high. The former method was chosen, as many fill values are due to undetectable aerosol features, which most likely represent near-zero extinction.

The $2^\circ \times 5^\circ$ monthly-mean 100 m vertically-gridded mean extinction coefficient dataset is integrated over four distinct layers – 0.0 to 0.5 km, 0.5 to 1.0 km, 1 to 2.0 km, and greater than 2.0 km (i.e., up to 30.1 km AGL), as determined from the vertical distribution of valid retrievals (Fig. 32), to derive corresponding layer-mean AOT. As shown in Fig. 32, for both daytime and nighttime conditions, the number of valid retrievals decreases by $\sim 75\%$ from 0.5 to 2.0 km AGL. Fewer data counts are found during daytime, due to the influence of the solar background signal. Aerosol particle extinction above 2.0 km can generally be assumed to be free-tropospheric, though this can be a coarse approximation over land in certain regions (e.g., desert dust). For this reason, AOT above 2.0 km AGL is reported as one value. Features that are not classified as aerosols by the CALIOP algorithms, such as clouds and stratospheric layers, are set to zero for this study.

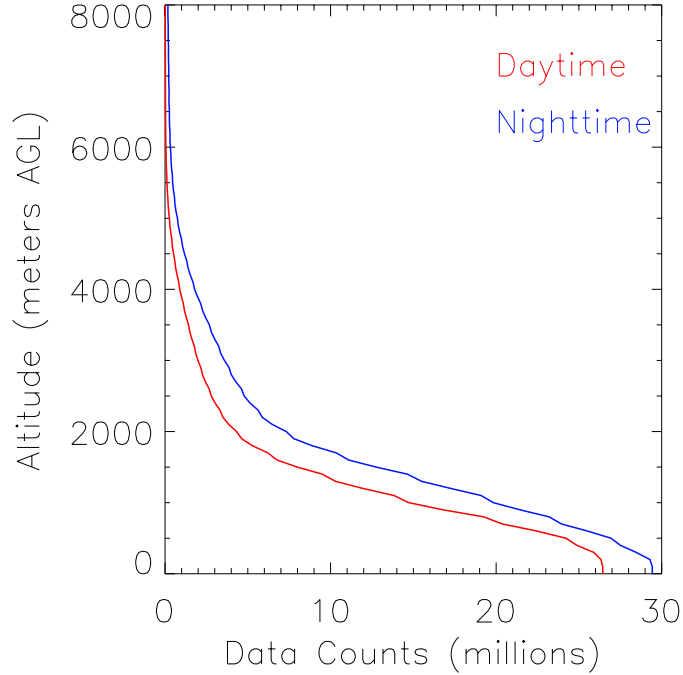


Figure 32. Vertical profiles of total number of valid CALIOP AOT observations for June 2006 through December 2014 for the daytime (in red) and nighttime (in blue) analyses.

Note that the CALIPSO L3 operational Aerosol Profile Product (CAL_LID_L3_APro) has been available to the scientific community since 2011, consisting of monthly-averaged extinction profiles (60 m resolution) and column-integrated extinction (i.e., AOT) on a $2^\circ \times 5^\circ$ latitude/longitude grid (Winker et al., 2013). These averages are constructed from Version 3.0 L2 aerosol extinction data after QC screening is performed. Various QC flags are utilized for this process, and include metrics such as Extinction_QC_532, extinction coefficient uncertainty, CAD score, and AVD parameter. Range bins containing fill values (i.e., -9999.00) attributed to clear air in the aerosol profile are given an extinction value of 0.0 km^{-1} . An exception to this is clear air found below 2.46 km for profiles in which the lowest aerosol layer base is below 2.46 km. Clear air bins are

ignored below this altitude in any resulting averages. Range bins that are cloudy or for which the signal is completely attenuated are also ignored.

For this study, a new L3 aerosol profile product was constructed, in contrast to using the product provided by the CALIPSO team, for several reasons. For one, the official product is referenced to MSL, but a dataset referenced to ground level was desired (such that aerosol presence can be referenced to the local surface). Accurate correction from MSL to AGL is not feasible on a $2^\circ \times 5^\circ$ grid ($\sim 120,000$ sq. km), as surface elevation over land can vary greatly over such an area. Secondly, the number of observations averaged is inhomogeneous throughout the profile (e.g., below the 2.46 km threshold) for the CAL_LID_L3_APro product, which is not ideal for a temporal variability study in the vertical domain. Also, it was required that profiles contain aerosol near the surface, consistent with the expectation of non-zero aerosol loading in the lowest part of the planetary boundary layer (e.g., Winker et al., 2013; Toth et al., 2014). Lastly, cases of AOT = 0 (those profiles containing completely fill values) are not considered for this dataset. While these profiles are currently included in the CAL_LID_L3_APro product, here they are ignored, as their presence creates a low bias in aerosol extinction (e.g., even over remote oceans, a baseline AOT of 0.05 is expected; Kaufman et al., 2001). Note that the filtering techniques of the methods described above are likely aggregating their results using very different populations of L2 profiles, but the population used by this study is likely a proper subset of the one used by the official CALIPSO L3 method.

A comparison of the official L3 aerosol profile product and that derived for this study is shown in Fig. 33. Extinction profiles from the all-sky CAL_LID_L3_APro (Standard V3-00) product for September 2006 were averaged for only those $2^\circ \times 5^\circ$ grid boxes with complete ocean coverage. The corresponding extinction profiles from this

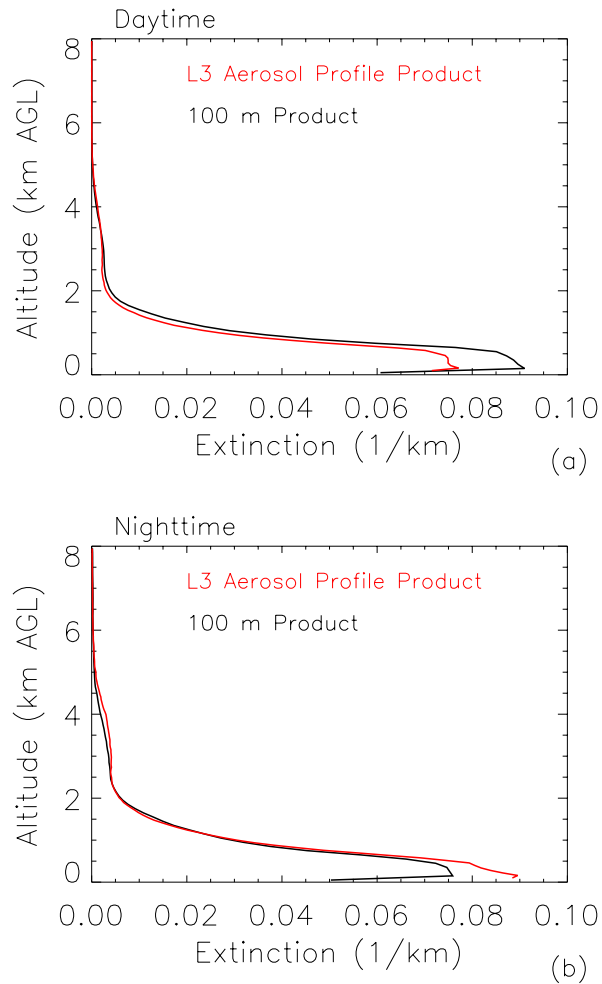


Figure 33. For September 2006 over global oceans, average profiles of $0.532\ \mu\text{m}$ extinction coefficient from the all-sky CALIPSO Version 3.0 Aerosol Profile Product (in red; CAL_LID_L3_APro_AllSky-Standard-V3-00) and the Level 3.0 dataset derived for this study (in black) for (a) daytime and (b) nighttime.

dataset found within those over-ocean $2^\circ \times 5^\circ$ grid boxes were averaged for comparison. The vertical distribution of aerosol extinction derived from each dataset is similar during both daytime (Fig. 33a) and nighttime (Fig. 33b) conditions, except near the surface. Tests revealed that this is due to differences in averaging between the two products and the near-surface aerosol presence requirement. It is suspected the treatment of clouds is also a factor. For example, the difference observed during nighttime (Fig. 33b) may be attributable to

pervasive marine cloud cover below 1 km (i.e., clouds are set to zero for the 100 m product but are ignored for the L3 aerosol profile product). The vertical re-gridding of the product created for this analysis from 60 m to 100 m may also contribute to the differences in the L3 profiles. Despite this disagreement in aerosol extinction near the surface, this dataset (i.e., surface aerosol requirement, registered to AGL rather than AMSL, consistent averaging vertically, etc.) is more appropriate for the purposes of studying the temporal variability in aerosol vertical distribution.

To estimate the linear trends for this study, both the linear least-squares fitting (LSF) model and Sen's method (Sen, 1968) are used. Sen's method provides a nonparametric estimate of the slope through computation of the median of pairwise slopes for all points in the dataset. Thus, different from the LSF method, Sen's method is less sensitive to noisy data (Sen, 1968). A minimum of sixty-eight of the one-hundred-three months ($\sim 2/3$ rd) of the study period to represent valid AOT data is required in order to perform trend analysis. The Mann-Kendall (MK) test (Mann, 1945; Kendall, 1975) was implemented to evaluate the significance of the temporal variations derived from this analysis. The MK test is a widely-used nonparametric statistical method, and is suitable for non-normally distributed and missing data (Li et al., 2014b). The test is applied to an ordered time series, for which the value of the statistic S is determined through comparison of each data value with all subsequent data values. The statistic S is analyzed against the variance of S to derive the standardized test statistic Z , which is then used to determine the statistical significance of the trend (Yue et al., 2002). Specifically, a method similar to the one described by Yue et al. (2002) is adopted, which involves estimation of the linear trend obtained from Sen's method (Sen, 1968) or the LSF model, and removing the effects of autocorrelation prior to

performing the MK test. Further details of this process are found in other studies (e.g., Yue et al., 2002; Li et al., 2014b).

Lastly, CALIOP AOT datasets have been investigated relative to passive sensors (e.g., MODIS) and global numerical model analyses, and shown to exhibit several biases that vary in sign and magnitude over land versus water (e.g., Kittaka et al., 2011; Redemann et al., 2012; Campbell et al., 2013; Toth et al., 2013). However, no study has evaluated the performance of the L2 algorithms over the length of the data collection period. Therefore, it is unclear whether or not these biases definitively vary in space and time through the archive or are a persistent artifact of the algorithms. Thus, in spite of these differences, the analysis is conducted with the understanding that the derived temporal variability likely contains uncorrected biases of an unknown magnitude and sign. The impact of this characteristic is discussed further in the concluding remarks of this chapter.

6.3 Results

6.3.1 Mean State of the AGL-referenced CALIOP AOT Dataset

The CALIOP-observed mean state of atmospheric aerosol particle presence is first examined globally. Figure 34 shows the spatial distribution of $2^\circ \times 5^\circ$ (latitude/longitude) 2006-2014 mean total-column CALIOP AOT for December through May (Fig. 34a, c) and June through November (Fig. 34b, d), including daytime and nighttime analyses. For both regimes, total-column AOTs over the remote oceans are 0.1 or smaller, and total-column AOTs greater than 0.35 are found over highly-polluted areas like the Middle East, India, and Asia. Other regions, such as northern South America and Africa, also exhibit high total-column aerosol loadings. Spatial AOT patterns depicted here are consistent with

those reported by previous passive and active-based studies (e.g., Zhang and Reid, 2010; Kittaka et al., 2011; Campbell et al., 2012; Hsu et al., 2012; Winker et al., 2013).

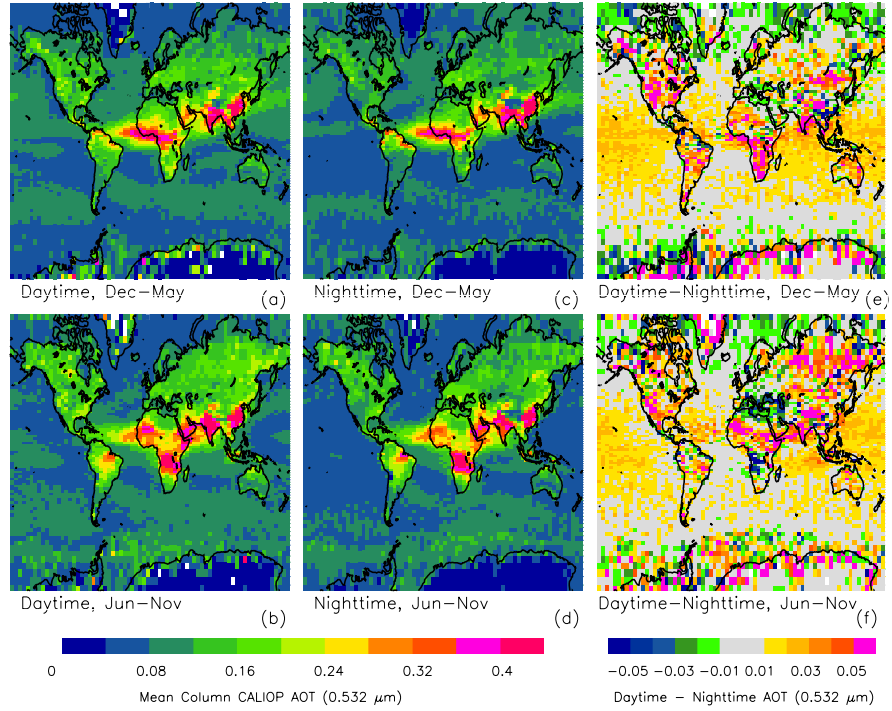


Figure 34. From June 2006 to December 2014, daytime and nighttime mean total-column CALIOP AOT for (a, c) December through May and (b, d) June through November, at $2^\circ \times 5^\circ$ (latitude/longitude) resolution. (e, f) Corresponding $2^\circ \times 5^\circ$ (latitude/longitude) daytime minus nighttime AOTs for each seasonal period are also shown.

Figure 34 also shows the spatial distribution ($2^\circ \times 5^\circ$ latitude/longitude) of daytime/nighttime differences in 2006-2014 mean total-column CALIOP AOT for December through May (Fig. 34e) and June through November (Fig. 34f). Over oceans, near-zero AOT differences are found, with slightly positive day/night differences (i.e., daytime AOT > nighttime AOT) over the Tropical oceans. Over land, most regions exhibit daytime column AOTs greater than those observed during nighttime. However, a few regions (e.g., Europe and the Middle East) exhibit nighttime column AOTs greater

than those acquired during daylight conditions. While these differences may be present in the monthly mean column AOTs, their corresponding trends are of the same sign for daytime/nighttime for the regions of focus in this study (Sect. 6.3.3).

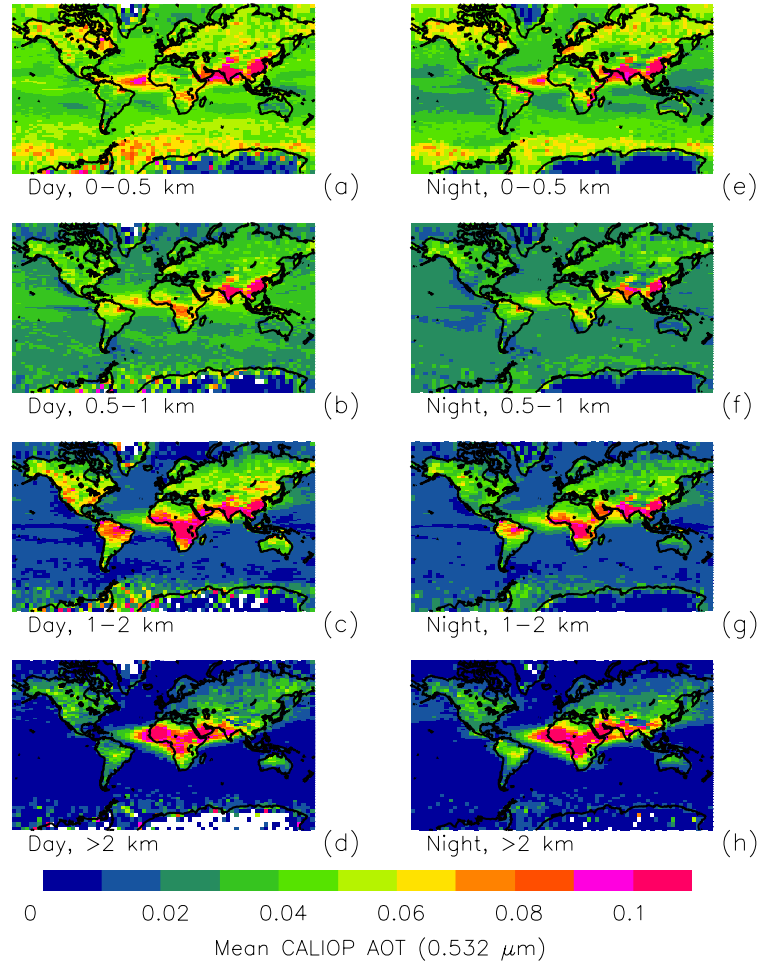


Figure 35. From June 2006 to December 2014, layer mean CALIOP AOT for (a, e) 0.0 – 0.5 km, (b, f) 0.5 – 1.0 km, (c, g) 1.0 – 2.0 km, and (d, h) > 2.0 km above ground level (AGL), at $2^\circ \times 5^\circ$ (latitude/longitude) resolution. Daytime analyses are shown in Figs. 35a-35d, with nighttime analyses in Figs. 35e-35h.

Consistent with Fig. 34, mean CALIOP layer-integrated AOT for 0.0-0.5 km (Fig. 35a, e), 0.5-1.0 km (Fig. 35b, f), 1.0-2.0 km (Fig. 35c, g), and > 2.0 km (Fig. 35d, h) are shown in Fig. 35 for daytime and nighttime, respectively. Again, the spatial patterns of

daytime AOT for each layer are generally consistent with those observed during nighttime. While values are higher for daytime than nighttime (possibly due to day/night disparities in CALIOP detection sensitivity, atmospheric structure, aggregation of profiles for averaging, and/or QA metrics used), these differences are small globally (e.g., global mean column AOT of 0.12 for daytime and 0.11 for nighttime). However, as discussed earlier, daytime/nighttime differences in column AOTs greater than 0.05 exist for some regions (Figs. 34e, f).

Table 11. For both daytime and nighttime analyses, and for each region, the signs of the total-column trend (AOT per year) from the linear least-squares fitting (LSF) method. Red indicates a positive trend and blue represents a negative trend. Those trends that are significant at the 90% confidence interval or greater, as determined by the Mann-Kendall (MK) test, are indicated. Also shown for each region are the altitudes of largest AOT and those of the primary contributor to the total-column trend.

Region	Daytime			Nighttime		
	Column Trend	Peak AOT	Primary Contributor to Column Trend	Column Trend	Peak AOT	Primary Contributor to Column Trend
Northern Africa	Significant	>2 km	1-2 km	Significant	>2 km	1-2 km
Southern Africa	Significant	1-2 km	1-2 km	Significant	>2 km	>2 km
Eastern China	Significant	0-0.5 km	0-0.5 km	Significant	0-0.5 km	1-2 km
India	Significant	0-0.5 km	0-0.5 km	Significant	0-0.5 km	0.5-1 km
Middle East	Significant	>2 km	>2 km	Significant	>2 km	>2 km
Indonesia	Significant	0.5-1 km	0.5-1 km	Significant	0-0.5 km	0-0.5 km
Europe	Significant	0-0.5 km	0-0.5 km	Significant	0-0.5 km	0-0.5 km
Eastern U.S.	Significant	0-0.5 km	1-2 km	Significant	0-0.5 km	1-2 km
Western U.S.	Significant	1-2 km	0-0.5 km	Significant	0-0.5 km	>2 km
South America	Significant	1-2 km	>2 km	Significant	1-2 km	>2 km

Overall, over-land AOT peaks at different altitudes for different regions. For example, peak AOT values observed over Northern Africa and the Middle East are for the > 2.0 km layer. Note that in some instances the values of largest layer AOT may be very similar to other values in the column (e.g., AOT = 0.07 for 0.0-0.5 km and AOT = 0.08

for > 2.0 km for the Middle East). Note also that AOTs over Northern Africa for the 0.0-0.5 km layer are lower than the 0.0-0.5 km layer AOTs implied by the CALIOP-derived extinction coefficient profiles reported in Amiridis et al. (2013). This may be due to differences in QA procedures (e.g., the surface aerosol requirement) and/or the misclassification of dense dust plumes as clouds (inherent in the Version 3.0 Level 2.0 aerosol products; Liu et al., 2009; Vaughan et al., 2009; Campbell et al., 2012). Also, a different CALIOP data processing scheme (e.g., dust only extinction, application of various lidar ratios, etc.) is employed for the Amiridis et al. (2013) study. In contrast to Northern Africa and the Middle East, peak AOT over Eastern China and India are found for the 0.0-0.5 km altitude range. Also, it is interesting to note the reduction of layer-mean AOT with altitude over the remote oceans, as marine aerosols are mostly confined to the layers nearest the surface (i.e., below 1.0 km AGL), with the exception of the sub-tropical Atlantic Ocean due to Saharan dust outflow. The altitudes of largest AOT for each region are summarized in Table 11.

6.3.2 Global Analysis

Next, inter-annual variation of global CALIOP AOT is studied. However, derived CALIOP AOT/layer trends may be affected by longer-term sensor-related anomalies, such as sensor deterioration, which need reconciling. In theory, one might expect a decrease in mean AOT, as the sensor would begin to fail to detect relatively diffuse aerosol layers as the signal-to-noise ratio (SNR) lowers. For this purpose, time series of monthly-mean L2 AOT at two AERONET sites are independently compared against the closest $2^\circ \times 5^\circ$ (latitude/longitude) daytime monthly mean CALIOP total-column AOT. The Amsterdam Island (37.8° S, 77.5° E, 30 m AMSL elevation) and Midway Island (28.2° N, 177.4° W,

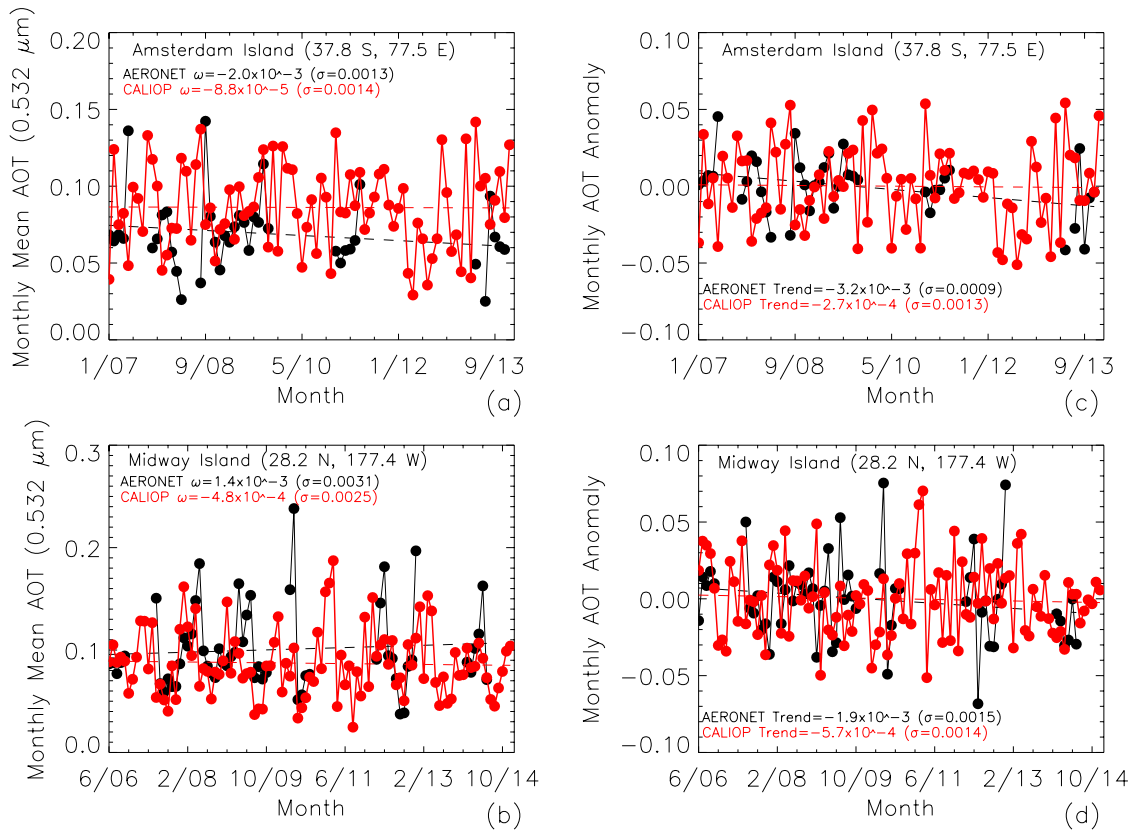


Figure 36. Time series of monthly mean AERONET AOT (interpolated to 0.532 μm) and the corresponding deseasonalized AOT anomalies at (a, c) Amsterdam Island (37.8° S, 77.5° E; January 2007 – December 2013) and (b, d) Midway Island (28.2° N, 177.4° W; June 2006 – December 2014). The time series of monthly mean 2° x 5° (latitude/longitude) daytime CALIOP AOT (0.532 μm) and the corresponding deseasonalized AOT anomalies for the closest grid box to each site is also shown. The trend (ω) and corresponding uncertainty (σ) for each time series are also included.

20 m AMSL elevation) stations are chosen because of their relatively-stable maritime aerosol loading conditions and long record of L2 QA data (see Omar et al., 2013 for a thorough analysis of the difficulties assessing collocated CALIOP AOT skill using the AERONET archive). The results of this analysis are shown in Fig. 36 for Amsterdam Island (January 2007 – December 2013; Figs. 36a and c) and Midway Island (June 2006 – December 2014; Figs. 36b and d), respectively. Differences in the monthly AOT anomalies

are apparent, as AERONET exhibits more variability over Midway Island compared to Amsterdam Island (possibly due to polluted dust transport from Asia, which also may not be captured by the sparseness of CALIOP coverage). However, the absolute differences between the CALIOP and AERONET trends are small, which suggests that the impact of sensor deterioration on CALIOP AOT retrievals over the length of the record studied here is insignificant.

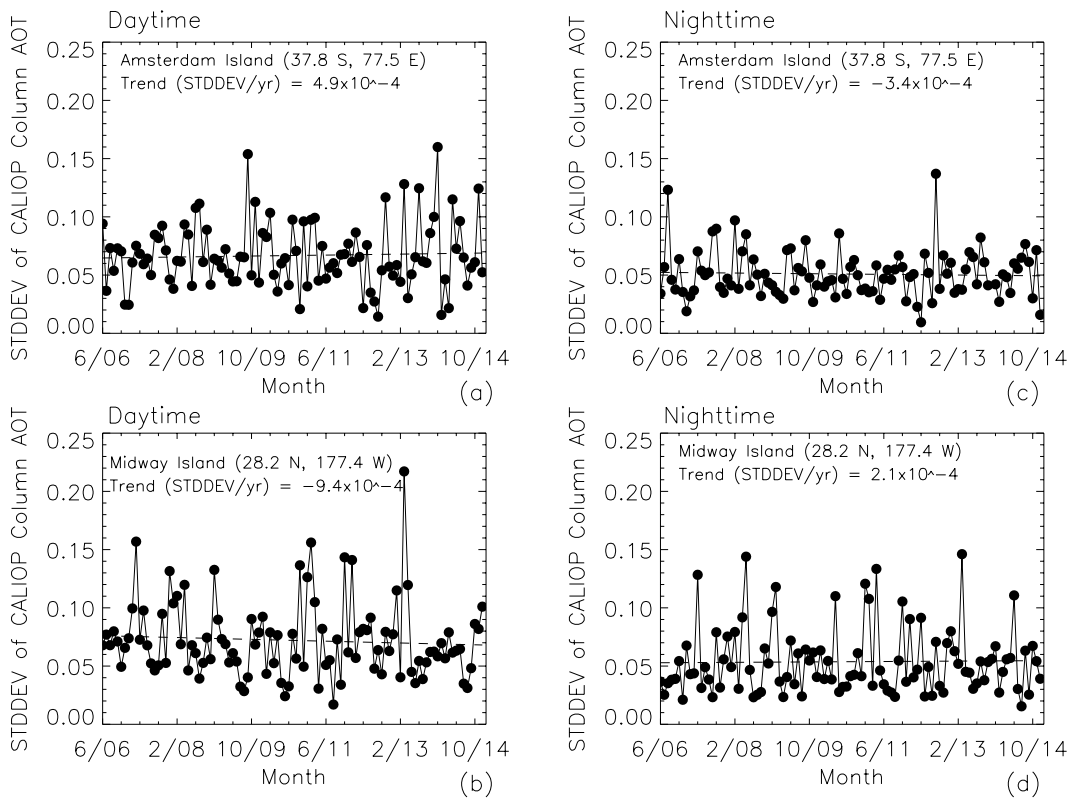


Figure 37. From June 2006 to December 2014, the standard deviation (STDDEV) of monthly mean CALIOP total-column AOT for the closest $2^\circ \times 5^\circ$ (latitude/longitude) grid box to (a, c) Amsterdam Island (37.8° S, 77.5° E) and (b, d) Midway Island (28.2° N, 177.4° W). Daytime analyses are shown in the left column, with nighttime analyses in the right column. The trends (STDDEV/year) of each dataset are also shown.

Besides sensor deterioration, uncertainties in CALIOP AOT could also vary with time systematically, affecting the computed trend significance. To examine this possibility,

the standard deviation corresponding to each monthly-mean CALIOP total-column AOT was computed on a $2^\circ \times 5^\circ$ (latitude/longitude) grid. Figure 37 shows the results of this analysis for the closest $2^\circ \times 5^\circ$ grid box to each of the two aforementioned island AERONET sites. Daytime (Fig. 37a, c) and nighttime (Fig. 37b, d) analyses for both sites exhibit no clear temporal shift in standard deviation. Thus, while an increase in AOT uncertainty is expected due to sensor deterioration and/or degradation of laser energy in theory, there is no definitive evidence that such an increase exists, or if the changes do exist they are marginal so as to be undetectable in comparison with the AERONET data used in this study.

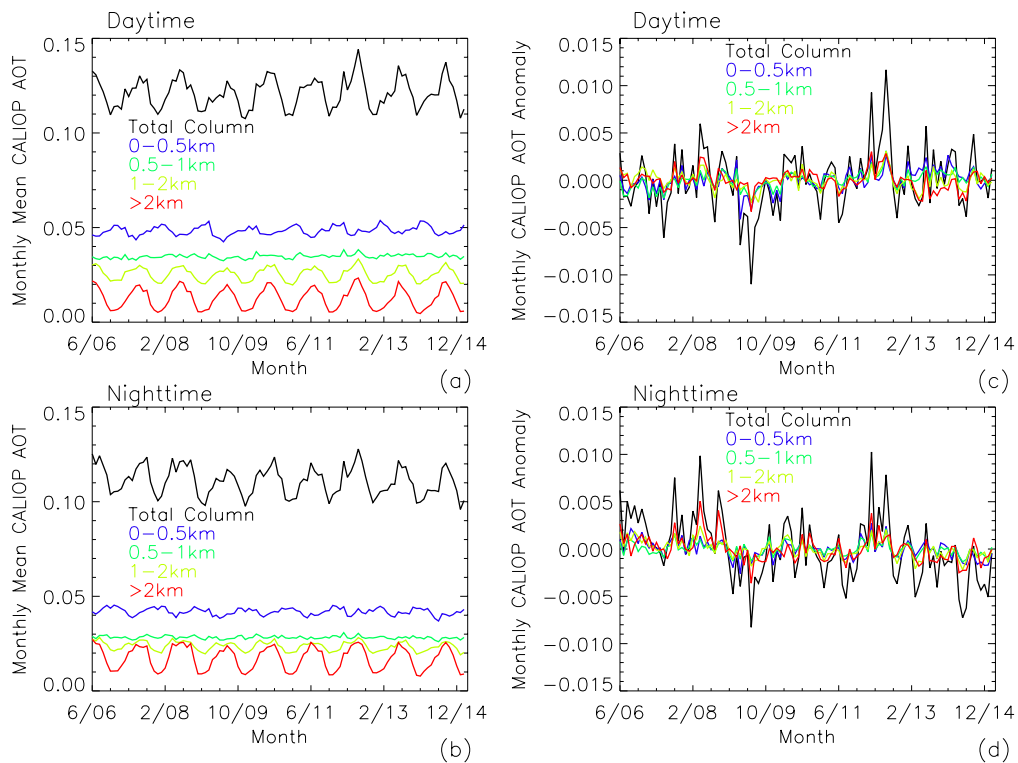


Figure 38. June 2006 to December 2014 monthly global mean CALIOP AOT, and corresponding deseasonalized AOT anomalies, for the total-column and each layer for (a, c) daytime and (b, d) nighttime.

Figure 38 includes a time series of monthly global-mean CALIOP AOT for the total-column and each respective analysis layer, for daytime (Fig. 38a) and nighttime (Fig. 38b) respectively. Globally-averaged monthly total-column AOTs are mostly greater than 0.1 for both daytime and nighttime. Monthly-mean AOT for elevated layers (i.e., 1.0 – 2.0 km and > 2.0 km AGL) are lower than those layers nearer the surface (0.0 – 0.5 km and 0.5 – 1.0 km AGL) for both daytime and nighttime analyses.

The deseasonalized time series of daytime monthly mean AOT shown in Fig. 38a reveals slightly positive trends for the near-surface layers, negative trends for the elevated layers, and an overall positive, though small, temporal variation ($0.0002/\text{year} \pm 0.0002$) for total-column AOT (Fig. 38c). For the deseasonalized nighttime monthly mean, all layers exhibit small negative trends, with a total-column AOT temporal variation of about $-0.0006/\text{year} \pm 0.0002$ (Fig. 38d). Based on the methods of Yue et al. (2002), the MK test showed that both trends are statistically significant at the 90% confidence level (Table 12). The day-night differences may be due to differences in atmospheric conditions (e.g., boundary layer evolution) between the two regimes, thus impacting aerosol vertical distribution.

These differences may also be due to the influence of the solar background during daytime. The decreased SNR during daytime degrades the sensitivity of the CALIOP L2 layer detection algorithm and introduces additional uncertainties into the extinction coefficients that are not present in the nighttime retrievals. As hypothesized by Campbell et al. (2012), these day-night differences in SNR may yield a larger number of diffuse aerosol detections (and hence extinction retrievals) at night, as these layers are more readily detected during night compared with day. The QA procedures implemented and the

Table 12. For the globe and selected regions, daytime and nighttime trends (AOT per 8.58 years) for the total-column and each layer. Trends computed from both the linear least-squares fitting (LSF) and Sen’s slope (SS; Sen, 1968) methods are shown. Bold values indicate trends that are significant at the 90% confidence interval or greater, as determined by the Mann-Kendall test.

Domain	Daytime												Nighttime											
	Column		0.0-0.5 km		0.5-1.0 km		1.0-2.0 km		>2.0 km		Column		0.0-0.5 km		0.5-1.0 km		1.0-2.0 km		>2.0 km					
	LSF	SS	LSF	SS	LSF	SS	LSF	SS	LSF	SS	LSF	SS	LSF	SS	LSF	SS	LSF	SS	LSF	SS				
Globe	0.002	0.002	0.002	0.001	0.001	0.001	-0.000	-0.000	-0.001	-0.000	-0.005	-0.005	-0.001	-0.001	-0.001	-0.001	-0.002	-0.002	-0.002	-0.002				
Northern Africa	-0.013	-0.013	-0.003	-0.003	-0.002	-0.003	-0.004	-0.003	-0.003	-0.001	-0.017	-0.017	-0.005	-0.004	-0.004	-0.004	-0.007	-0.006	-0.002	-0.003				
Southern Africa	0.019	0.019	0.003	0.003	0.003	0.003	0.008	0.008	0.005	0.004	-0.002	-0.002	-0.003	-0.002	-0.001	-0.001	-0.002	-0.002	0.006	0.007				
Eastern China	-0.028	-0.029	-0.009	-0.009	-0.006	-0.007	-0.007	-0.007	-0.006	-0.006	-0.029	-0.033	-0.008	-0.008	-0.007	-0.007	-0.009	-0.008	-0.008	-0.006				
India	0.021	0.019	0.008	0.008	0.008	0.004	0.004	0.004	0.002	0.001	0.012	0.012	0.004	0.002	0.004	0.003	0.002	0.001	0.001	0.000				
Middle East	-0.000	0.003	-0.001	-0.001	0.001	0.001	0.000	-0.000	-0.001	-0.000	-0.009	-0.004	0.000	0.001	-0.001	-0.001	-0.003	-0.003	-0.004	-0.003				
Indonesia	-0.002	-0.003	-0.001	-0.002	0.003	0.003	-0.002	-0.003	-0.002	-0.001	-0.016	-0.015	-0.006	-0.006	-0.001	-0.001	-0.005	-0.005	-0.004	-0.003				
Europe	-0.012	-0.010	-0.004	-0.004	-0.003	-0.003	-0.004	-0.002	-0.001	-0.001	-0.018	-0.017	-0.006	-0.006	-0.004	-0.004	-0.005	-0.004	-0.002	-0.003				
Eastern U.S.	-0.011	-0.011	-0.002	-0.003	0.000	0.000	-0.005	-0.005	-0.004	-0.003	-0.019	-0.017	-0.005	-0.005	-0.004	-0.004	-0.007	-0.006	-0.004	-0.002				
Western U.S.	-0.004	-0.005	-0.002	-0.001	-0.001	-0.001	-0.001	-0.002	-0.000	-0.000	-0.010	-0.011	-0.003	-0.003	-0.002	-0.002	-0.002	-0.002	-0.003	-0.004				
South America	-0.011	0.000	-0.002	-0.001	-0.001	0.000	-0.003	0.000	-0.006	-0.004	-0.042	-0.032	-0.008	-0.007	-0.008	-0.006	-0.013	-0.010	-0.013	-0.010				

manner in which CALIOP profiles are aggregated for averaging may also have an impact on day-night differences in mean AOT (Campbell et al., 2012).

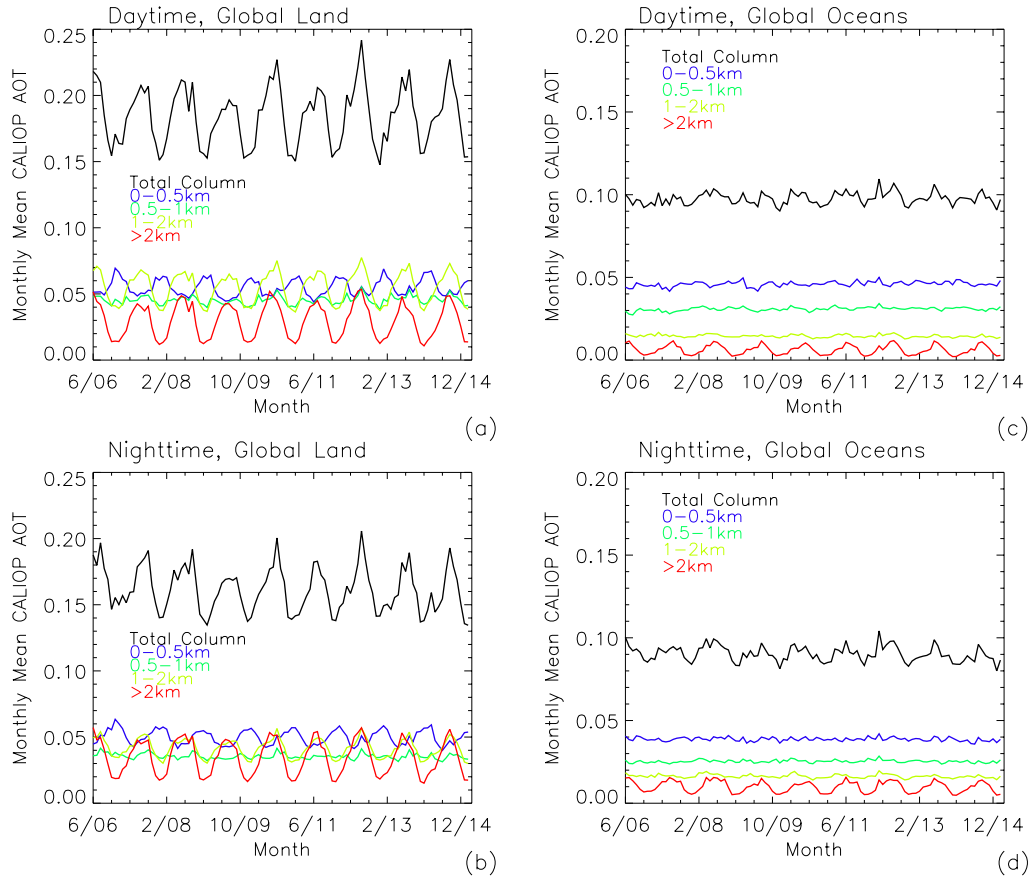


Figure 39. For the June 2006 to December 2014 period, monthly mean CALIOP AOT for the total-column and each of the four layers for global (a, b) land and (c, d) oceans. Daytime analyses are shown in Figs. 39a and 39c, with nighttime analyses in Figs. 39b and 39d.

Seasonal variability in CALIOP AOT is also found from examining Fig. 38, with maxima occurring for the > 2.0 km layer during the Northern Hemisphere (NH) summer months and minima for the NH winter months. The opposite is true for the 0.0-0.5 km layer, as AOT peaks are found during the NH winter months. The increase in aerosol loading for the > 2.0 km layer during NH summer could be due to elevated dust transport,

while the increase in aerosol loading in NH winter for the lowest layer may be due to increased human activity (e.g., fossil fuel burning), more inversion layers over continental polluted regions, and/or sea salt maxima over the remote oceans. Overall, the seasonality of total-column AOT closely resembles that of the > 2.0 km layer, and the 0.5-1.0 km layer conspicuously shows no seasonality. Similar seasonal patterns are found for nighttime conditions (Fig. 38b).

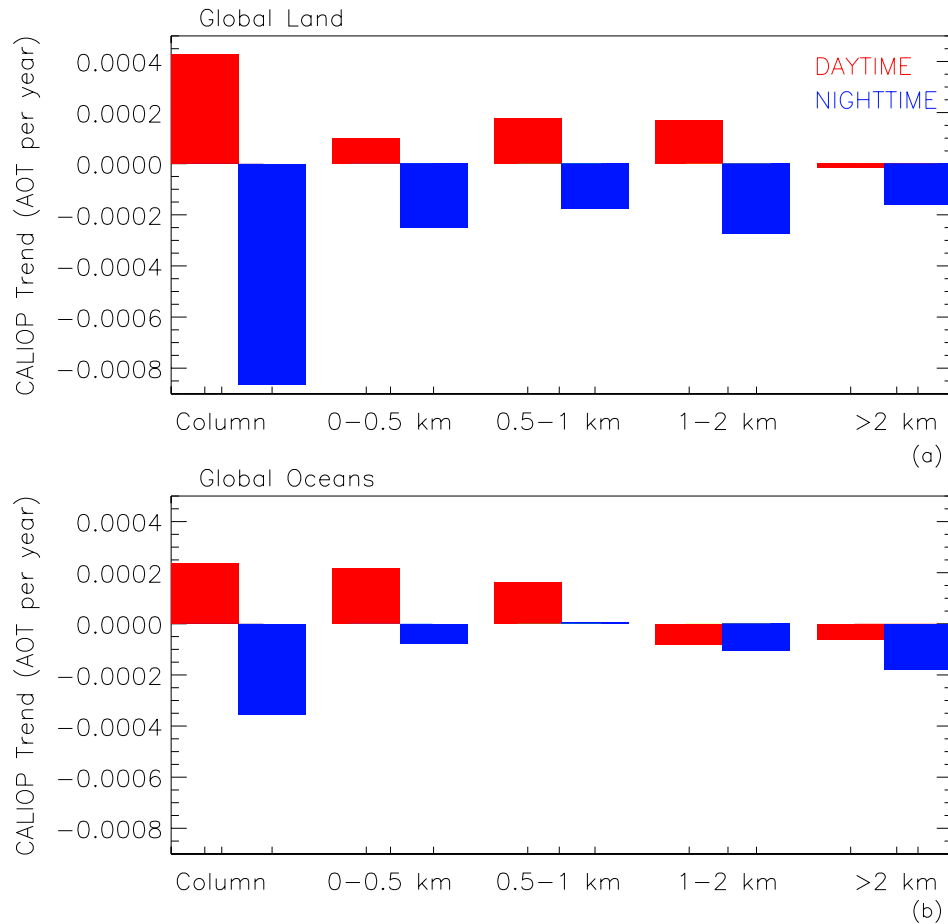


Figure 40. For June 2006 to December 2014, daytime and nighttime trends per year of the de-seasonalized monthly mean CALIOP AOT for the total-column and each of the four layers for global (a) land and (b) oceans.

To further explore the counter-phase between the time series of layer-mean AOT for the 0.0-0.5 km and the > 2.0 km layer, time series of monthly-mean total-column and layer CALIOP AOT are shown in Fig. 39 for global land (Figs. 39a, b) and oceans (Figs. 39c, d). Comparison of these plots reveals that over-land AOTs are greater than those over oceans, consistent with Figs. 34 and 35. Also, in a pattern similar to that shown in Fig. 38, seasonality of CALIOP AOT is apparent, most notably for the total-column and elevated layers. It is thus likely that elevated over-land aerosol particles during the NH summer months are mostly responsible for the counter-phase in the time series between the 0.0-0.5 km and the > 2.0 km layers. The sources of this seasonality (e.g., biomass burning, Saharan and/or Asian dust, etc.) are out of the general scope of this study and not explored here.

Temporal variability of deseasonalized CALIOP monthly AOT for global land and oceans are shown in Fig. 40. Positive (daytime) and negative (nighttime) trends in total-column AOT are found for both land (Fig. 40a) and oceans (Fig. 40b). For daytime, positive trends are found for most layers, except > 2.0 km for global land and 1.0-2.0 km and > 2.0 km for global oceans. Figure 40a also suggests that the total-column AOT trend for global land is significantly influenced by a positive result at the 0.5-1.0 km and 1.0-2.0 km layers. For nighttime, negative trends are observed for all layers other than 0.5-1.0 km for global oceans, and the dominant contributor to the negative total-column AOT result is from the > 2.0 km layer for global oceans.

Over global land, a positive near-zero AOT variation of $\sim 0.0004/\text{year}$ is found (also see Table 13) for CALIOP daytime total-column AOT, which is similar to the trend ($\sim 0.00058/\text{year}$) reported by Hsu et al. (2012) using SeaWiFS AOT data. A positive near-zero variation in AOT of $\sim 0.0002/\text{year}$ is also found during daytime over global oceans. This value is comparable to both SeaWiFS (Hsu et al., 2012; $\sim 0.0008/\text{year}$) and MODIS

(Zhang and Reid, 2010; $\sim 0.0003/\text{year}$), but is inconsistent with the negative result reported using MISR (Zhang and Reid, 2010). This inconsistency could be due to several reasons, such as differences in calibration, sensitivity, and detectability between satellite sensors.

6.3.3 Regional Analysis

6.3.3.1 Daytime analysis of total-column AOT and comparison with passive-based AOT trend studies. Prior study of column-integrated AOT temporal variability has been based almost exclusively on passive sensor measurements from both space-borne and ground observations. Therefore, it is interesting to inter-compare active-based total-column CALIOP AOT daytime trends with those of column-integrated AOT derived through passive sensors on a regional scale. Three such studies are selected (i.e., Zhang and Reid, 2010; Hsu et al., 2012; Li et al., 2014b) that share study periods similar to the one in this work, which generally report statistically significant trends in column-integrated AOT. AVHRR-based analyses are not considered because they are reported for much longer periods than this study (e.g., Mishchenko et al., 2007; Zhao et al., 2008; Li et al., 2014a).

The results of these comparisons (in terms of AOT variation per year) are shown in Table 13. Note that the Terra MODIS/MISR study is over global oceans only (Zhang and Reid, 2010) and the AERONET one is mostly for over-land sites (as opposed to coastal ones; Li et al., 2014b). Also, both Level 1.5 and Level 2.0 AERONET data are used in Li et al. (2014b), but only those AERONET analyses that use the more rigorous QA Level 2.0 data are selected.

Table 13. Trends (AOT per year) for selected regions from Terra MODIS/MISR (Zhang and Reid, 2010), SeaWiFS (Hsu et al., 2012), and AERONET (Li et al., 2014b) observations. Also shown are daytime total-column trend from CALIOP aerosol profile observations. The number in parentheses for the Terra MODIS/MISR and SeaWiFS columns represents the CALIOP total-column trends using the latitude/longitude boundaries defined by each passive-based study.

Region	Zhang and Reid (2010)		Hsu et al. (2012)		Li et al. (2014b)		This Study	
	Terra MODIS/MISR		SeaWiFS		AERONET		CALIOP	
	March 2000 – December 2009	January 1998 – December 2010	2000 – 2013 (station-dependent)	June 2006 – December 2014	Latitude Longitude	Trend (AOT/year)	Latitude Longitude	Trend (AOT/year)
Northern Africa	8°N-24°N 60°W-18°W	10°N-15°N 5°W-15°E	13.3°N 5.9°W	0°N-30°N 20°W-20°E		-0.007	0°N-30°N 20°W-20°E	-0.0016
Southern Africa	29°S-7°S 20°W-15°E			30°S-0°N 10°E-30°E			30°S-0°N 10°E-30°E	0.0023
Eastern China	20°N-40°N 110°E-125°E	35°N-40°N 110°E-120°E	40°N 116.4°E	20°N-40°N 100°E-120°E		-0.01	20°N-40°N 100°E-120°E	-0.0032
India	10°N-25°N 78°E-103°E	20°N-30°N 75°E-85°E	26.5°N 80.2°E	5°N-30°N 70°E-90°E		0.008	5°N-30°N 70°E-90°E	0.0025
Middle East	5°N-23°N 50°E-78°E	10°N-35°N 35°E-60°E		15°N-40°N 40°E-60°E			15°N-40°N 40°E-60°E	-0.00005
Indonesia	15°S-10°N 80°E-120°E	15°S-10°N 80°E-120°E		10°S-5°N 95°E-130°E			10°S-5°N 95°E-130°E	-0.0003
Europe	30°N-45°N 0°E-40°E	43°N-55°N 0°E-30°E		40°N-60°N 10°W-30°E			40°N-60°N 10°W-30°E	-0.0014
Eastern U.S.	30°N-45°N 80°W-60°W	30°N-45°N 70°W-90°W		25°N-50°N 95°W-65°W			25°N-50°N 95°W-65°W	-0.0013
Western U.S.				25°N-50°N, 125°W-95°W			25°N-50°N, 125°W-95°W	-0.0005
South America		10°S-20°S 40°W-65°W		30°S-0°N 80°W-50°W			30°S-0°N 80°W-50°W	-0.0013
Global Land								0.0004
Global Oceans								0.0002
Globe								0.0002

Comparisons are performed for ten selected areas. The latitude and longitude boundaries for these regions are: Northern Africa (0° N - 30° N, 20° W - 20° E), Southern Africa (30° S - 0° N, 10° E - 30° E), Eastern China (20° N - 40° N, 100° E - 120° E), India (5° N - 30° N, 70° E - 90° E), Middle East (15° N - 40° N, 40° E - 60° E), Indonesia (10° S

- 5° N, 95° E - 130° E), Europe (40° N - 60° N, 10° W - 30° E), Eastern U.S. (25° N - 50° N, 95° W - 65° W), Western U.S. (25° N - 50° N, 125° W - 95° W), and South America (30° S - 0° N, 80° W - 50° W). Figure 41 depicts the spatial distribution of yearly deseasonalized temporal variability of monthly-mean total-column CALIOP AOT at 2° x 5° (latitude/longitude) resolution. Grid cells having insufficient data (i.e., fewer than sixty-eight months) are shown in black.

For the daytime (Fig. 41a) analysis, negative trends are observed over several regions, including the Eastern U.S. (-0.0013/year), South America (-0.0013/year), Northern Africa (-0.0016/year), Europe (-0.0014/year), and Eastern China (-0.0032/year). Positive trends, however, are found for Southern Africa (0.0023/year) and India (0.0025/year). Five of these regional total-column AOT trends (Southern Africa, Eastern China, India, Europe, and the Eastern U.S.) are statistically significant at the 90% confidence level, while the others are not (Table 12). Near-zero trends in column AOT are found over the remote oceans, possibly due to the common low aerosol loadings for these regions. Note that the decreasing AOTs over Northern Africa are consistent with the findings of a recent AVHRR-based study concerning the dust transport path from northwest Africa over the Atlantic Ocean (Ridley et al., 2014). Also, the fact that most regions exhibit negative trends, while the near-zero column AOT trend for global lands is positive (~ 0.0004 /year; Table 13), implies there are land areas outside the selected regions that feature positive trends.

For all satellite sensors included in Table 13, India is the sole region of focus with consistent positive AOT trends, while Europe, South America, and the Eastern U.S. exhibit consistent negative trends. Mostly positive values are found for Eastern China, Indonesia, and the Middle East, with most satellite sensors indicating negative trends over Northern

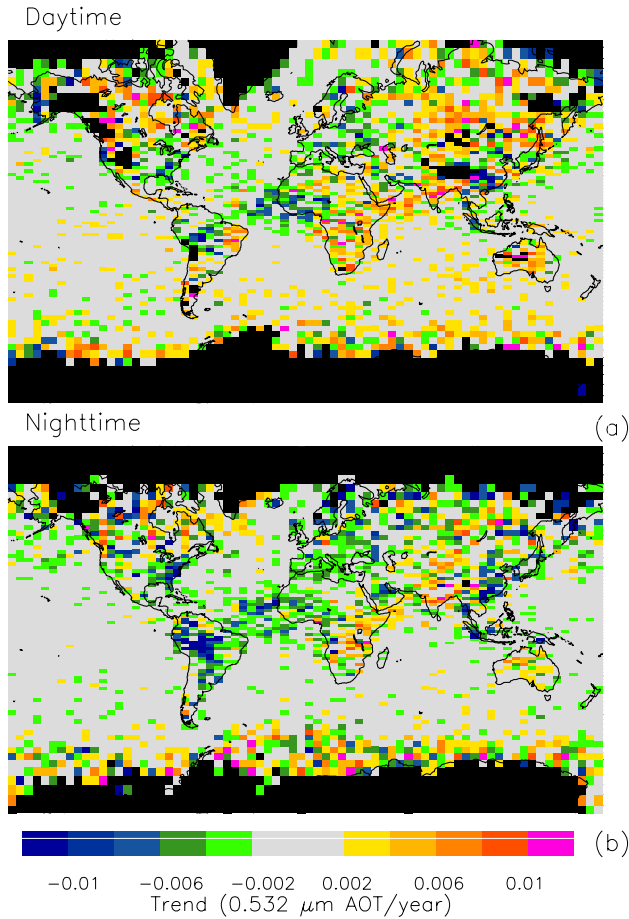


Figure 41. From June 2006 to December 2014, trends (AOT per year) of the de-seasonalized monthly mean total-column CALIOP AOT for every $2^\circ \times 5^\circ$ (latitude/longitude) for (a) daytime and (b) nighttime.

Africa. For Eastern China, Terra MODIS, MISR, and SeaWiFS trends are positive (see Table 13 for the exact values from each sensor). However, CALIOP observations indicate a negative trend over this region ($-0.0032/\text{year}$), as do AERONET measurements collected at Beijing, China ($-0.01/\text{year}$; 40.0° N , 116.4° E , 92 m AMSL elevation). Note that while the negative trend found over Eastern China from some datasets may be due to the reduction in aerosol loading after the 2008 Olympics in Beijing, some AERONET-based studies have found positive trends in AOT over this region (e.g., de Meij et al., 2012; Yoon

et al., 2012). Similar to Eastern China, the AOT trend from the passive satellite sensors for Indonesia are positive, with a negative trend found with CALIOP (-0.0003/year). Over-land CALIOP AOTs have been reported higher than over-land MODIS AOTs for Southeast Asia due most likely to mischaracterization of lidar ratios used in the CALIOP algorithms (Campbell et al., 2013). The impact of this point is discussed in the concluding remarks of this chapter. Lastly, all satellite sensors indicate a negative trend for Northern Africa, with the exception of SeaWiFS (Table 13). However, as was the case for Eastern China, AERONET-derived AOT from the Cinzana, Mali station (13.3° N, 5.9° W, 285 m AMSL elevation) in Northern Africa also exhibits a negative trend (-0.007/year).

6.3.3.2 Nighttime analysis. At present, CALIOP is the only instrument that can assess the temporal variability in nighttime AOT globally. At night, negative trends are found for the same regions as daytime: Western and Eastern U.S. (-0.0011/year and -0.0022/year, respectively), South America (-0.0049/year), Northern Africa (-0.0022/year), Europe (-0.0021/year), Eastern China (-0.0038/year), and Indonesia (-0.0019/year). These trends are generally stronger during night. The Middle East exhibits a stronger (but now negative) total-column value (-0.0010/year), with a weaker positive trend found over India (0.0014/year). With the exception of Southern Africa, India, and the Middle East, all of these trends are statistically significant at the 90% confidence level (Table 12).

Nighttime variability in total-column CALIOP AOT is depicted spatially in Fig. 41b. Although both day and nighttime results exhibit similar patterns over most regions, negative values are more predominant over the Middle East and Asia during nighttime. These day/night differences could be introduced by differences in aerosol loading between

the two regimes. However, it is also likely that less variance is expected from CALIOP-based methods at nighttime (e.g., Campbell et al., 2012; Winker et al., 2013). Day versus night aerosol detection performance should also be considered here, as CALIOP only retrieves extinction coefficients where it detects aerosol layers, and the detection of weakly scattering aerosol layers (i.e., the vast majority of aerosols) is much more difficult during daytime due to the solar background signal.

6.3.3.3 Examining the sources of total-column AOT in the vertical domain. Similar to total-column CALIOP AOT results of Fig. 41, Fig. 42 shows the spatial distribution of variability for each of the four subject layers. For both day (left column) and night (right column), the negative trends observed over the Eastern U.S., South America, and Northern Africa are generally stronger within the elevated layers (Figs. 42c, g and Figs. 42d, h) relative to lower ones (Figs. 42a, e and Figs. 42b, f). Also, positive trends over Southern Africa are mostly stronger for the elevated layers compared with those closer to the surface. Note that data gaps in the elevated layers (especially Fig. 42d) are reflected as those grid boxes for which no trends are computed, as they do not meet the sixty-eight-month requirement described in Sec. 6.2.

To summarize the temporal variation shown spatially in Figs. 41 and 42, Fig. 43 consists of bar plots representing the regionally-averaged values for deseasonalized monthly-mean CALIOP AOT for the total-column and four layers, respectively. For daytime conditions (Fig. 43a), negative trends are found for the total-column for Western and Eastern U.S., South America, Northern Africa, Europe, Eastern China, and Indonesia. With the exception of Europe, Eastern China, Indonesia, and the Western U.S., these negative values are due mostly to changes in elevated (i.e., 1.0-2.0 km and >2.0 km) aerosol

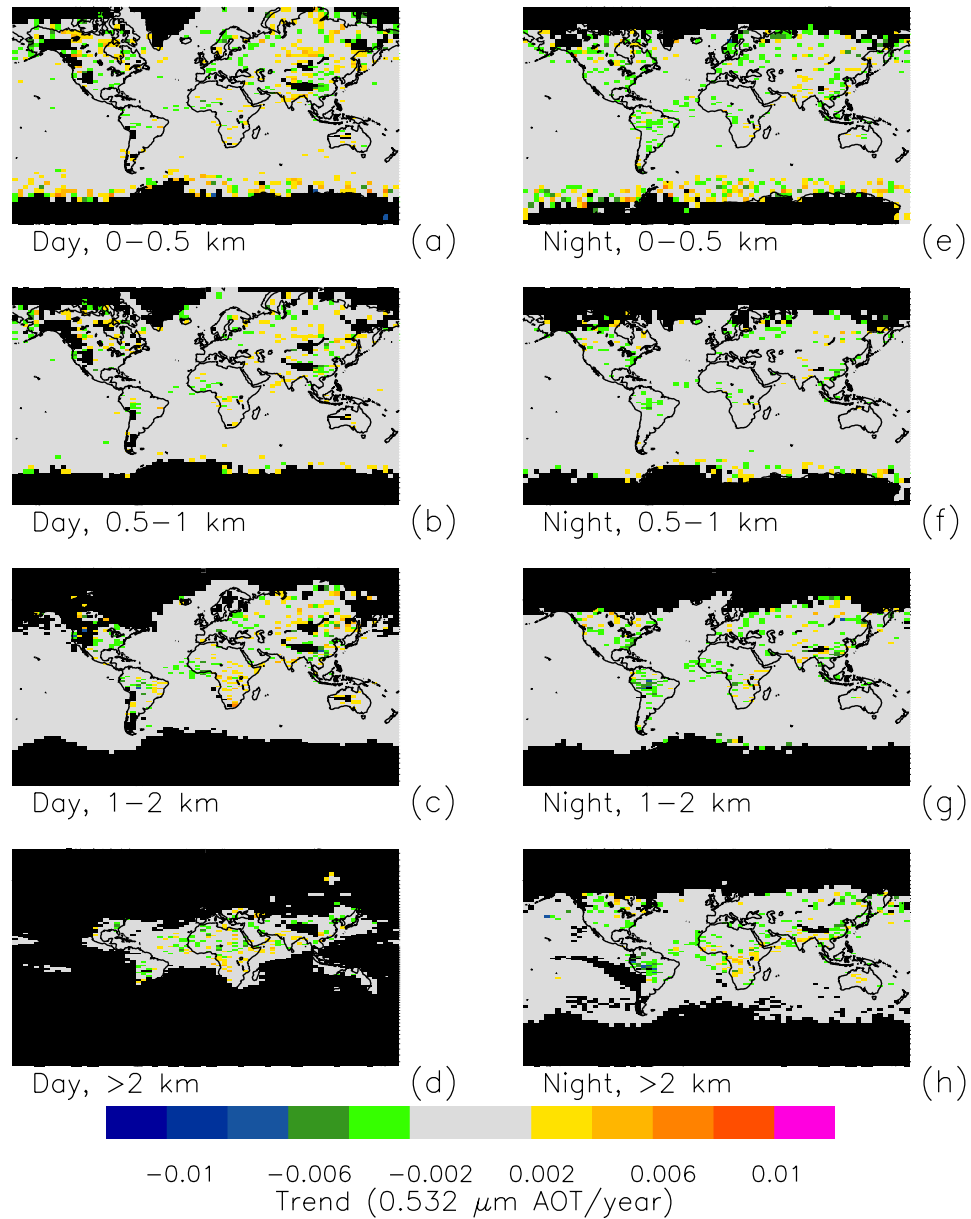


Figure 42. From June 2006 to December 2014, trends (AOT per year) of the de-seasonalized monthly mean layer CALIOP AOT for (a, e) 0.0 - 0.5 km, (b, f) 0.5 - 1.0 km, (c, g) 1.0 - 2.0 km, and (d, h) > 2.0 km for every $2^\circ \times 5^\circ$ (latitude/longitude). Daytime analyses are shown in Figs. 42a-42d, with nighttime analyses in Figs. 42e-42h.

presence. On the other hand, Southern Africa and India exhibit positive trends in total-column AOT. Aerosol particles between 1.0 and 2.0 km AGL predominantly contribute to the total-column variation in Southern Africa, and aerosol particles in the 0.0-0.5 km

layers are the primary contribution for total-column trends for India (Table 11). For those regions with statistically significant total-column AOT trends (Southern Africa, Eastern China, India, Europe, and the Eastern U.S.), the trends for the layer of primary contribution to the total-column trend for each region are also statistically significant (Table 12).

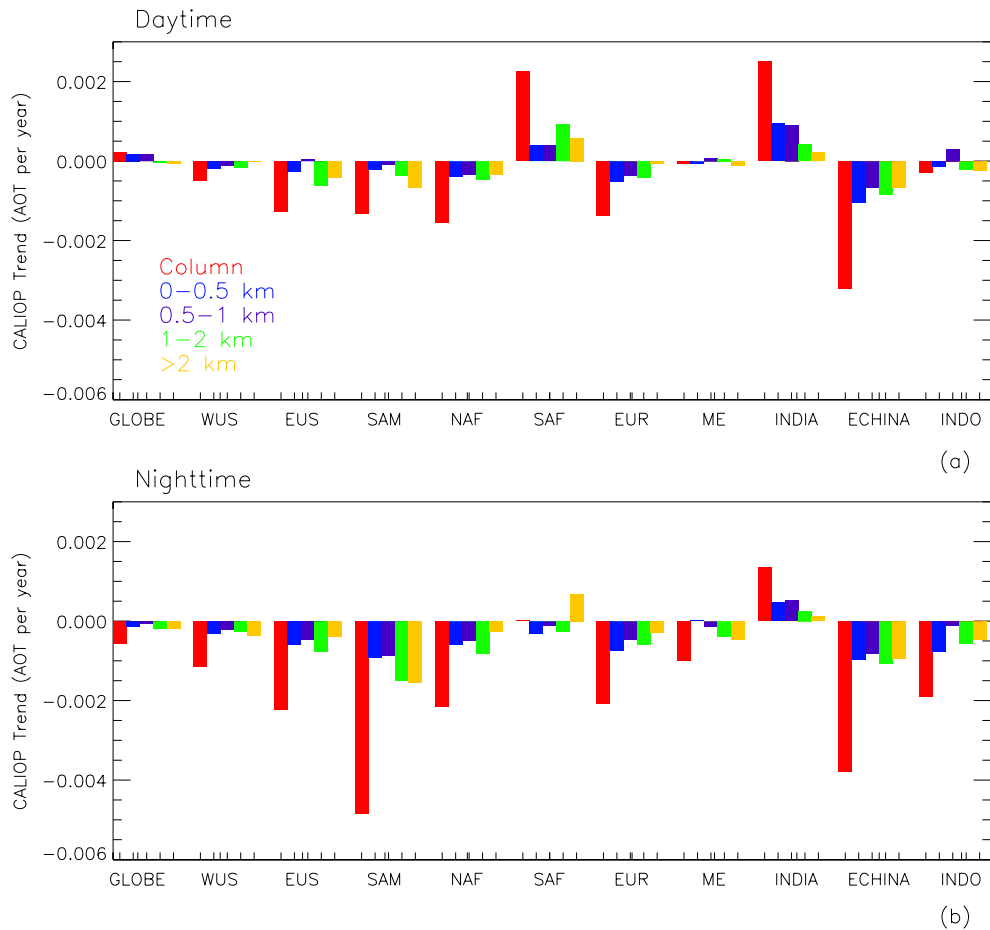


Figure 43. For June 2006 to December 2014, trends (AOT per year) of the de-seasonalized monthly mean CALIOP AOT for the total-column and each of the four layers for the globe and each region for (a) daytime and (b) nighttime. The ten regions presented are Western U.S. (WUS), Eastern U.S. (EUS), South America (SAM), Northern Africa (NAF), Southern Africa (SAF), Europe (EUR), the Middle East (ME), India (INDIA), Eastern China (ECHINA), and Indonesia (INDO).

Five of the ten selected focus regions exhibit the same altitude segment of primary contribution (i.e., largest bars in Fig. 43) to total-column trend for both day (Fig. 43a) and night (Fig. 43b): Northern Africa (1.0-2.0 km), the Middle East (> 2.0 km), Europe (0.0-0.5 km), Eastern U.S. (1.0-2.0 km), and South America (> 2.0 km). Four regions (Southern Africa, Eastern China, India, and the Western U.S.) experience an increase in the altitudes with greatest contribution to total variation. Lastly, contributions in Indonesia decrease monotonically from 0.5-1.0 km to the layer nearest the surface (i.e., 0.0-0.5 km). These day-night similarities and differences are summarized in Table 11. As is the case with the daytime analysis, those regions with statistically significant total-column AOT trends during nighttime also exhibit statistically significant trends for the layer of primary contribution to the total-column trend (Table 12).

6.3.3.4 Sensitivity studies. Prior studies have reported uncertainties in CALIOP extinction profiles and AOT (e.g., Kacenelenbogen et al., 2011; Campbell et al., 2012). For example, surface contamination is possible, and can occur as large negative extinction values (i.e., noise excursions; Winker et al., 2013) or beneath surface-attached opaque aerosol layers (https://eosweb.larc.nasa.gov/PRODOCS/calipso/Quality_Summaries/CALIOP_L3A_ProProducts_1-00.html). Also, although rigorous QA procedures have been implemented for this analysis (including the surface aerosol requirement described in Sec. 6.2), there still exists the possibility of cloud presence over a small portion of the 5 km aerosol profile, as determined by the CALIOP vertical feature mask (VFM). Therefore, two sensitivity studies (Fig. 44) are conducted to examine the effect these issues may have on temporal variation in CALIOP AOT.

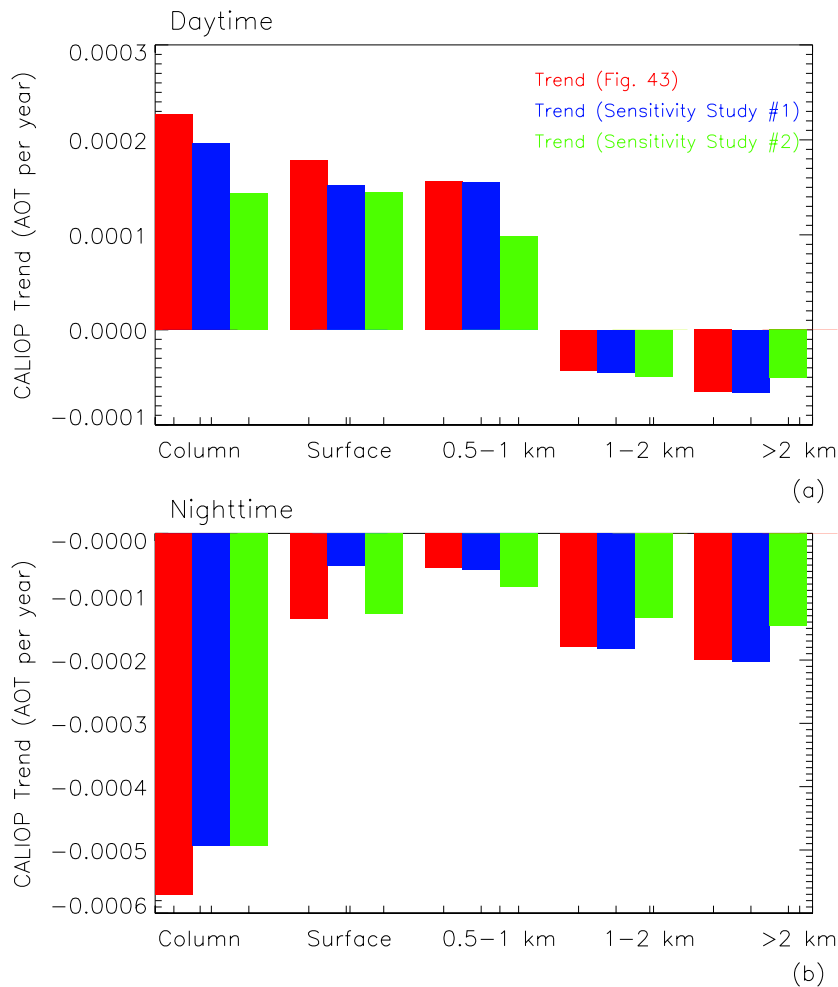


Figure 44. For June 2006 to December 2014, global total-column/layer trends (AOT per year) of the de-seasonalized monthly mean CALIOP AOT from the analysis shown in Fig. 43 and two sensitivity studies for (a) daytime and (b) nighttime. See the text for details of each sensitivity study.

The ground contamination issue (i.e., Sensitivity Study #1) is investigated by re-computing CALIOP AOT trends and ignoring the lowest 200 m of the profile, such that the surface layer represents 200-500 m AGL. For the daytime analysis, smaller values for the total-column and surface are found when ignoring the lowest 200 m (Fig. 44a), as compared with corresponding results in Fig. 43. However, the nighttime analysis of the sensitivity study yields larger temporal variability for the total-column and surface (Fig.

44b). For both daytime and nighttime, results are mostly unchanged for the top three layers. A minor discrepancy exists in the top three layers because of a small sampling bias, resulting from columns that only contain aerosol in the lowest 200 m. Overall, no large differences exist globally, suggesting that ground contamination has an insignificant effect on overall trend results. This may be partially due to the screening of the ‘negative surface anomaly’ (Amiridis et al., 2013; Winker et al., 2013) during QA procedures.

To investigate potential cloud-related issues (i.e., Sensitivity Study #2), CALIOP AOT trends are re-computed with the requirement that the VFM classifies no clouds in the entire 5 km aerosol profile. This requirement is not used in this initial analysis, as it is a strict requirement that excludes a significant portion of the 5 km granules that are for the most part cloud-free. Comparison between results in Fig. 43 and those of this sensitivity study reveals no clear correlative pattern for daytime and nighttime conditions, as changes vary with altitude (Fig. 44). However, as is the case for the first sensitivity study, overall trends are of the same sign and similar magnitude. Therefore, since no large differences exist globally, it is concluded that the presence of clouds (as determined by the VFM) does not have a significant impact on CALIOP-derived AOT trends.

6.3.3.5 Temporal variability of collocated CALIOP and Aqua MODIS observations. In Sec. 6.3.3.1, temporal variability in daytime total-column CALIOP AOT is compared with those from previous passive-based studies, like from MODIS and MISR, for which significant regional differences are found. However, these comparisons do not address the causes of the differences (e.g., differences in algorithm performance and/or spatial/temporal sampling) found. Thus, as the final step for this study, the variation of daytime AOT is examined from a spatially (5 km) and temporally (30 minutes)

collocated Collection 6 (C6) Aqua MODIS (Levy et al., 2013) and CALIOP dataset. The Aqua MODIS C6 Level 2.0 aerosol product (MYD04_L2; 0.550 μm) is reported at 10 x 10 km^2 spatial resolution, and only those retrievals flagged as “marginal” or better are used. Note that this analysis provides an initial perspective of collocated Aqua MODIS/CALIOP C6 AOT trends, as a full study is required to investigate calibration drift as was done for C5 in Zhang and Reid (2010). Also, the collocation is performed at the MYD04_L2 data domain (10 x 10 km^2 resolution), and thus the collocated data size is reduced in comparison with the CALIOP dataset used in previous sections.

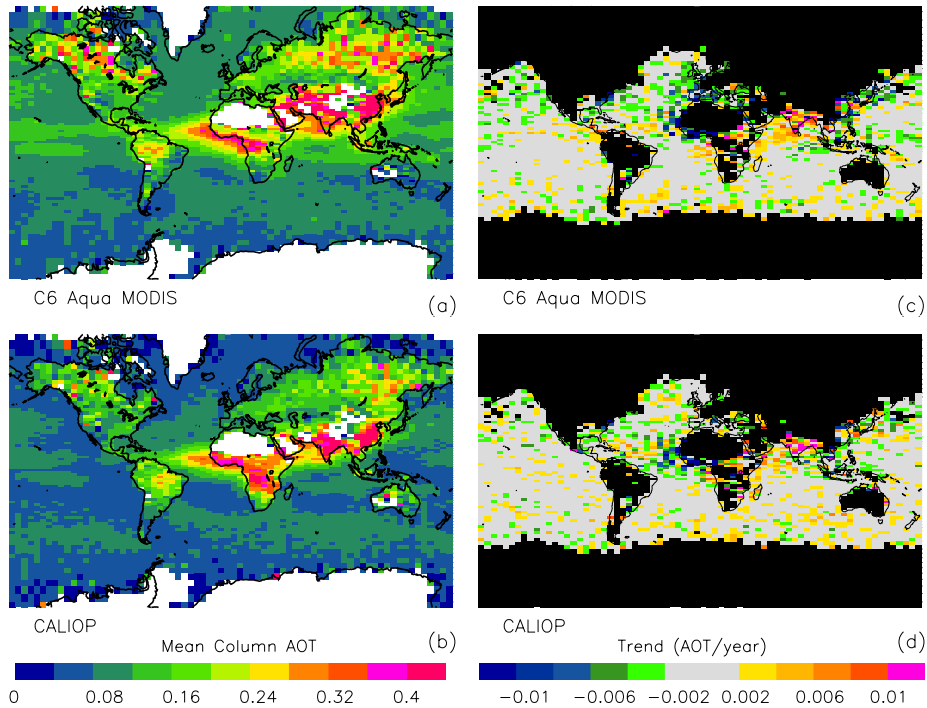


Figure 45. For June 2006 to December 2014, (a, b) mean total-column daytime AOT and (c, d) trends (AOT per year) of the de-seasonalized monthly mean total-column daytime AOT at $2^\circ \times 5^\circ$ (latitude/longitude) resolution, from the collocated Collection 6 (C6) Aqua MODIS (Figs. 45a and 45c) and CALIOP (Figs. 45b and 45d) analyses.

Figure 45 depicts the mean state of collocated column-integrated AOT for C6 Aqua MODIS (Fig. 45a) and CALIOP (Fig. 45b) for the study period (June 2006 through

December 2014). AOT spatial distributions are again generally consistent between the two instruments, with high aerosol loadings off the western coast of Northern Africa, India, and China, and lower AOT over the remote oceans. However, some notable differences exist, such as in the Tropical Pacific, Indonesia, and the coastal regions of East Asia. Consistent with previous studies (e.g., Kittaka et al., 2011; Redemann et al., 2012; Toth et al., 2013), the CALIOP low AOT bias (i.e., compared to MODIS) is apparent for most regions. Also shown in Fig. 45 are the corresponding spatial distributions of yearly trends in the collocated deseasonalized monthly-mean total-column AOT from C6 Aqua MODIS (Fig. 45c) and CALIOP (Fig. 45d). Stronger trends are generally observed for C6 Aqua MODIS than for CALIOP. Regional variations are similar to those shown in Fig. 45, with negative values found over the Eastern U.S., western coast of Northern Africa, Europe, and Eastern China, and positive ones found over Southern Africa and India.

Bar plots from Fig. 43 are reconstructed for the collocated C6 Aqua MODIS/CALIOP analysis, and are shown in Fig. 46. While the temporal variations in aerosol vertical distribution for most regions are consistent with those shown in Fig. 43 and outlined in Table 11, some differences exist. This is expected, as MODIS does not provide AOT retrievals for glint regions over oceans and also bright land surfaces (whereas CALIOP does; e.g., Levy et al., 2013). The magnitudes and signs of the CALIOP-based total-column AOT trends are similar to those presented in Fig. 43, and are consistent with those regionally depicted in Fig. 45. As for corresponding results from a passive perspective, the collocated C6 Aqua MODIS AOT values are stronger than those from CALIOP and are of the same sign for all but one (i.e., the Middle East) of the ten study regions. The different trend observed over the Middle East may be due to sampling issues or uncertainties in the retrieval.

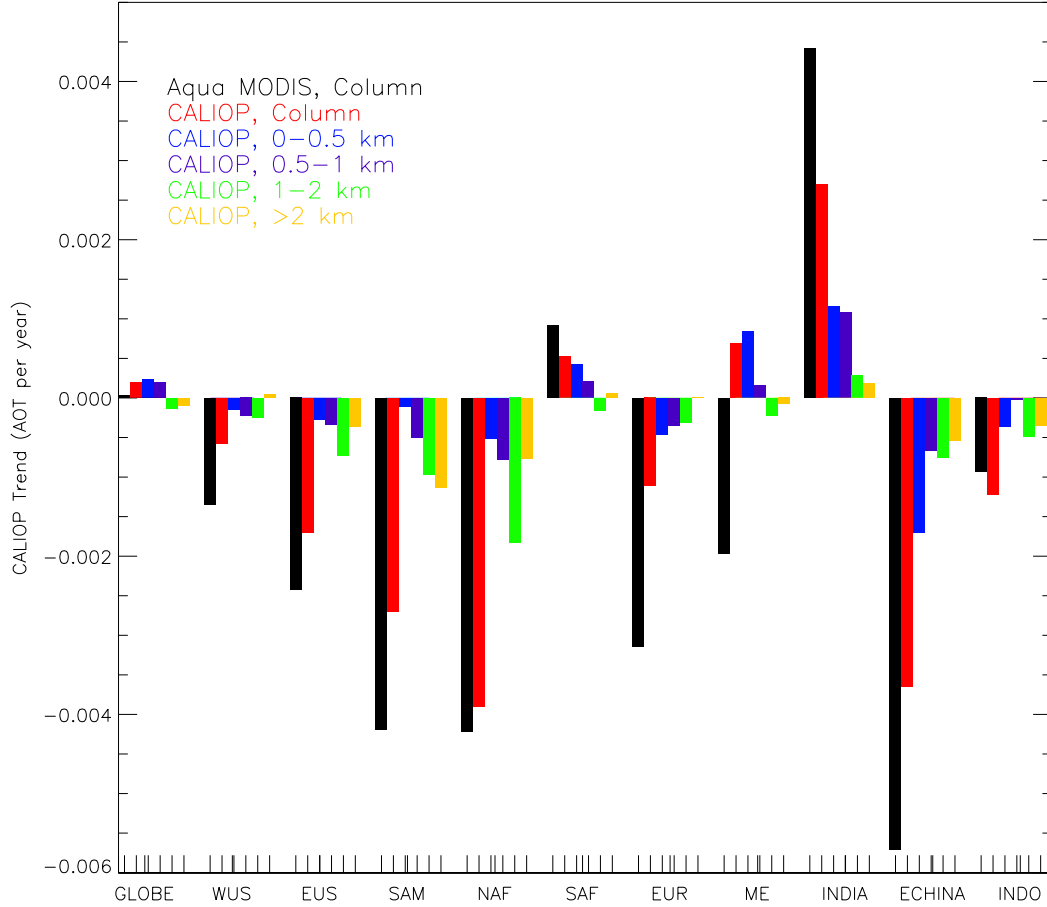


Figure 46. For June 2006 to December 2014, global and regional trends (AOT per year) of the de-seasonalized monthly mean daytime AOT for the total-column and each layer from the collocated Collection 6 (C6) Aqua MODIS/CALIOP analysis. The ten regions presented are Western U.S. (WUS), Eastern U.S. (EUS), South America (SAM), Northern Africa (NAF), Southern Africa (SAF), Europe (EUR), the Middle East (ME), India (INDIA), Eastern China (ECHINA), and Indonesia (INDO).

Globally, CALIOP total-column AOT variation is slightly stronger than that of C6 Aqua MODIS AOT. This may seem inconsistent with the bar plots presented in Fig. 46, as many of the ten selected regions exhibit stronger C6 Aqua MODIS AOT values than that of CALIOP. This implies that areas outside the ten selected regions may exhibit smaller C6 Aqua MODIS AOT values. For some regions (e.g., Eastern China), the negative trend exhibited by the C6 Aqua MODIS AOT data is in disagreement with results

found from independent C5 Aqua MODIS observations reported in past studies (Table 13). However, their signs are the same for CALIOP and C6 Aqua MODIS when the two datasets are collocated, and thus indicates that differences in column-integrated AOT trends are related to differences in the spatial and temporal sampling between the two sensors. Additional research is necessary to determine if this is the only cause of the discrepancy, as other factors exist (e.g., the difference between C5 and C6 Aqua MODIS data).

6.4 Conclusions

The temporal variability of the vertical distribution of aerosol particles in the atmosphere has been assessed through the use of aerosol optical thickness (AOT) and extinction coefficient retrievals derived from both satellite and ground-based passive remote sensors. Limited to only column-integrated measurements, previous passive sensor-based investigations necessarily focus solely on total-column AOT trends. A corresponding study that characterizes aerosol vertical distribution, however, is crucial to furthering the understanding of the effect aerosols have on climate and air quality. The Cloud-Aerosol Lidar with Orthogonal Polarization (CALIOP) is a space-based active remote sensor that acquires vertical profiles of particulate loading within the atmosphere, and thus is an ideal platform for studying aerosol particle presence, and by proxy AOT, as a function of altitude.

Using eight and a half years (June 2006 – December 2014) of CALIOP aerosol observations, the temporal variation of vertically distributed aerosol extinction is quantified regionally and globally. The ten regions of focus are Northern Africa, Southern Africa, Eastern China, India, Middle East, Indonesia, Europe, Eastern U.S., Western U.S., and South America. Analysis is performed both for total-column AOT and at four discrete

levels: 0.0 to 0.5 km, 0.5 to 1.0 km, 1.0 to 2.0 km, and greater than 2.0 km above ground level (AGL). Trend analyses from this study are compared with similar analyses based on passive satellite- and Aerosol Robotic Network (AERONET)-based methods. Regions with consistent trends among active- and passive-based studies are highlighted and the sources in the vertical domain are examined. The Mann-Kendall (MK) test is used to evaluate the statistical significance of the trends computed in this study. The main findings of this study are:

- (1) Statistically-significant near-zero global total-column AOT trends of 0.0002 and -0.0006 per year are found for daytime and nighttime conditions, respectively. These are primarily due to near-surface (i.e., 0.0-0.5 km and 0.5-1.0 km AGL) for daytime, and elevated (i.e., 1.0-2.0 km and > 2.0 km AGL) for nighttime, aerosol particles.
- (2) Statistically-significant increasing total-column daytime AOTs are found over Southern Africa (0.0023/year) and India (0.0025/year), with statistically-significant decreasing total-column daytime AOT trends found over Europe (-0.0014/year), Eastern U.S. (-0.0013/year), and Eastern China (-0.0032/year).
- (3) Although differing in both spatial and temporal coverage, total-column AOT trends derived from both passive- and active-based methods are consistent for most regions.
- (4) While a positive trend in total-column AOT is found over Eastern China from passive satellite sensors, CALIOP and some AERONET observations indicate a negative value. However, results from collocated Collection 6 Moderate Resolution Imaging Spectroradiometer (MODIS) and CALIOP data are consistent over China,

indicating that AOT trends in Eastern China are likely horizontal sampling-dependent.

(5) Increasing daytime AOT trends found in Southern Africa and India are mostly due to changes in aerosol loading at the 1.0-2.0 km and 0.0-0.5 km layers, respectively. Decreasing values over Northern Africa, Eastern U.S., and South America are due mostly to elevated (i.e., 1.0-2.0 km or >2.0 km AGL) aerosol loading, while the largest contributor to decreasing values in Eastern China, Indonesia, and Europe is nearer the surface (i.e., 0.0-0.5 km or 0.5-1.0 km AGL) layers.

(6) Globally, the time series of 0.0-0.5 km aerosol loading is in counter-phase with that of > 2.0 km aerosol particle presence. This pattern is most influenced by aerosol vertical distribution over global land compared to that over global oceans.

(7) An increasing (but marginal) daytime trend in near-surface aerosols (i.e., 0.0-0.5 km layer) found over India (0.0010/year) suggests slightly deteriorating air quality over this region. In contrast, a marginal decreasing daytime near-surface aerosol trend over Eastern China (-0.0010/year) implies a slight improvement in air quality for this area.

The results from this research will be helpful in studying evolving air quality for regions with limited surface-based air pollution measurement sites. Similarly, aerosol-related climate studies, especially those concerning longwave aerosol forcing, may also benefit from resolving changes in aerosol vertical distribution. Aerosol transport, particularly the differentiation between local aerosol sources and transported plumes over representative periods, is another possible area of future work. Ultimately, aerosol speciation can play a key role in all of the aforementioned topics, and thus remains an

important aspect of future studies involving temporal variations in the vertical distribution of atmospheric aerosols.

This study is not without several limitations, including the accuracy of CALIOP-derived AOT, in part due to the assumption of the lidar ratio (i.e., extinction-to-backscatter ratio) to compute extinction (discussed in more detail below). Also, the time period (8.5 years) used to analyze trends is relatively short, in the context of environmental and instrument uncertainties. The inconsistency of CALIOP-based AOT trends with those derived from passive satellite sensors over regions with large AOTs (e.g., Asia), and the disparity between daytime and nighttime global AOT trends, are other areas that require further investigation.

As a final thought, note that errors exist in CALIOP Level 2.0 data. For example, the misclassification of dense aerosol layers as clouds results in the elimination of highly polluted scenes from the dataset, and could affect the AOT profile temporal variations derived in this study. Also, past studies report biases in CALIOP AOT when compared to other sensors, and some attribute this to incorrect lidar ratios used in the CALIOP algorithms (e.g., Wandinger et al., 2010; Campbell et al., 2013; Tesche et al., 2013). As an elastic lidar, an inherent limitation of CALIOP is that, absent a collocated measurement of layer optical depth, an a priori estimate of lidar ratio is required to retrieve extinction. This can cause offsets in this trend analysis. High Spectral Resolution Lidar (HSRL) can be leveraged here, as prior knowledge of lidar ratios is not necessary to make retrievals of extinction (e.g., Burton et al., 2013). Also, the use of ground-based lidars can provide a means to evaluate the representativeness (i.e., due to detection sensitivity) of the CALIOP aerosol profiles and their corresponding trends derived in this analysis. A recent study investigates this issue using Raman lidars, with a focus on the aerosol direct radiative effect

(Thorsen and Fu, 2015). Ultimately, the temporal variability of the CALIOP AOT profile is analyzed in this study, with the acknowledgement that these derived variations are likely offset by some uncharacterized amount. While this study provides an initial perspective on global aerosol profile temporal variability, stronger conclusions can likely be made in future studies given the inclusion of aerosol optical parameters from HSRL and comparison with ground-based lidars.

CHAPTER VII

SUMMARY AND CONCLUSIONS

Space-borne passive aerosol measurements are prominent tools for studying air pollution, including particulate matter less than $2.5\ \mu\text{m}$ ($\text{PM}_{2.5}$). Specifically, aerosol optical thickness (AOT) observations, like those from the Moderate Resolution Imaging Spectroradiometer (MODIS) and Multi-angle Imaging Spectroradiometer (MISR), have been leveraged for this task. In this doctoral dissertation, issues with estimating $\text{PM}_{2.5}$ from passively-sensed AOT were explored. The feasibility of, and issues with, using near-surface aerosol measurements from the active space-borne Cloud-Aerosol Lidar with Orthogonal Polarization (CALIOP) instrument to directly derive $\text{PM}_{2.5}$ concentrations were also investigated. In order to obtain knowledge of possible temporal variations in surface air quality, this dissertation research concluded with a study examining trends in aerosol vertical distribution, including those of aerosols near the ground.

As a first step, using purely measurement-based methods, the impacts of satellite AOT data quality and representativeness of satellite-derived AOT to surface aerosol particle mass concentration on the $\text{PM}_{2.5}$ /AOT relationship for the contiguous United States (CONUS) were explored. This was done through temporally and spatially collocated datasets of $\text{PM}_{2.5}$ and Level 2 (L2) AOT retrievals from MODIS, MISR, and CALIOP. These analyses showed that improving data quality of satellite AOT, such as done with data assimilation-grade retrievals, increases their correlation with $\text{PM}_{2.5}$. However, overall correlation was relatively low across CONUS. Also, integrated extinction

observed within 500 m above ground level (AGL), as measured by CALIOP, was not well representative of the total column AOT. Surface aerosol in eastern CONUS was better correlated than in the western CONUS. The best correlation values were found for estimated dry mass CALIOP extinction at 200-300 m AGL and $PM_{2.5}$, as shown by an initial investigation into the ability of using actively sensed aerosol observations as a proxy for $PM_{2.5}$ concentrations.

Second, issues related to CALIOP aerosol data processing were explored. For example, due to instrument sensitivities and algorithm detection limits, L2 CALIOP 532 nm aerosol extinction profile retrievals are often populated with retrieval fill values (RFVs), which indicate the absence of detectable levels of aerosol within the profile. In the CALIOP data products, the AOT of any CALIOP all-RFV profile (i.e., a profile consisting entirely of RFVs) is reported as being zero, which may introduce a bias in CALIOP-based AOT and aerosol vertical distribution (including near-surface aerosol extinction) climatologies. In this study, four years (2007-2008 and 2010-2011) of CALIOP L2 aerosol data were used to quantify the occurrence frequency of daytime CALIOP all-RFV profiles, after which revised estimates of AOT for all-RFV profiles were derived using collocated MODIS Dark Target (DT) and, where available, Aerosol Robotic Network (AERONET) data. Globally, all-RFV profiles comprised roughly 71% of all daytime CALIOP L2 aerosol profiles (i.e., including completely attenuated profiles), accounting for nearly half (45%) of all daytime cloud-free L2 aerosol profiles. The mean collocated MODIS DT (AERONET) 550 nm AOT was found to be near 0.06 (0.08) for CALIOP all-RFV profiles. Further, a global mean aerosol extinction profile was estimated, a so-called “noise floor”, for CALIOP all-RFV profiles. The global mean CALIOP AOT was then recomputed by replacing RFV values with the derived noise floor values for both all-RFV and non-all-RFV profiles. This

process yielded an improvement in the agreement of CALIOP and MODIS over-ocean AOT.

Next, a 2-year (2008-2009) concept-demonstration study was conducted to retrieve $PM_{2.5}$ concentrations over the CONUS by applying a bulk-mass-modeling-based method using CALIOP observations. Different from previous approaches that rely on empirical relationships between AOT and $PM_{2.5}$, daytime and nighttime $PM_{2.5}$ concentrations were derived from near surface CALIOP aerosol extinction retrievals using bulk mass extinction and model-based hygroscopicity. Preliminary results from this study showed a good agreement ($r^2 \sim 0.50$; mean bias of $-3.5 \mu\text{g m}^{-3}$) between the averaged nighttime CALIOP-derived $PM_{2.5}$ and ground-based $PM_{2.5}$ (with a lower r^2 of ~ 0.24 for daytime; mean bias of $-1.1 \mu\text{g m}^{-3}$), suggesting that $PM_{2.5}$ concentrations can be obtained from active-based space borne observations with reasonable accuracy. However, as this initial study has also shown, there are spatial, temporal, and retrieval biases related to this method. These issues, along with more carefully quantifying the uncertainties related to the values of the bulk parameters assumed in this study, all require further research.

Lastly, the temporal variability in the vertical distribution of AOT derived from the $0.532 \mu\text{m}$ aerosol extinction coefficient was investigated using CALIOP observations over eight and a half years (June 2006 – December 2014). Temporal variability of CALIOP column-integrated AOT was largely consistent with total-column AOT trends from several passive satellite sensors, such as the MODIS, MISR, and the Sea-viewing Wide Field-of-view Sensor (SeaWiFS) instruments. Globally, a 0.0002 AOT per year positive trend in deseasonalized CALIOP total-column AOT for daytime conditions was attributed to corresponding changes in near-surface (i.e., 0.0-0.5 km or 0.5-1.0 km AGL) aerosol particle loading, while a -0.0006 AOT per year trend during nighttime was attributed to elevated

(i.e., 1.0-2.0 km or > 2.0 km AGL) aerosols. Trends in CALIOP aerosol vertical distribution were also investigated regionally. For example, both the Eastern and Western CONUS exhibited slightly negative trends in near-surface aerosols, suggesting a marginal improvement in air quality for these areas.

This dissertation research advances the study of PM_{2.5} pollution using passive and active remote sensing techniques, and there are several areas in which this topic can be further explored in future work. For one, responding to the importance of air quality trends as outlined in the most recent Decadal Survey, temporal variations of CALIOP-derived PM_{2.5} can be examined, building upon the trends of near-surface aerosol extinction found in this study. Also, additional research is necessary for applying the bulk-mass-modeling-based method on a global scale. This is especially important for highly polluted regions with little to no readily available PM_{2.5} observations, such as China. Overall, this doctoral research helps pave the way for future studies in applying aerosol extinction derived from lidar observations for PM_{2.5} monitoring and forecasts, like those from the Earth Cloud Aerosol Radiation Explorer (EarthCARE) and Aerosol-Clouds-Ecosystems (ACE) satellite missions.

BIBLIOGRAPHY

- Akimoto, H. (2003). Global air quality and pollution. *Science*, 302(5651), 1716-1719.
- Alfaro-Contreras, R., Zhang, J., Campbell, J. R., & Reid, J. S. (2016). Investigating the frequency and interannual variability in global above-cloud aerosol characteristics with CALIOP and OMI. *Atmospheric Chemistry and Physics*, 16(1), 47-69.
- Amaral, S. S., de Carvalho, J. A., Costa, M. A. M., & Pinheiro, C. (2015). An overview of particulate matter measurement instruments. *Atmosphere*, 6(9), 1327-1345.
- Amiridis, V., Marinou, E., Tsekeri, A., Wandinger, U., Schwarz, A., Giannakaki, E., Mamouri, R., Kokkalis, P., Biniotoglou, I., Solomos, S., Herekakis, T., Kazadzis, S., Gerasopoulos, E., Balis, D., Papayannis, A., Kontoes, C., Kourtidis, K., Papagiannopoulos, N., Mona, L., Pappalardo, G., Le Rille, O., & Ansmann, A. (2015). LIVAS: a 3-D multi-wavelength aerosol/cloud climatology based on CALIPSO and EARLINET, *Atmos. Chem. Phys. Discuss.*, 15, 2247-2304, doi:10.5194/acpd-15-2247-2015.
- Amiridis, V., Wandinger, U., Marinou, E., Giannakaki, E., Tsekeri, A., Basart, S., Kazadzis, S., Gkikas, A., Taylor, M., Baldasano, J., & Ansmann, A. (2013). Optimizing CALIPSO Saharan dust retrievals. *Atmos. Chem. Phys.*, 13, 12089-12106, doi:10.5194/acp-13-12089-2013.

- Anderson, T. L., Charlson, R. J., White, W. H., & McMurry, P. H. (1994). Comment on “Light scattering and cloud condensation nucleus activity of sulfate aerosol measured over the Northeast Atlantic Ocean” by D.A. Hegg et al. *J. Geophys. Res.*, 99(D12), 25947–25949, doi:10.1029/94JD02608.
- Anderson, T. L., Charlson, R. J., Winker, D. M., Ogren, J. A., & Holmén, K. (2003). Mesoscale variations of tropospheric aerosols. *J. Atmos. Sci.*, 60, 119–136.
- Atwood, S. A., Reid, J. S., Kreidenweis, S. M., Cliff, S. S., Zhao, Y., Lin, N.-H., Tsay, S.-C., Chu, Y.-C., & Westphal, D. L. (2013). Size resolved measurements of springtime aerosol particles over the northern South China Sea. *Atmospheric Environment*, 78, 134-143.
- Ban-Weiss, G. A., Cao, L., Bala, G., & Caldeira, K. (2012). Dependence of climate forcing and response on the altitude of black carbon aerosols. *Climate Dynamics*, 38 (5-6), 897-911.
- Boucher, O. (2015). *Atmospheric aerosols: Properties and climate impacts*. Springer.
- Boyouk, N., Léon, J. F., Delbarre, H., Podvin, T., & Deroo, C. (2010). Impact of the mixing boundary layer on the relationship between PM_{2.5} and aerosol optical thickness. *Atmospheric Environment*, 44(2), 271-277.
- Burton, S. P., Ferrare, R. A., Vaughan, M. A., Omar, A. H., Rogers, R. R., Hostetler, C. A., & Hair, J. W. (2013). Aerosol classification from airborne HSRL and comparisons with the CALIPSO vertical feature mask. *Atmospheric Measurement Techniques*, 6(5), 1397-1412.

- Campbell, J. R., Reid, J. S., Westphal, D. L., Zhang, J., Hyer, E. J., & Welton, E. J. (2010). CALIOP aerosol subset processing for global aerosol transport model data assimilation. *IEEE Journal of Selected Topics in Applied Earth Observations and Remote Sensing*, 3(2), 203-214.
- Campbell, J. R., Reid, J. S., Westphal, D. L., Zhang, J., Tackett, J. L., Chew, B. N., Welton, E. J., Shimizu, A., Sugimoto, N., Aoki K., & Winker D. M. (2013). Characterizing the vertical profile of aerosol particle extinction and linear depolarization over Southeast Asia and the Maritime Continent: the 2007-2009 view from CALIOP. *Atmos. Res.*, doi:10.1016/j.atmosres.2012.05.007.
- Campbell, J. R., Tackett, J. L., Reid, J. S., Zhang, J., Curtis, C. A., Hyer, E. J., Sessions, W. R., Westphal, D. L., Prospero, J. M., Welton, E. J., Omar, A. H., Vaughan, M. A., & Winker, D. M. (2012). Evaluating nighttime CALIOP 0.532 μm aerosol optical depth and extinction coefficient retrievals. *Atmospheric Measurement Techniques*, 5, 2143-2160, doi:10.5194/amt-5-2143-2012.
- Chand, D., Wood, R., Anderson, T. L., Satheesh, S. K., & Charlson, R. J. (2009). Satellite-derived direct radiative effect of aerosols dependent on cloud cover. *Nature Geoscience*, 2(3), 181-184.
- Charlson, R. J., Ahlquist, N. C., & Horvath, H. (1968). On the generality of correlation of atmospheric aerosol mass concentration and light scatter. *Atmospheric Environment* (1967), 2(5), 455-464.
- Chen, W.-T., Liao, H., & Seinfeld, J. H. (2007). Future climate impacts of direct radiative forcing of anthropogenic aerosols, tropospheric ozone, and long-lived greenhouse gases. *Journal of Geophysics Research*, 112, D14209, doi:10.1029/2006JD008051.

- Chew, B. N., Campbell, J. R., Hyer, E. J., Salinas, S. V., Reid, J. S., Welton, E. J., Holben, B. N., & Liew, S. C. (2016). Relationship between aerosol optical depth and particulate matter over Singapore: Effects of aerosol vertical distributions. *Aerosol and Air Quality Research*, 16, 2818-2830.
- Chew, B. N., Campbell, J. R., Reid, J. S., Giles, D. M., Welton, E. J., Salinas, S. V., & Liew, S. C. (2011). Tropical cirrus cloud contamination in sun photometer data, *Atmospheric Environment*, 45(37), 6724-6731.
- Chew, B. N., Campbell, J. R., Salinas, S. V., Chang, C. W., Reid, J. S., Welton, E. J., Holben, B. N., & Liew, S. C. (2013). Aerosol particle vertical distributions and optical properties over Singapore. *Atmospheric Environment*, 79, 599-613.
- Chow, J. C., Watson, J. G., Park, K., Robinson, N. F., Lowenthal, D. H., Park, K., & Magliano, K. A. (2006). Comparison of particle light scattering and fine particulate matter mass in central California. *Journal of the Air & Waste Management Association*, 56(4), 398-410.
- Chu, D. A., Kaufman, Y. J., Zibordi, G., Chern, J. D., Mao, J., Li, C., & Holben, B. N. (2003). Global monitoring of air pollution over land from the Earth Observing System-Terra Moderate Resolution Imaging Spectroradiometer (MODIS). *J. Geophys. Res.*, 108, 4661, doi:10.1029/2002JD003179,D21.
- Chu, D. A., Tsai, T. C., Chen, J. P., Chang, S. C., Jeng, Y. J., Chiang, W. L., & Lin, N. H. (2013). Interpreting aerosol lidar profiles to better estimate surface PM_{2.5} for columnar AOT measurements. *Atmospheric environment*, 79, 172-187.

- Colarco, P. R., Kahn, R. A., Remer, L. A., & Levy, R. C. (2014). Impact of satellite viewing-swath width on global and regional aerosol optical thickness statistics and trends. *Atmos. Meas. Tech.*, 7, 2313-2335, <https://doi.org/10.5194/amt-7-2313-2014>.
- Dawson, K. W., Meskhidze, N., Josset, D., & Gassó, S. (2015). Spaceborne observations of the lidar ratio of marine aerosols. *Atmos. Chem. Phys.*, 15, 3241-3255, <https://doi.org/10.5194/acp-15-3241-2015>.
- de Meij, A., Pozzer, A., & Lelieveld, J. (2012). Trend analysis in aerosol optical depths and pollutant emission estimates between 2000 and 2009. *Atmospheric Environment*, 51, 75–85, doi:10.1016/j.atmosenv.2012.01.059.
- Devara, P. C. S., Maheskumar, R. S., Raj, P. E., Pandithurai, G., and Dani, K. K. (2002). Recent trends in aerosol climatology and air pollution as inferred from multi-year lidar observations over a tropical urban station, *International Journal of Climatology*, 22 (4), 435-449.
- Di, Q., Wang, Y., Zanobetti, A., Wang, Y., Koutrakis, P., Choirat, C., Dominici, F., & Schwartz, J. D. (2017). Air pollution and mortality in the Medicare population, *New England Journal of Medicine*, 376(26), 2513-2522.
- Diner, D. J., Beckert, J. C., Reilly, T. H., Bruegge, C. J., Conel, J. E., Kahn, R. A., Martonchik, J. V., Ackerman, T. P., Davies, R., Gerstl, S. A. W., Gordon, H. R., Muller, J.-P., Myneni, R. B., Sellers, P. J., Pinty, B., & Verstraete, M. M. (1998). Multi-angle Imaging SpectroRadiometer (MISR) instrument description and experiment overview, *IEEE Trans. Geosci. Remote Sens.*, 36, 1072–1087.

- Eck, T. F., Holben, B. N., Reid, J. S., Dubovik, O., Smirnov, A., O'Neill, N. T., Slutsker, I., & Kinne, S. (1999). Wavelength dependence of the optical depth of biomass burning, urban, and desert dust aerosols, *Journal of Geophysical Research: Atmospheres*, 104(D24), 31333-31349.
- Engel-Cox, J. A., Hoff, R. M., Rogers, R., Dimmick, F., Rush, A. C., Szykman, J., Al-Saadi, J., Chu, D. A., & Zell, E. R. (2006). Integrating lidar and satellite optical depth with ambient monitoring for 3-dimensional particulate characterization, *Atmos. Environ.*, 40, 8056–8067.
- Engel-Cox, J. A., Holloman, C. H., Coutant, B. W., & Hoff, R. M. (2004). Qualitative and quantitative evaluation of MODIS satellite sensor data for regional and urban scale air quality, *Atmos. Environ.*, 38, 2495–2509.
- Federal Register: National ambient air quality standards for particulate matter. (1997).
Final Rule Federal Register/vol. 62, no. 138/Friday, July 18, 1997/Final Rule, 40 CFR Part 50.
- Federal Register: National ambient air quality standards for particulate matter. (2006).
Proposed Rule Federal Register/vol. 71, no. 10/Tuesday, January 17, 2006/Proposed Rules, 40 CFR Part 50.
- Fuzzi, S., Baltensperger, U., Carslaw, K., Decesari, S., Denier van der Gon, H., Facchini, M. C., Fowler, D., Koren, I., Langford, B., Lohmann, U., Nemitz, E., Pandis, S., Riipinen, I., Rudich, Y., Schaap, M., Slowik, J. G., Spracklen, D. V., Vignati, E., Wild, M., Williams, M., & Gilardoni, S. (2015). Particulate matter, air quality and climate: lessons learned and future needs, *Atmos. Chem. Phys.*, 15, 8217-8299, <https://doi.org/10.5194/acp-15-8217-2015>.

- Getzewich, B. J., Tackett, J. L., Kar, J., Garnier, A., Vaughan, M. A., & Hunt, B. (2016). CALIOP Calibration: Version 4.0 Algorithm Updates, The 27th International Laser Radar Conference (ILRC 27), EPJ Web of Conferences, 119, 04013, doi:10.1051/epjconf/201611904013.
- Greenstone, M. (2002). The impacts of environmental regulations on industrial activity: Evidence from the 1970 and 1977 clean air act amendments and the census of manufactures, *Journal of political economy*, 110(6), 1175-1219.
- Gupta, P., Christopher, S.A., Wang, J., Gehrig, R., Lee, Y.C., & Kumar, N. (2006). Satellite remote sensing of particulate matter and air quality over global cities, *Atmospheric Environment* 40 (30), 5880–5892.
- Hand, J. L., & Malm, W. C. (2007). Review of aerosol mass scattering efficiencies from ground-based measurements since 1990, *Journal of Geophysical Research: Atmospheres*, 112(D16).
- Hand, J. L., Schichtel, B. A., Malm, W. C., & Frank, N. H. (2013). Spatial and temporal trends in PM_{2.5} organic and elemental carbon across the United States, *Advances in Meteorology*.
- Hanel, G. (1976). The properties of atmospheric aerosol particles as functions of relative humidity at thermodynamic equilibrium with surrounding moist air, *Adv. Geophys.*, 19, 73–188.
- Hegg, D. A., Ferek, R. J., & Hobbs, P. V. (1993). Light scattering and cloud condensation nucleus activity of sulfate aerosol measured over the northeast Atlantic Ocean, *J. Geophys. Res.*, 98(D8), 14887–14894, doi:10.1029/93JD01615.

- Hess, M., Koepke, P., & Schult, I. (1998). Optical properties of aerosols and clouds: The software package OPAC, *Bulletin of the American Meteorological Society*, 79(5), 831-844.
- Hoff, R. M. & Christopher, S. A. (2009). Remote sensing of particulate pollution from space: have we reached the promised land?, *J Air Waste Manag Assoc.*, 59:645–675.
- Holben, B. N., Eck, T. F., Slutsker, I., Tanre, D., Buis, J. P., Setzer, A., Vermote, E., Reagan, J.A., Kaufman, Y.J., Nakajima, T. & Lavenue, F. (1998). AERONET - A Federated Instrument Network and Data Archive for Aerosol Characterization, *Remote Sens. Environ.*, 66, 1-16.
- Hsu, N. C., Gautam, R., Sayer, A. M., Bettenhausen, C., Li, C., Jeong, M. J., Tsay, S.-C., & Holben, B. N. (2012). Global and regional trends of aerosol optical depth over land and ocean using SeaWiFS measurements from 1997 to 2010, *Atmospheric Chemistry and Physics*, 12, 8037-8053, doi:10.5194/acp-12-8037-2012.
- Hu, Z. (2009). Spatial analysis of MODIS aerosol optical depth, PM_{2.5}, and chronic coronary heart disease, *Int. J. Health Geogr.*, 8, 27, doi:10.1186/1476-072X-8-27.
- Huang, J., Hsu, N. C., Tsay, S. C., Holben, B. N., Welton, E. J., Smirnov, A., Jeong, M. J., Hansell, R.A., Berkoff, T.A., Liu, Z. & Liu, G. R. (2012). Evaluations of cirrus contamination and screening in ground aerosol observations using collocated lidar systems, *Journal of Geophysical Research: Atmospheres*, 117(D15).
- Huang, J., Minnis, P., Yi, Y., Tang, Q., Wang, X., Hu, Y., Liu, Z., Ayers, K., Trepte, C. & Winker, D. (2007). Summer dust aerosols detected from CALIPSO over the Tibetan Plateau, *Geophysical Research Letters*, 34(18).

- Hunt, W. H., Winker, D. M., Vaughan, M. A., Powell, K. A., Lucker, P. L., & Weimer, C. (2009). CALIPSO lidar description and performance assessment, *J. Atmos. Oceanic Technol.*, 26, 1214–1228, doi:10.1175/2009JTECHA1223.1.
- Hutchison, K. D., Faruqui, S. J., & Smith, S. (2008). Improving correlations between MODIS aerosol optical thickness and ground-based PM_{2.5} observations through 3D spatial analyses, *Atmospheric Environment*, 42(3), 530-543.
- Hyer, E. J. & Chew, B. N. (2010). Aerosol transport model evaluation of an extreme smoke episode in Southeast Asia, *Atmos. Environ.*, 44(11), 1422–1427.
- Hyer, E. J., Reid, J. S., & Zhang, J. (2011). An over-land aerosol optical depth data set for data assimilation by filtering, correction, and aggregation of MODIS Collection 5 optical depth retrievals, *Atmos. Meas. Tech.*, 4, 379–408, doi:10.5194/amt-4-379-2011.
- Illingworth, A. J., Barker, H. W., Beljaars, A., Ceccaldi, M., Chepfer, H., Clerbaux, N., Cole, J., Delanoë, J., Domenech, C., Donovan, D.P. & Fukuda, S. (2015). The EarthCARE satellite: The next step forward in global measurements of clouds, aerosols, precipitation, and radiation, *Bulletin of the American Meteorological Society*, 96(8), 1311-1332.
- Kacenelenbogen, M., Vaughan, M. A., Redemann, J., Hoff, R. M., Rogers, R. R., Ferrare, R. A., Russell, P. B., Hostetler, C. A., Hair, J. W., & Holben, B. N. (2011). An accuracy assessment of the CALIOP/CALIPSO version 2/version 3 daytime aerosol extinction product based on a detailed multi-sensor, multi-platform case study, *Atmos. Chem. Phys.*, 11, 3981-4000, doi:10.5194/acp-11-3981-2011.

- Kahn, R. A., Gaitley, B. J., Garay, M. J., Diner, D. J., Eck, T., Smirnov, A. & Holben, B. N. (2010). Multiangle Imaging Spectroradiometer global aerosol product assessment by comparison with Aerosol Robotic Network, *J. Geophys. Res.*, 115, D23209, doi:10.1029/2010JD014601.
- Kahn, R. A., Gaitley B. J., Martonchik J. V., Diner D. J., Crean K. A., & Holben B. N. (2005). Multiangle Imaging Spectroradiometer (MISR) global aerosol optical depth validation based on 2 years of coincident Aerosol Robotic Network (AERONET) observations, *J. Geophys. Res.*, 110, D10S04, doi:10.1029/2004JD004706.
- Kaku, K. C., Reid, J. S., Hand, J. L., Edgerton, E. S., Holben, B. N., Zhang, J. & Holz, R. E. (2018). Assessing the challenges of surface-level aerosol mass estimates from remote sensing and modeling during the SEAC⁴RS campaign: Baseline surface observations and remote sensing in the Southeastern United States, submitted to *Journal of Geophysical Research: Atmospheres*.
- Kanitz, T., Ansmann, A., Foth, A., Seifert, P., Wandinger, U., Engelmann, R., Baars, H., Althausen, D., Casaccia, C. & Zamorano, F. (2014). Surface matters: limitations of CALIPSO V3 aerosol typing in coastal regions, *Atmospheric Measurement Techniques*, 7(7), 2061-2072.
- Kaufman, Y. J., Boucher, O., Tanré, D., Chin, M., Remer, L. A., & Takemura, T. (2005). Aerosol anthropogenic component estimated from satellite data, *Geophys. Res. Lett.*, 32, L17804, doi:10.1029/2005GL023125.
- Kaufman, Y., Smirnov, A., Holben, B., & Dubovik, O. (2001). Baseline maritime aerosol: Methodology to derive the optical thickness and scattering properties, *Geophys. Res. Lett.*, 28(17), 3251–3254.

- Kaufman, Y. J., Tanré, D., & Boucher, O. (2002). A satellite view of aerosols in the climate system, *Nature*, 419(6903), 215.
- Kendall, M. G. (1975). *Rank Correlation Methods*. Griffin, London.
- Kim, M. H., Kim, S. W., Yoon, S. C., & Omar, A. H. (2013). Comparison of aerosol optical depth between CALIOP and MODIS-Aqua for CALIOP aerosol subtypes over the ocean, *Journal of Geophysical Research: Atmospheres*, 118(23).
- Kim, M. H., Omar, A. H., Vaughan, M. A., Winker, D. M., Trepte, C. R., Hu, Y., Z. Liu, Z., & Kim, S.-W. (2017). Quantifying the low bias of CALIPSO's column aerosol optical depth due to undetected aerosol layers, *J. Geophys. Res. Atmos.*, 122, 1098–1113, doi:10.1002/2016JD025797.
- Kittaka, C., Winker, D. M., Vaughan, M. A., Omar, A., & Remer, L. A. (2011). Intercomparison of column aerosol optical depths from CALIPSO and MODIS Aqua, *Atmospheric Measurement Techniques*, 4(2), 131-141.
- Kumar, N., Chu, A., & Foster, A. (2007). An empirical relationship between PM_{2.5} and aerosol optical depth in Delhi Metropolitan, *Atmos. Environ.*, 41, 4492–4503.
- Lau, K. M., Kim, M.K., & Kim, K.M. (2006). Asian monsoon anomalies induced by aerosol direct effects, *Climate Dynamics*, 26, 855–864, doi:10.1007/s00382-006-0114-z.
- Levy, R. C., Mattoo, S., Munchak, L. A., Remer, L. A., Sayer, A. M., Patadia, F., & Hsu, N. C. (2013). The Collection 6 MODIS aerosol products over land and ocean, *Atmos. Meas. Tech.*, 6, 2989-3034, doi:10.5194/amt-6-2989-2013.
- Levy, R. C., Remer L. A., Kleidman R. G., Mattoo S., Ichoku C., Kahn R., & Eck, T. F. (2010). Global evaluation of the Collection 5 MODIS dark-target aerosol products over land. *Atm. Chem. Phys.* 10, 10399-10420, doi:10.5194/acp-10-10399-2010.

- Li, J., Carlson, B. E., Dubovik, O., & Lacis, A. A. (2014b). Recent trends in aerosol optical properties derived from AERONET measurements, *Atmospheric Chemistry and Physics*, 14, 12271-12289, doi:10.5194/acp-14-12271-2014.
- Li, J., Carlson, B. E. & Lacis, A.A. (2014a). Revisiting AVHRR tropospheric aerosol trends using principal component analysis, *J. Geophys. Res. Atmos.*, 119, no. 6, 3309-3320, doi:10.1002/2013JD020789.
- Li, Z., Zhao, X., Kahn, R., Mishchenko, M., Remer, L., Lee, K.-H., Wang, M., Laszlo, I., Nakajima, T., & Maring, H. (2009). Uncertainties in satellite remote sensing of aerosols and impact on monitoring its long-term trend: a review and perspective, *Ann. Geophys.*, 27, 2755–2770.
- Liou, Kuo-Nan. (2002). *An introduction to atmospheric radiation*, Vol. 84. Academic press.
- Liu, Y., Franklin, M., Kahn, R., & Koutrakis, P. (2007). Using aerosol optical thickness to predict ground-level PM_{2.5} concentrations in the St. Louis area: A comparison between MISR and MODIS, *Remote sensing of Environment*, 107(1-2), 33-44.
- Liu, Y., Park, R.J., Jacob, D.J., Li, Q., Kilaru, V., & Sarnat, J. A. (2004). Mapping annual mean ground-level PM_{2.5} concentrations using Multiangle Imaging Spectroradiometer aerosol optical thickness over the contiguous United States, *Journal of Geophysical Research: Atmospheres*, 109 (D22).
- Liu, Y., Sarnat, J. A., Kilaru, V., Jacob, D. J., & Koutrakis, P. (2005). Estimating ground-level PM_{2.5} in the eastern United States using satellite remote sensing, *Environmental science & technology*, 39(9), 3269-3278.

- Liu, Z., Vaughan, M., Winker, D., Kittaka, C., Getzewich, B., Kuehn, R., Omar, A., Powell, K., Trepte, C., & Hostetler, C. (2009). The CALIPSO lidar cloud and aerosol discrimination: Version 2 algorithm and initial assessment of performance, *Journal of Atmospheric and Oceanic Technology* 26, no. 7: 1198-1213.
- Lynch, P., Reid, J. S., Westphal, D. L., Zhang, J., Hogan, T. F., Hyer, E. J., Curtis, C.A., Hegg, D.A., Shi, Y., Campbell, J.R. & Rubin, J. I. (2016). An 11-year global gridded aerosol optical thickness reanalysis (v1. 0) for atmospheric and climate sciences, *Geosci. Model Dev.*, 9, 1489–1522.
- Ma, X., Bartlett, K., Harmon, K, & Yu, F. (2013). Comparison of AOD between CALIPSO and MODIS: significant differences over major dust and biomass burning regions, *Atmospheric Measurement Techniques*, 6(9), 2391-2401.
- Malm, W.C. & Hand, J.L. (2007). An examination of the physical and optical properties of aerosols collected in the IMPROVE program, *Atmospheric Environment*, 41(16), pp.3407-3427.
- Mann, H. B. (1945). Nonparametric tests against trend, *Econometrica: Journal of the Econometric Society*, 245-259.
- Marais, W., Holz, R. E., Hui, Y. H., Kuehn, R. E., Eloranta, E. E., & Willett, R. M. (2016). Approach to simultaneously denoise and invert backscatter and extinction from photon-limited atmospheric lidar observations, *Appl. Opt.*, 55, 8316-8334, doi: 10.1364/AO.55.008316.
- Martin, R. V. (2008). Satellite remote sensing of surface air quality, *Atmospheric Environment*, 42(34), 7823-7843.

- Martonchik, J. V., Diner, D. J., Kahn, R. A., Ackerman, T. P., Verstraete, M. M., Pinty, B., & Gordon, H. R. (1998). Techniques for the retrieval of aerosol properties over land and ocean using multiangle imaging, *IEEE Transactions on Geoscience and Remote Sensing*, 36(4), 1212-1227.
- Martonchik, J. V., Kahn, R. A., & Diner, D. J. (2009). Retrieval of aerosol properties over land using MISR observations, In *Satellite aerosol remote sensing over land* (pp. 267-293). Springer, Berlin, Heidelberg.
- Mishchenko, M. I., Geogdzhayev, I. V., Rossow, W. B., Cairns, B., Carlson, B.E., A. A. Lacis, A. A., & Travis, L. D. (2007). Long-term satellite record reveals likely recent aerosol trend, *Science*, 315 (5818), 1543–1543.
- National Academies of Sciences, Engineering, and Medicine. (2018). *Thriving on Our Changing Planet: A Decadal Strategy for Earth Observation from Space*. Washington, DC: The National Academies Press. <https://doi.org/10.17226/24938>.
- Noble, C. A., Vanderpool, R. W., Peters, T. M., McElroy, F. F., Gemmill, D. B., & Wiener, R. W. (2001). Federal reference and equivalent methods for measuring fine particulate matter. *Aerosol Science & Technology*, 34(5), 457-464.
- Omar, A.H., Winker, D.M., Tackett, J.L., Giles, D.M., Kar, J., Liu, Z., Vaughan, M.A., Powell, K.A., & Trepte, C.R. (2013). CALIOP and AERONET aerosol optical depth comparisons: One size fits none, *Journal of Geophysical Research Atmospheres*, 118, 4748–4766, doi:10.1002/jgrd.50330.

- Omar, A. H., Winker, D. M., Vaughan, M. A., Hu, Y., Trepte, C. R., Ferrare, R. A., Lee, K.P., Hostetler, C.A., Kittaka, C., Rogers, R.R. & Kuehn, R. E. (2009). The CALIPSO automated aerosol classification and lidar ratio selection algorithm, *Journal of Atmospheric and Oceanic Technology*, 26(10), 1994-2014.
- Omar, A. H., Won, J. G., Winker, D. M., Yoon, S. C., Dubovik, O., & McCormick, M. P. (2005). Development of global aerosol models using cluster analysis of Aerosol Robotic Network (AERONET) measurements, *Journal of Geophysical Research: Atmospheres*, 110(D10).
- Paciorek, C., Liu, Y., Moreno-Macias, H., & Kondragunta, S. (2008). Spatio-temporal associations between GOES aerosol optical depth retrievals and ground-level PM_{2.5}, *Environ Sci Technol* 42:5800–5806.
- Pappalardo, G., Wandinger, U., Mona, L., Hiebsch, A., Mattis, I., Amodeo, A., Ansmann, A., Seifert, P., Linne, H., Apituley, A. & Alados Arboledas, L. (2010). EARLINET correlative measurements for CALIPSO: First intercomparison results, *Journal of Geophysical Research: Atmospheres*, 115(D4).
- Park, S. S., Kim, Y.J., Lee, K. W., Chun, K. J., Lee, J. Y., Lim, Y. S., & Han, J. S. (2001). Development of an automatic beta gauge particulate sampler with filter cassette mechanism, *Aerosol Science & Technology*, 35(4), 844-851.
- Pope III, C. A., Burnett, R. T., Thun, M.J., Calle, E. E., Krewski, D., Ito, K., & Thurston, G.D. (2002). Lung cancer, cardiopulmonary mortality, and long-term exposure to fine particulate air pollution, *Journal of the American Medical Association* 287, 1132–1141.

- Prados, A. I., Kondragunta, S., Ciren, P., & Knapp, K. R. (2007). GOES Aerosol/Smoke Product (GASP) over North America: Comparisons to AERONET and MODIS observations, *J. Geophys. Res.*, 112, D15201, doi:10.1029/2006JD007968.
- Prados, A. I., Leptoukh, G., Lynnes, C., Johnson, J., Rui, H., Chen, A., & Husar, R. B. (2010). Access, visualization, and interoperability of air quality remote sensing data sets via the Giovanni online tool, *IEEE Journal of Selected Topics in Applied Earth Observations and Remote Sensing*, 3(3), 359-370.
- Prospero, J. M. (1999). Long-term measurements of the transport of African mineral dust to the southeastern United States: Implications for regional air quality, *J. Geophys. Res.*, 104(D13), 15917–15927, doi:10.1029/1999JD900072.
- Rajeev, K., Ramanathan, V., & Meywerk, J. (2000). Regional aerosol distribution and its long-range transport over the Indian Ocean, *Journal of Geophysical Research-Atmospheres*, 105:2029-2043.
- Ramanathan, V. C., Crutzen, P. J., Kiehl, J. T., & Rosenfeld, D. (2001). Aerosols, climate, and the hydrological cycle, *Science*, 294(5549), 2119-2124.
- Redemann, J., Vaughan, M. A., Zhang, Q., Shinozuka, Y., Russell, P. B., Livingston, J. M., Kacenelenbogen, M., & Remer, L. A. (2012). The comparison of MODIS-Aqua (C5) and CALIOP (V2 & V3) aerosol optical depth, *Atmos. Chem. Phys.*, 12, 3025-3043, doi:10.5194/acp-12-3025-2012.
- Reid, J. S., Kaku, K., Xian, P., Benedetti, A., Colarco, P. R., da Silva Jr, A. M., Holben, B.N., Rubin, J., Tanaka, T.Y. & Zhang, J. (2016). Skill of Operational Aerosol Forecast Models in Predicting Aerosol Events and Trends of the Eastern United States. In AGU Fall Meeting Abstracts.

- Reid, J. S., Kuehn, R. E., Holz, R. E., Eloranta, E. W., Kaku, K. C., Kuang, S., Newchurch, M.J., Thompson, A.M., Trepte, C.R., Zhang, J. & Atwood, S. A. (2017). Ground-based High Spectral Resolution Lidar observation of aerosol vertical distribution in the summertime Southeast United States, *Journal of Geophysical Research: Atmospheres*, 122(5), 2970-3004.
- Remer, L. A., Kaufman, Y.J., Tanre, D., Mattoo, S., Chu, D. A., Martins, J. V., Li, R. R., Ichoku, C., Levy, R. C., Kleidman, R. G., Eck, T. F., Vermote, E., & Holben, B. N. (2005). The MODIS aerosol algorithm, products, and validation, *J. Atmos. Sci.*, 62, 947–973.
- Ridley, D. A., Heald, C. L., & Prospero, J. M. (2014). What controls the recent changes in African mineral dust aerosol across the Atlantic?, *Atmos. Chem. Phys.*, 14, 5735-5747, doi:10.5194/acp-14-5735-2014.
- Rogers, R. R., Vaughan, M. A., Hostetler, C. A., Burton, S. P., Ferrare, R. A., Young, S. A., Hair, J.W., Obland, M.D., Harper, D.B., Cook, A.L. & Winker, D. M. (2014). Looking through the haze: evaluating the CALIPSO level 2 aerosol optical depth using airborne high spectral resolution lidar data, *Atmospheric Measurement Techniques*, 7(12), 4317-4340.
- Sayer, A. M., Smirnov, A., Hsu, N. C., & Holben, B. N. (2012). A pure marine aerosol model for use in remote sensing applications, *J. Geophys. Res.*, 117, D05213, doi:10.1029/2011JD016689, 2012.
- Schuster, G. L., Vaughan, M., MacDonnell, D., Su, W., Winker, D., Dubovik, O., Lapyonok, T., & Trepte, C. (2012). Comparison of CALIPSO aerosol optical depth retrievals to AERONET measurements, and a climatology for the lidar ratio of dust, *Atmos. Chem. Phys. Discuss.*, 12, 11641– 11697.

- Schwartz, J., & Neas, L. M. (2000). Fine particles are more strongly associated than coarse particles with acute respiratory health effects in school children. *Epidemiology*, 11, 6–10.
- Sekiyama, T. T., Tanaka, T. Y., Shimizu, A., & Miyoshi, T. (2010). Data assimilation of CALIPSO aerosol observations, *Atmospheric Chemistry and Physics*, 10(1), 39-49.
- Sen, P. K. (1968). Estimates of the regression coefficient based on Kendall's tau, *Journal of the American Statistical Association*, 63(324), 1379-1389.
- Sessions, W. R., J. S. Reid, A. Benedetti, P. R. Colarco, A. da Silva, S. Lu, T., Sekiyama, T. Y. Tanaka, J. M. Baldasano, S. Basart, M. E. Brooks, T. F. Eck, M. Iredell, J. Hansen, O. C. Jorba, H.-M. Juang, P. Lynch, J.-J. Morcrette, S. Moorthi, J. Mulcahy, Y. Pradhan, M. Razinger, C. B. Sampson, J. Wang, & D. L. Westphal. (2015). Development towards a global operational aerosol consensus: basic climatological characteristics of the International Cooperative for Aerosol Prediction Multi-Model Ensemble (ICAP-MME), *Atmos. Chem. Phys.*, 15, 335-362, doi:10.5194/acp-15-335-2015.
- Shi, Y., Zhang, J., Reid, J. S., Campbell, J. R., Hsu, N. Y. C. & McHardy, T. M. (2015). An investigation of a potential low bias in the MODIS aerosol products over Asia, In AGU Fall Meeting Abstracts.
- Shi, Y., Zhang, J., Reid, J. S., Holben, B., Hyer, E. J., & Curtis, C. (2011a). An analysis of the Collection 5 MODIS over-ocean aerosol optical depth product for its implication in aerosol assimilation, *Atmos. Chem. Phys.*, 11, 557–565.

- Shi, Y., Zhang, J., Reid, J. S., Hyer, E. J., Eck, T. F., Holben, B. N., & Kahn, R. A. (2011c). A critical examination of spatial biases between MODIS and MISR aerosol products - application for potential AERONET deployment, *Atmospheric Measurement Techniques*, Vol. 4, No. 12, 2823-2836.
- Shi, Y., Zhang, J., Reid, J. S., Liu, B., & Deshmukh, R. (2011b). Multi-sensor analysis on data-assimilation-quality MISR aerosol products, In AGU Fall Meeting Abstracts.
- Shi, Y., Zhang, J., Reid, J. S., Liu, B., & Deshmukh, R. (2012). Critical evaluation of cloud contamination in MISR aerosol product using collocated MODIS aerosol and cloud products, In AGU Fall Meeting Abstracts.
- Shinozuka, Y., Clarke, A. D., Howell, S.G., Kapustin, V. N., McNaughton, C. S., Zhou, J., & Anderson, B. E. (2007). Aircraft profiles of aerosol microphysics and optical properties over North America: Aerosol optical depth and its association with PM_{2.5} and water uptake, *J. Geophys. Res.*, 112, D12S20, doi:10.1029/2006JD007918.
- Silva, R. A., West, J. J., Zhang, Y., Anenberg, S. C., Lamarque, J. F., Shindell, D. T., Collins, W.J., Dalsoren, S., Faluvegi, G., Folberth, G. & Horowitz, L. W. (2013). Global premature mortality due to anthropogenic outdoor air pollution and the contribution of past climate change, *Environmental Research Letters*, 8(3), 034005.
- Smirnov, A., Holben, B. N., Eck, T. F., Dubovik, O., & Slutsker, I. (2000). Cloud-screening and quality control algorithms for the AERONET database, *Remote Sensing of Environment*, 73(3), 337-349.

- Smirnov, A., Holben, B. N., Giles, D. M., Slutsker, I., O'Neill, N. T., Eck, T. F., Macke, A., Croot, P., Courcoux, Y., Sakerin, S.M. & Smyth, T. J. (2011). Maritime aerosol network as a component of AERONET-first results and comparison with global aerosol models and satellite retrievals, *Atmospheric Measurement Techniques*, 4(3), 583.
- Stephens, G. L., Vane, D. G., Boain, R. J., Mace, G. G., Sassen, K., Wang, Z., Illingworth, A. J., O'Connor, E. J., Rossow, W. B., Durden, S. L., Miller, S. D., Austin, R. T., Benedetti, A., & Mitrescu, C. (2002). The CloudSat mission and the A-Train: A new dimension of space-based observations of clouds and precipitation, *Bull. Amer. Meteorol. Soc.*, 83, 1771–1790, doi:10.1175/BAMS-83-12-1771.
- Tesche, M., Wandinger, U., Ansmann, A., Althausen, D., Müller, D., & Omar, A. H. (2013). Ground-based validation of CALIPSO observations of dust and smoke in the Cape Verde region, *J. Geophys. Res. Atmos.*, 118, 2889–2902, doi:10.1002/jgrd.50248.
- Tesche, M., Zieger, P., Rastak, N., Charlson, R. J., Glantz, P., Tunved, P., & Hansson, H. C. (2014). Reconciling aerosol light extinction measurements from spaceborne lidar observations and in situ measurements in the Arctic, *Atmospheric Chemistry and Physics*, 14(15), 7869-7882, 2014.
- Thorsen, T. J. & Fu, Q. (2015). CALIPSO-inferred aerosol direct radiative effects: Bias estimates using ground-based Raman lidars, *J. Geophys. Res. Atmos.*, 120, 12, 209–12, 220, doi:10.1002/2015JD024095.

- Toth, T. D., Campbell, J. R., Reid, J. S., Tackett, J. L., Vaughan, M. A., Zhang, J., & Marquis, J. W. (2018). Minimum aerosol layer detection sensitivities and their subsequent impacts on aerosol optical thickness retrievals in CALIPSO level 2 data products, *Atmospheric Measurement Techniques*, 11, 499-514, <https://doi.org/10.5194/amt-11-499-2018>.
- Toth, T. D., Zhang, J., Campbell, J. R., Hyer, E. J., Reid, J. S., Shi, Y., & Westphal, D. L. (2014). Impact of data quality and surface-to-column representativeness on the PM_{2.5}/satellite AOD relationship for the contiguous United States, *Atmospheric Chemistry and Physics*, 14(12), 6049-6062.
- Toth, T. D., Zhang, J., Campbell, J. R., Reid, J. S., Shi, Y., Johnson, R. S., Smirnov, A., Vaughan, M.A. & Winker, D. M. (2013). Investigating enhanced Aqua MODIS aerosol optical depth retrievals over the mid-to-high latitude Southern Oceans through intercomparison with co-located CALIOP, MAN, and AERONET data sets, *Journal of Geophysical Research: Atmospheres*, 118(10), 4700-4714.
- Toth, T. D., Zhang, J., Campbell, J. R., Reid, J. S., & Vaughan, M. A. (2016). Temporal variability of aerosol optical thickness vertical distribution observed from CALIOP, *Journal of Geophysical Research: Atmospheres*, 121(15), 9117-9139.
- van Donkelaar A., Martin, R. V., Brauer, M., Kahn, R., Levy, R., Verduzco, C., & Villeneuve, P. J. (2010). Global estimates of ambient fine particulate matter concentrations from satellite-based aerosol optical depth: development and application, *Environ Health Perspect*, 118:847–855.
- van Donkelaar, A., Martin, R. V., & Park, R. J. (2006). Estimating ground-level PM_{2.5} using aerosol optical depth determined from satellite remote sensing, *Journal of Geophysical Research* 111, D21201, doi:10.1029/2005JD006996.

- van Donkelaar, A., Martin, R. V., Spurr, R. J., & Burnett, R. T. (2015). High-resolution satellite-derived PM_{2.5} from optimal estimation and geographically weighted regression over North America, *Environmental Science & Technology*, 49(17), 10482-10491.
- Vaughan, M. A., Powell, K. A., Kuehn, R. E., Young, S. A., Winker, D. M., Hostetler, C. A., Hunt, W. H., Liu, Z., McGill, M. J., & Getzewich, B. J. (2009). Fully automated detection of cloud and aerosol layers in the CALIPSO lidar measurements, *J. Atmos. Ocean. Tech.*, 26, 2034–2050.
- Vaughan, M. A., Trepte, C. R., Winker, D. M., Avery, M. A., Campbell, J., Hoff, R., Young, S., Getzewich, B. J., Tackett, J. L. & Kar, J. (2011). Adapting CALIPSO climate measurements for near real time analyses and forecasting, *Proceedings of the 34th International Symposium on Remote Sensing of Environment*, 10–15 April 2011, Sydney, Australia, http://www.calipso.larc.nasa.gov/resources/pdfs/VaughanM_211104015final00251.pdf.
- Waggoner, A. P., & Weiss, R. E. (1980). Comparison of fine particle mass concentration and light scattering extinction in ambient aerosol, *Atmospheric Environment* (1967), 14(5), 623-626.
- Wandinger, U., Hiebsch, A., Mattis, I., Pappalardo, G., Mona, L., & Madonna, F. (2011). Aerosols and clouds: long-term database from spaceborne lidar measurements, Final report, ESTEC, Noordwijk, The Netherlands.
- Wandinger, U., Tesche, M., Seifert, P., Ansmann, A., Müller, D., & Althausen, D. (2010). Size matters: Influence of multiple scattering on CALIPSO light-extinction profiling in desert dust, *Geophys. Res. Lett.*, 37, L10801, doi:10.1029/2010GL042815.

- Wang, J., & Christopher, S. A. (2003). Intercomparison between satellite derived aerosol optical thickness and PM_{2.5} mass: implications for air quality studies, *Geophysical Research Letters* 30 (21), 2095, doi:10.1029/2003GL018174.
- Winker, D. M., Hunt, W. H., & McGill, M. J. (2007). Initial performance assessment of CALIOP, *Geophys. Res. Lett.*, 34, L19803, doi:10.1029/2007GL030135.
- Winker, D. M., Pelon, J., Coakley Jr, J. A., Ackerman, S. A., Charlson, R. J., Colarco, P. R., Flamant, P., Fu, Q., Hoff, R.M., Kittaka, C. & Kubar, T. L. (2010). The CALIPSO mission: A global 3D view of aerosols and clouds, *Bulletin of the American Meteorological Society*, 91(9), 1211-1230.
- Winker, D. M., Tackett, J. L, Getzewich, B. J., Liu, Z., Vaughan, M. A., & Rogers, R. R. (2013). The global 3-D distribution of tropospheric aerosols as characterized by CALIOP, *Atmospheric Chemistry and Physics*, 13, 3345-3361, doi:10.5194/acp-13-3345-2013.
- Winker, D. M., Vaughan, M. A., Omar, A., Hu, Y., Powell, K. A., Liu, Z., Hunt, W. H., & Young, S. A. (2009). Overview of the CALIPSO Mission and CALIOP Data Processing Algorithms, *J. Atmos. Oceanic Technol.*, 26, 2310–2323.
- Yoon, J., von Hoyningen-Huene, W., Kokhanovsky, A. A., Vountas, M., & Burrows, J. P. (2012). Trend analysis of aerosol optical thickness and Ångström exponent derived from the global AERONET spectral observations, *Atmos. Meas. Tech.*, 5, 1271-1299, doi:10.5194/amt-5-1271-2012.
- Yoon, J., von Hoyningen-Huene, W., Vountas, M., & Burrows, J. P. (2011). Analysis of linear long-term trend of aerosol optical thickness derived from SeaWiFS using BAER over Europe and South China, *Atmos. Chem. Phys.*, 11, 12149-12167, doi:10.5194/acp-11-12149-2011.

- Yorks, J. E., McGill, M., Rodier, S., Vaughan, M., Hu, Y., & Hlavka, D. (2009). Radiative effects of African dust and smoke observed from Clouds and the Earth's Radiant Energy System (CERES) and Cloud-Aerosol Lidar with Orthogonal Polarization (CALIOP) data, *J. Geophys. Res.*, 114, D00H04, doi:10.1029/2009JD012000.
- Young, S. A. & Vaughan, M. A. (2009). The retrieval of profiles of particulate extinction from Cloud Aerosol Lidar Infrared Pathfinder Satellite Observations (CALIPSO) data: Algorithm description, *J. Atmos. Oceanic Technol.*, 26, 1105–1119, doi:10.1175/2008JTECHA1221.1.
- Young, S. A., Vaughan, M. A., Kuehn, R. E., & Winker, D. M. (2013). The retrieval of profiles of particulate extinction from Cloud–Aerosol Lidar and Infrared Pathfinder Satellite Observations (CALIPSO) data: Uncertainty and error sensitivity analyses. *Journal of Atmospheric and Oceanic Technology*, 30(3), 395-428.
- Yu, H., Chin, M., Winker, D. M., Omar, A. H., Liu, Z., Kittaka, C., & Diehl, T. (2010). Global view of aerosol vertical distributions from CALIPSO lidar measurements and GOCART simulations: Regional and seasonal variations, *Journal of Geophysical Research: Atmospheres* (1984–2012), 115 (D4).
- Yue, S., Pilon, P., Phinney, B., & Cavadias, G. (2002). The influence of autocorrelation on the ability to detect trend in hydrological series, *Hydrological Processes*, 16(9), 1807-1829.
- Zhang, J., Campbell, J. R., Hyer, E. J., Reid, J. S., Westphal, D. L., & Johnson, R. S. (2014). Evaluating the impact of multisensory data assimilation on a global aerosol particle transport model, *J. Geophys. Res. Atmos.*, 119, 4674–4689, doi:10.1002/2013JD020975.

- Zhang, J., Campbell, J. R., Reid, J. S., Westphal, D. L., Baker, N. L., Campbell, W. F., & Hyer, E. J. (2011). Evaluating the impact of assimilating CALIOP-derived aerosol extinction profiles on a global mass transport model, *Geophysical Research Letters*, 38(14).
- Zhang, J., & Christopher, S. A. (2003). Longwave radiative forcing of Saharan dust aerosols estimated from MODIS, MISR, and CERES observations on Terra, *Geophysical Research Letters*, Vol. 30, No. 23, 2188, doi: 10.1029/2003GL018479.
- Zhang, J., Christopher, S. A., & Holben, B. N. (2001). Intercomparison of smoke aerosol optical thickness derived from GOES 8 imager and ground-based Sun photometers, *J. Geophys. Res.*, 106, D7, doi: 10.1029/2000JD900540.
- Zhang, J., & Reid, J. S. (2006). MODIS aerosol product analysis for data assimilation: Assessment of over-ocean level 2 aerosol optical thickness retrievals, *J. Geophys. Res.*, 111, D22207, doi:10.1029/2005JD006898.
- Zhang, J. & Reid, J. S. (2009), An analysis of clear sky and contextual biases using an operational over ocean MODIS aerosol product, *Geophysical Research Letters*, 36, L15824, doi:10.1029/2009GL038723.
- Zhang, J. & Reid, J. S. (2010). A decadal regional and global trend analysis of the aerosol optical depth using a data-assimilation grade over-water MODIS and Level 2 MISR aerosol products, *Atmospheric Chemistry and Physics*, 10, 10949-10963, doi:10.5194/acp-10-10949-2010.
- Zhang, J., Reid, J. S., Westphal, D. L., Baker, N. L., & Hyer, E. J. (2008). A system for operational aerosol optical depth data assimilation over global oceans, *J. Geophys. Res.*, 113, D10208, doi:10.1029/2007JD009065.

Zhang, Z. Y., Wong, M. S., & Nichol, J. (2016). Global trends of aerosol optical thickness using the ensemble empirical mode decomposition method, *International Journal of Climatology*, 36(13), 4358-4372.

Zhao, T. X.-P., Laszlo, I., Guo, W., Heidinger, A., Cao, C. Jelenak, A., Tarpley, D., & Sullivan, J. (2008). Study of long-term trend in aerosol optical thickness observed from operational AVHRR satellite instrument, *J. Geophys. Res.*, 113, D07201, doi:10.1029/2007JD009061.